P O S I T R O N A N N I H I L A T I O N I N P U R E A N D D E F E C T E D M E T A L S

ILPER CHAGLAR

B.Sc., M.Sc. (Ankara); M.Sc. (Lond.)

A Thesis Submitted for the Degree of

DOCTOR OF PHILOSOPHY

in the

University of London

Physics Department

Bedford College

London

1978

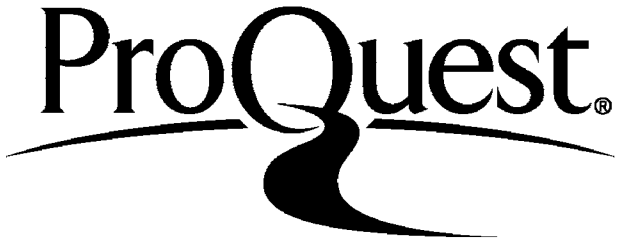

DEDICATED TO MY WIFE WHOSE PATIENCE
AND SUPPORT PLAYED AN IMPORTANT ROLE
IN THE COMPLETION OF THIS WORK

A B S T R A C T

The Doppler-broadening technique has been applied to positron annihilation studies in plastically deformed and annealed specimens of zinc, indium, cadmium, lead, gold, and silver in the temperature range down to 4.2 K .

Annealing studies in metals deformed at room temperature or under liquid nitrogen provided information on recrystallisation and on the nature of defects produced by plastic deformation. It has been shown that the specific trapping rate of positrons by deformation-induced dislocations is temperature independent.

The equilibrium measurements, which extended up to their melting points in well annealed samples (except for gold and silver) , enabled us to compare the models proposed to take into account the intermediate temperature dependence of the line-shape parameter. Also the mono-vacancy formation energies could be determined.

The model fittings to the annihilation gamma-ray peak, which consisted of a Gaussian and an inverted parabola convoluted with the instrumental resolution function, provided the probabilities of positron annihilation with core and conduction electrons in the deformed and annealed samples.

The annihilation spectra were recorded with a high resolution Ge(Li) detector whose resolution at a count rate of 5000 cps was 1.15 keV for the 514 keV line in ^{85}Sr .

Further results on the temperature dependence of the width parameters of the Gaussian and parabolic distributions which characterise the momentum distributions of the core and conduction electrons, respectively, are presented.

TABLE OF CONTENTS

CHAPTER 1 POSITRONS AND THEIR ANNIHILATION IN MATTER

1.1 General Introduction

After the theoretical predictions of their existence (Dirac, 1930) positrons were experimentally observed by Anderson (1933) as a constituent of cosmic rays in a bubble chamber at Pasadena, California.

After the first angular correlation measurements of annihilation photons by Beringer and Montgomery (1942) were performed, it was found that annihilation pairs are radiated, within limits of one degree, in exactly opposite directions. Measurements with a far greater accuracy (De Benedetti et al, 1950) showed that the mean angular departure from antiparallelism of two photons is about 1/137 radians, and arise from the motion of centre of mass of the annihilating pair.

Practically, all the positrons survive the atom ionisation and excitation processes without annihilation. This finding gave the idea, for the first time, to indicate the possibility of determination of the energy distribution (Du Mond et al, 1949) for free electrons according to the line-width in the spectrum of the annihilation photons.

Experimental, as well as theoretical, investigations on positron annihilation in the 1950 's continued in the 1960 's with a continuously growing interest, and increasing numbers of scientists entered the field. By 1970 it was fully realised that positrons were potentially capable

of being a very sensitive probe in the investigations on the nature and properties of lattice defects and their agglomerations, as well as in the studies of the internal structure of materials.

The present day positron annihilation studies can broadly be divided into two catagories : (i) measurements in annealed materials to study the electron momentum distributions ; thus the shape and the size of the Fermi surfaces. (ii) Defect studies ; capture and subsequent annihilation of positrons in various types defects.

The ever increasing, vast amount of data, encountered in the field of materials research, promises the solutions to several long-standing problems where other conventional metallurgical techniques are not capable of giving.

1.2 The Behaviour of Positrons in Matter

1.2.1 Slowing-down to Thermal Energies

From the rate of loss of energy, by inelastic collisions with thermally vibrating lattice atoms - or ions- of the annihilation medium, Lee-Whiting (1955) showed that positrons slow down to thermal energies in 3×10^{-12} seconds. This is short compared to the known positron lifetimes in metals, typically in the order of 10^{-10} second. Later, by examining the momentum distribution of annihilation photons in the region corresponding to Fermi momentum, where the electron energy distribution has a sharp cut-off, Kim et al (1967) defined the positron effective temperature. Their angular

correlation measurements in alkali metals showed that, as the temperature of the specimen was raised, the smearing at the cut-off was increased and this was interpreated as a result of increased motion of the positron in the hotter metal. At high temperatures the observed effective positron temperature rises linearly with increasing specimen temperature and the linearity is taken as good evidence of thermalisation. The deviation from the linearity towards low temperatures was interpreated as the result of annihilation of positrons prior to complete thermalisation. Analysis in Na showed a positron effective temperature 160 K at the lowest temperature.

Contrary to what was suggested by Kim et al (1967), Kubica and Stewart (1975) presented direct evidence to show that, in certain cases at least, positrons or positronium atoms (hereafter abreviated Ps) at the time of annihilation could be close to thermal equilibrium when in the liquid helium temperature regime. They reckoned that, although the small contribution from the motion of thermal positron could be seen as a smearing of the electron momentum distribution at the Fermi cut-off, this could not be entirely due to the thermal motion of positrons. Positron localisation in various types of defcts can also be a contributing factor. In addition, contribution from the instrumental resolution and uncertainity in the actual resolution function can generate systematic errors. Therefore, very high instrumental resolution is required.

With their high resulution angular correlation apparatus, capable of measuring thermal motion of positrons at helium temperature, Kubica and Stewart (1975), assuming that the best fit to the total smearing of the angular correlation curve at the Fermi cut-off reflects just the instrumental resolution, positron penetretion into the sample, and the Maxwell-Boltzman distribution of free positrons at temperature T, measured the lowest positron temperatures in K, Mg, and Al as $T=25\pm25$ K , $T=10\pm10$ K , and $T=30\pm25$ K, respectively, and concluded that the precision of the results is determined mainly by the instrumental resolution rather than the thermal motion of positrons.

1.2.2 Annihilation of Thermal Positrons

Thermalised positrons interact with the atomic environment of the medium and these interactions are governed by the laws of quantum electrodynamics (Berestetskii et al, 1971). As a result of this, a positron-electron pair can be radiated in the form of electromagnetic energy. The amount of energy liberated in the process, from the conservation of energy, can be written in the form

$$E = 2m_o c^2 + E_K + E_B \qquad (1.1)$$

where $m_o c^2$ is the rest mass energy of each particle, E_K and E_B are the total knetic enrgy and the binding enrgy of the positron-electron system, respectively. Prior to their annihilation with an electron of the medium, practically all positrons survive the slowing down process. Therefore, the total knetic enrgy of the system is due mainly to that of

the electron, which is in the order of a few electron volts and much smaller than the total rest mass energy of the pair ($2m_0c^2$ = 1.02 MeV). The binding energy, if a bound state exists at all, is also very small. In free space the binding energy of a Ps atom is 6.8 eV and may be even smaller in matter (Ore and Powell, 1949 ; Wallace, 1960). As a result of this, the annihilation quanta have to carry the huge total rest mass energy with a relatively very small net momentum. Conservation of momentum requires at least two quanta should be emitted (Yang, 1950). Single-quantum annihilation is only possible in the presence of a third body, an electron or a nucleus, which can absorbe the recoil momentum (Wallace, 1960).

A positron-electron pair, if not free, can, in certain cases, form a bound system known as the Ps atom. Ps formation is found only in the substances, among them non-metallic elements, with complex molecular structure or imperfect crystal status (De Benedetti, 1967). These substances contain empty spaces which enable slow positrons to localise. Decay modes of such a system satisfy the conservation laws ; conservation of energy, momentum, spin, and charge. The effect of these laws on the decay modes are more easily demonstrated if the initial state of the annihilating pair is well defined (Muirhead, 1965).

If the positron-electron pair forms a Ps atom in the ground state (i.e., the total angular momentum L=0) then, depending on their spin orientation the atom can either be in the

singlet, $^1S_0$, state (para-Ps) -where the total spin is zero - or in the triplet, $^3S_1$, state (ortho-Ps), in which the total spin is unity.

The charge parity, P_c, of a positron-electron system, given by Berestetskii et al (1971), is a combination of the intrinsic, spatial, and spin parities ($P_c=P_i\ P_L\ P_s$). For a particle-antiparticle pair the intrinsic parity P_i is negative. The spatial and the spin parities are given, respectively, in the forms $P_L=(-1)^L$ and $P_s=(-1)^{s+1}$. Since the charge parity of a photon is negative, for an annihilating positron-electron bound system invariance under charge conjugation implies that

$$(-1)^{L+s} = (-1)^n \qquad (1.2)$$

where n is the number of photons emitted as a result of the annihilation.

If Ps decays only from the ground state, the two possible decay modes are :
(i) Singlet state (para-Ps) ; J=L+s=0 —i.e., n is even
(ii) Triplet state (ortho-Ps) ; J=L+s=1 —i.e., n is odd .

Typically, para-Ps decays into two photons and ortho-Ps decays into three photons. Statistically, one-quarter of the total number of Ps atoms are formed in the singlet state and the rest in the triplet. Kerr (1974) showed that, in polymers, the amount of para-Ps formed is one-third that of the ortho-Ps . This figure is of course based on the assumption that there is no appreciable triplet-singlet conversion.

On the other hand the three-to-two photon annihilation ratio from a bound state may be affected by "pick-off" annihilation which is a direct annihilation of a positron with a foreign electron from the surrounding medium with which the Ps atom collides.

1.2.3 Annihilation Rates

The problem of two-photon annihilation in the circumtances permitted by the selection rules was first discussed and the cross-section for the annihilation of a slow free positron with a slow electron of the system, ignoring the effect of Coulomb interaction between them, was given by Dirac (1930) :-

$$\sigma_2 = \pi r_o^2 \, c/v \qquad (1.3)$$

where v is the positron velocity and $r_o = e^2/(m_o c^2)$ is the classical electron radius.

In an environment having n electrons per unit volume the annihilation rate of positron is given by

$$\lambda_2 = \sigma_2 \, vn = \pi r_o^2 \, cn \qquad (1.4)$$

The Ps atom ground state wave functions, given by West (1974), have the form

$$\psi(r) = (\pi a^3)^{-\frac{1}{2}} \exp(-r/a) \qquad (1.5)$$

where $a = 2\hbar^2/(m_o e^2)$ is the Bohr radius of Ps atom and r is the relative coordinate. The electron density at the positron is

$$n = |\psi(o)|^2 \qquad (1.6)$$

Since the annihilation cross-section of a free positron with an electron is averaged over four possible spin orientations whereas the Ps decays from a specific spin state, the decay rate of para-Ps from Dirac's formula is

$$\lambda_{para} = 4\pi r_o^2 \, c \, |\psi(o)|^2 \qquad (1.7)$$

Substituting the values for r_o and a, the para-Ps lifetime can be calculated :-

$$\tau_{para} = \lambda_{para}^{-1} = 1.25 \times 10^{-10} \text{ sec.}$$

It has been shown by Ore and Powell (1949) that the three-to-two photon annihilation ratio for slowly moving, unbound positron-electron pairs is 1/370 . Since ortho-Ps formation is three times more likely than the para-Ps, the ratio of their lifetimes will be approximatelly $3 \times 370 = 1100$. Therefore the ortho-Ps lifetime becomes

$$\tau_{ortho} = \tau_{para} \times 1100 = 1.4 \times 10^{-7} \text{ sec.}$$

The three-photon annihilation rate can be assessed by a triplet coincidence technique or from a study of the energy spectra of the annihilation photons (De Blonde et al, 1972 ; Gainotti et al, 1964).

1.2.4 Energetics of Positron Annihilation in Matter

At the final stage of their thermalisation, positrons lose almost half of their energy in each collision with the electrons of the medium until their energy becomes less than the typical energy required for the excitation of the

electrons to higher bands. Calculations by Lee-Whiting (1955) of the time required for the positrons to reduce their energy to a few electron volts yields a time of 3×10^{-15} seconds. Also, for 1 eV to 0.1 eV , 2×10^{-13} seconds and from 0.1 eV to 0.025 eV , 3×10^{-12} seconds. Thus, most of the time is required for the last stage of the slowing-down process.

The situation in insulators, after slowing down in the initial stages of the process, is more complicated. Energy losses in excitations of the electrons to higher bands is inhibited by energy gaps, therefore, the thermalisation stages, below 1 eV , can only proceed by excitation of lattice vibrations. Calculations by De Benedetti et al (1950) deduced a thermalisation time of the order of 300 pseconds.

The binding energy of the Ps atom in solids, quoted by Wallace (1960), is slightly less than 6.8 eV and for most materials the ionisation energy, E_i, of molecules is about 10 eV . Ps formation is most probable when the positron energy, E, is within the range

$$E_e > E > E_i - 6.8 \quad eV \qquad (1.8)$$

where E_e is the lowest electronic excitation energy. This energy range is known as the "Ore gap" .

1.2.4.1 Positron Annihilation in Molecular Substances and in Ionic Crystals

Concerning the annihilation of positrons in molecular materials, in which Ps can be formed (Wallace, 1960), the

subctances investigated in greatest detail are polymers.

Measurements with recently improved, fast coincidence systems and data analysis show a long lifetime component, typically, ranging from 2 to 4 nseconds and intensities from 10% to 30% of total annihilations. This is attributed to the pick-off annihilations of positrons bound in ortho-Ps. The short lifetime component of 125 pseconds, ideally with an intensity one-third as large as that of the long lifetime, emerges from the self-annihilation of para-Ps. Nevertheless, at present, the experiments, or the methods, of analysis cannot definitely decide whether this component is single or a composition. The rest arise from the annihilation of unbound positrons, with lifetimes approximatelly 500 pseconds.

The intermediate lifetime which accounts for the decay of positrons have not formed Ps appears to be independent to changes in temperature or volume (Brandt and Spirn, 1966). On the other hand, the long lived component shows sensitive response to such changes. Temperature dependence of the pick-off annihilation modes have been discussed by Brandt et al (1960) and Brandt (1967) with that of a free volume model. The thermal motion of molecules raises the electron density in the free volume. Therefore, the net result is a decrease in the long lifetime relative to its value at low temperatures.

The work by Bell and Graham (1953) in ionic crystals yielded

a mean life of 230 pseconds in NaCl. Farrell (1956) also showed that there is simply not enough room for a Ps atom. Angular correlation studies in alkali halides by Stewart and Pope (1960) confirmed the annihilation of positrons with the outer electrons of negative ions.

Measurements of the temperature effect on the lifetime spectra of positrons annihilating in additively coloured KCl by Bosi and Dupasquier (1975) showed that the rate of positron trapping at F-centres (positive ion induced free-cation vacancies), per unit F-centre concentration, is temperature independent in the range 7 - 300 K . They concluded that the trapping process in ionic crystals is not diffusion limited.

1.2.4.2 Annihilation in Metals

It has been well established, since the early days of positron annihilation work, due to several reasons, Ps formation in metals is not favourable (Ore and Powell,1949). Energetics of positron annihilation inhibits such a possibility. The large conduction electrons density in metals, which screen the interaction of a positron with a particular electron, provides further reason to doubt the possibility of positron binding to single electrons.

The average density of electrons at the site of a thermalised positron in metals determines its lifetime. Single component positron lifetimes in metals range from 100 to 500 pseconds (Weisberg and Berko, 1967 ; Hautojarvi et al, 1970 ;

Mc Kee et al, 1972b).

Due to its positive charge the positron is repelled from the positive ions at the lattice site. Thus, they annihilate mainly with conduction band electrons. Positron annihilation gamma-ray lines in metals, after the subtruction of the instrumental broadening effect, are classified as a superposition of a broad, approximatelly Gaussian and an inverted parabola. Contributions to the parabolic component come from the annihilations with conduction electrons and the broad Gaussian component is due mainly to the annihilations with more tightly bound electrons, usually refered to as core electrons.

Because of its positive charge, the positron perturbs the electrons of the medium surrounding it. Therefore, the annihilation electrons are no longer in pure Bloch states. Although, inclusion of many-body effects requires relatively small modification of the angular correlation distributions (Kahana, 1963), they lead much shorter lifetimes than are predicted if the Coulomb interaction between a positron and an electron is neglected. These many-body effects have been dealt with extensively in the literature (Carbotte and Kahana, 1965 ; Carbotte and Salvadori, 1967 ; Fujiwara et al, 1972 ; Bhattacharyya and Singwi, 1972).

1.3 Methods for Observing the Features of Positron Annihilation

1.3.1 Positron Sources

Among the commonly used positron sources (listed in table 1.3.1) ^{22}Na , without doubt, takes the first place. The emission of a 545 keV positron is accompanied, promptly (3.3 pseconds), by the emission of a 1.28 MeV gamma-ray. In addition, its long lifetime and commercial availability makes it the most favourable for lifetime measurements. Commercially available ^{22}Na positron sources are commonly carrier-free $^{22}NaCl$ in aqueous solutions.

Despite its short lifetime, ^{64}Cu is, also, often used in angular correlation and in Doppler-broadening measurements, because of its easy production. Absence of the emission of gamma-rays in coincidence with positrons eliminates its use in lifetime measurements.

^{68}Ge and ^{58}Co are also used in positron annihilation studies. Especially ^{68}Ge has a relatively long lifetime and it gives rise to a very small background from nuclear gamma-rays. On the other hand their production to suit the experimental requirements, in particular the sample preparation, is rather difficult.

In the source-specimens sandwich arrangement, positron absorption in the source itself is undesirable, and to minimise it the source has to be either a very thin foil or evaporated directly on to the specimens.

Table 1.3.1 List of commonly used positron sources.

Isotope	Half-life	Positron end point energy (keV)	Intensity of coincident gamma-rays (%)
Na-22	2.58 y	545	90
Cu-64	12.9 h	650	0
Ge-68	275 d	1880	1.5
Co-58	71.3 d	480	15

1.3.2 Measurements of Positron Lifetimes

Positrons injected into a sample, normally, thermalise in times short compared to their lifetime. The lifetime of thermalised positrons in a metal is determined by the average density of electrons at the positron coordinates. To measure the time delay between the injection of a positron into a sample and its annihilation, a marker to indicate the time of injection is required. Therefore, it is basically this requirement which restricts the contemporary positron lifetime experiments to the use of the isotope ^{22}Na .

A typical, schematic experimental arrangement for measuring positron lifetimes in metals is shown in figure 1.1 . Detectors used in lifetime measurements are fast plastic scintillators mounted on fast photomultiplier tubes in which the light pulses produced in the scintillators are detected and amplified. The fast timing discriminators are used to process the pulses from the photomultipliers into standard, well defined pulses. A time to pulse-height converter (TPHC)

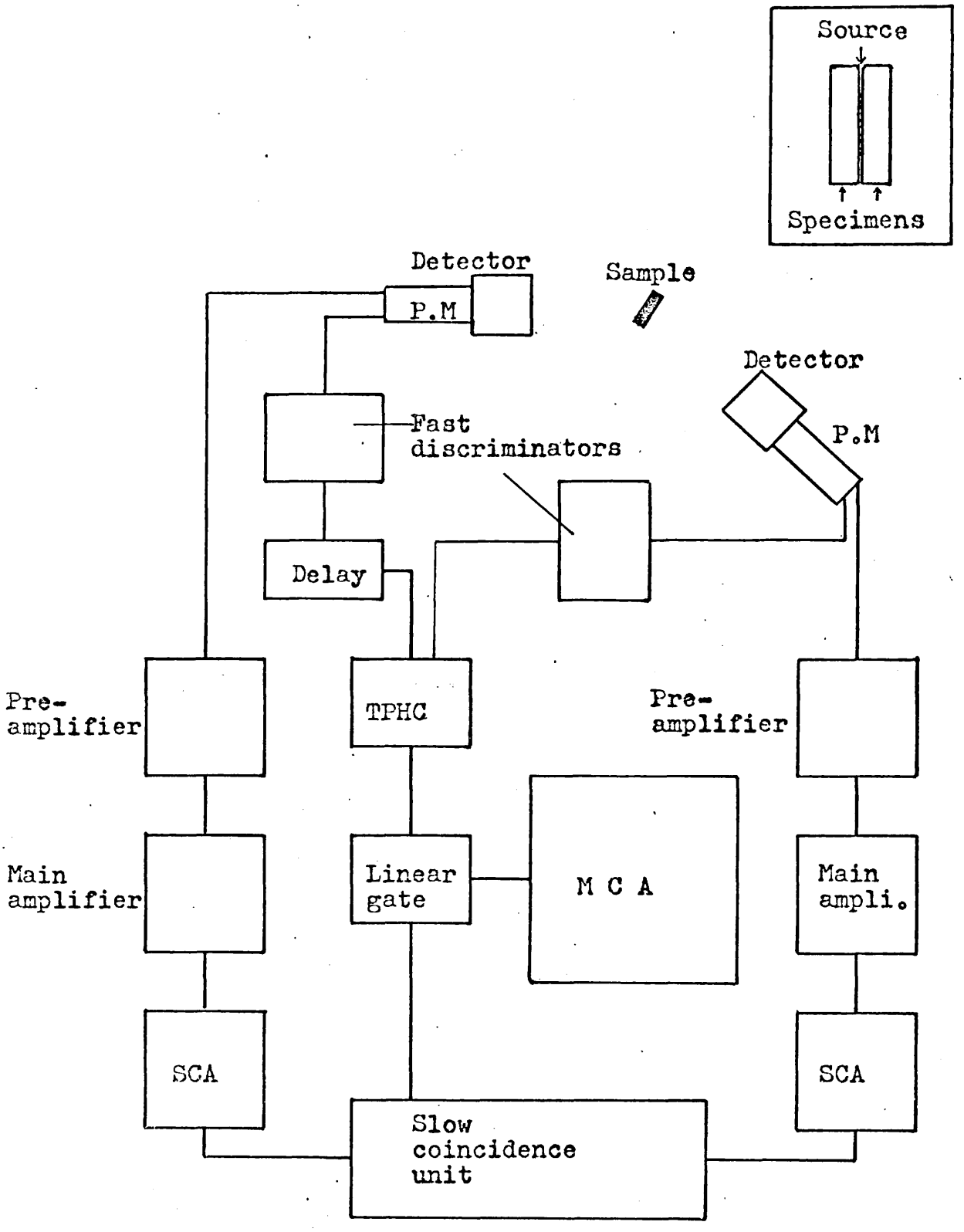

FIG. 1.1 A typical schematic block diagram for lifetime measurements. Inset shows the source-specimen arrangement.

is then used to generate a pulse with an amplitude which is a measure of the time delay between the detection of a pair of events in the detectors. The slow, energy selection, coincidence system, consisting of two pre-amplifiers, two main amplifiers, two single channel analysers (SCA) and a coincidence unit, is used to ensure the isolation of relevant coincidence events. Finally, the identified pulses from the time to pulse-height converter are digitised and sorted by a multi channel analyser (MCA).

The quality and success of such a system, described above, depends on several factors. Fast, and stable, electronics is essential. Coincidence circuits with a 10 nseconds resolving time can give a moderate time resolution. Chance coincidence contributions play an important role in the smearing of a true time spectrum. This demands a modest source strength, normally a few microcuries.

The intrinsic time resolution of a lifetime system can be determined from the full width at half maximum (FWHM) of the coincidence curve of ^{60}Co, which emits two prompt coincident gamma-rays. The best, present day, intrinsic resolutions obtained in positron lifetime measurements are about 2 nseconds (Scharma et al, 1976).

The positron relative mean lifetime measurements in different materials or in the same specimen, subjected to different treatments, may be obtained from the centroid shift of the delayed coincidence curve obtained from the prompt ^{60}Co curve. However, the centroid shift measurements are bound

to be very sensitive to electronic stability, the amount of annihilations in the source material and errors resulting from changing the geometrical position of the prompt and the delayed sources. Newertheless, recently improved lifetime measurements, reported by Myllyla (1978), allowing the simultaneous accumulation of the propt and delayed data with a higher counting rate, good time resolution and good electronics stability, eliminates -or, at least, weakens - some of the difficulties outlined above.

The positron lifetime analysis is usually rather complicated, therefore large computer programs are necessary (Kirkegaard and Eldrup, 1972 ; 1974). If a lifetime spectrum contains only a single component, the task is not difficult. On the other hand, a serious problem arises when a spectrum contains more than one component, in particular when two lifetimes are present having values close to each other.

1.3.3 Angular Correlation of Annihilation Radiation

The angular distribution of the two photons, emitted when a positron-electron pair annihilates in matter, reflects the momentum distribution of the centre of mass of the annihilating particles at the time of annihilation. In principle, all the positrons injected into the sample survive the thermalisation process, as noted earlier in section 2.1 of this chapter. Therefore, the observed angular correlation is due mainly to the momentum distribution of the electrons of the annihilation medium and, thus, provides information about the size and shape of the Fermi surface.

The high momentum component of angular correlation curves is due mainly to the annihilations with core electrons. The departure of the two photons from collinearity can be as high as 20 milliradians for annihilation of positrons, even with the loosely bound localised electrons.

A typical, experimental arrangement for angular correlation measurements is shown in figure 1.2 . The annihilation photons are detected by scintillation counters where one of them is fixed and the other is moveable. The coincidence count rates measured as a function of the position of the moveable arm gives the angular correlation curve.

The scintillation counters are shielded from direct view of the source by lead collimators. The additional detector collimators (shown in the inset in figure 1.2) and the source-detector distance, determine the angular resolution. By choosing large source-detector distances and narrow slits the angular resolution can be improved, at the expense of the counting rate.

An angular correlation apparatus, shown in figure 1.2 , with long slit geometry, can define only one component, say P_z , of the transverse momentum of the photon pair. P_x is parallel to the direction of photons.

A less common detector collimator type is the crossed-slit geometry. Figure 1.3 displays the geometry for a typical crossed-slit angular correlation experiment (Berko and Mader, 1975). For a positron-free electron pair momentum $\underline{P}$

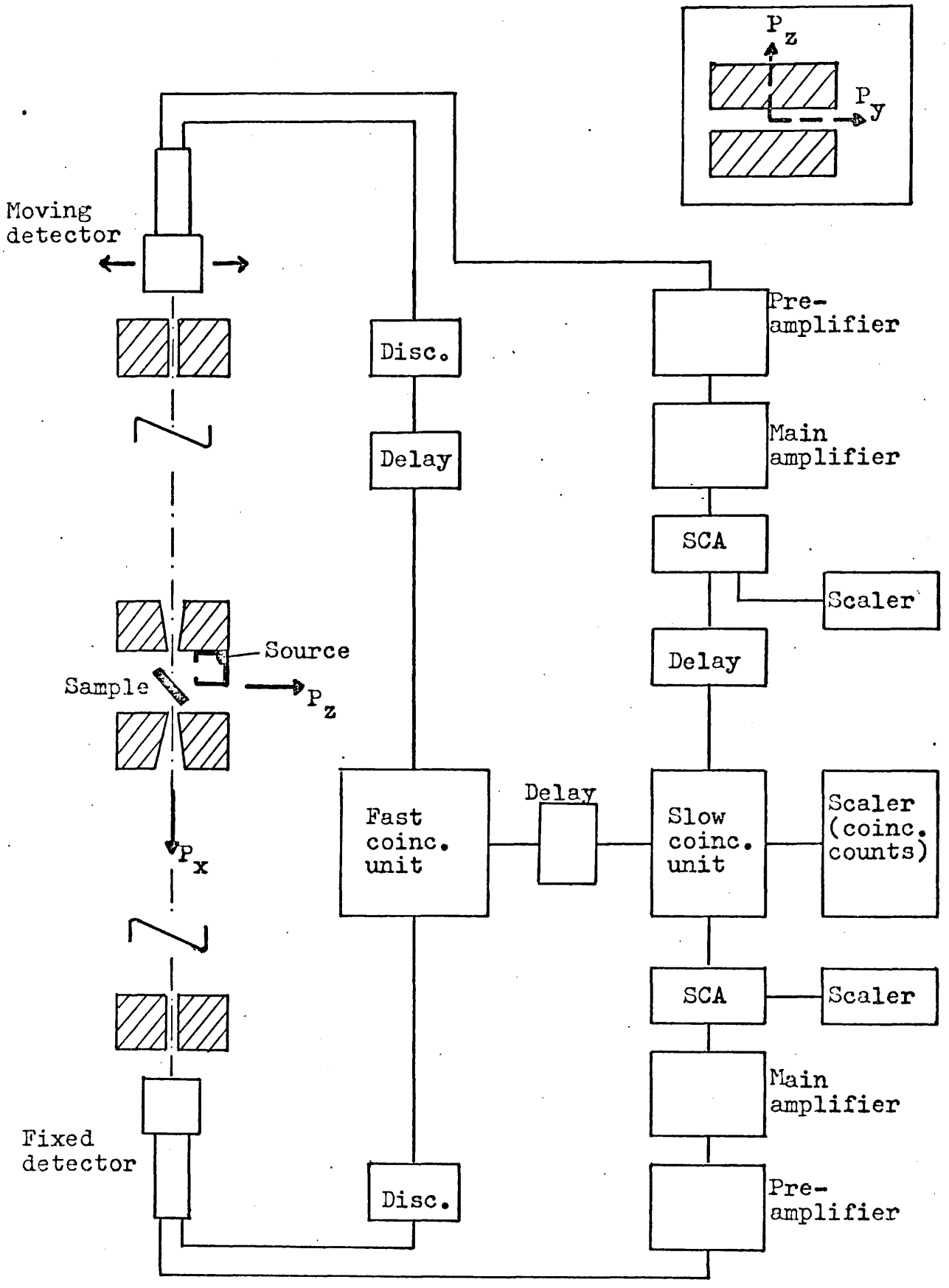

FIG. 1.2 A typical experimental arrangement for angular correlation experiments. The inset shows the long slit geometry.

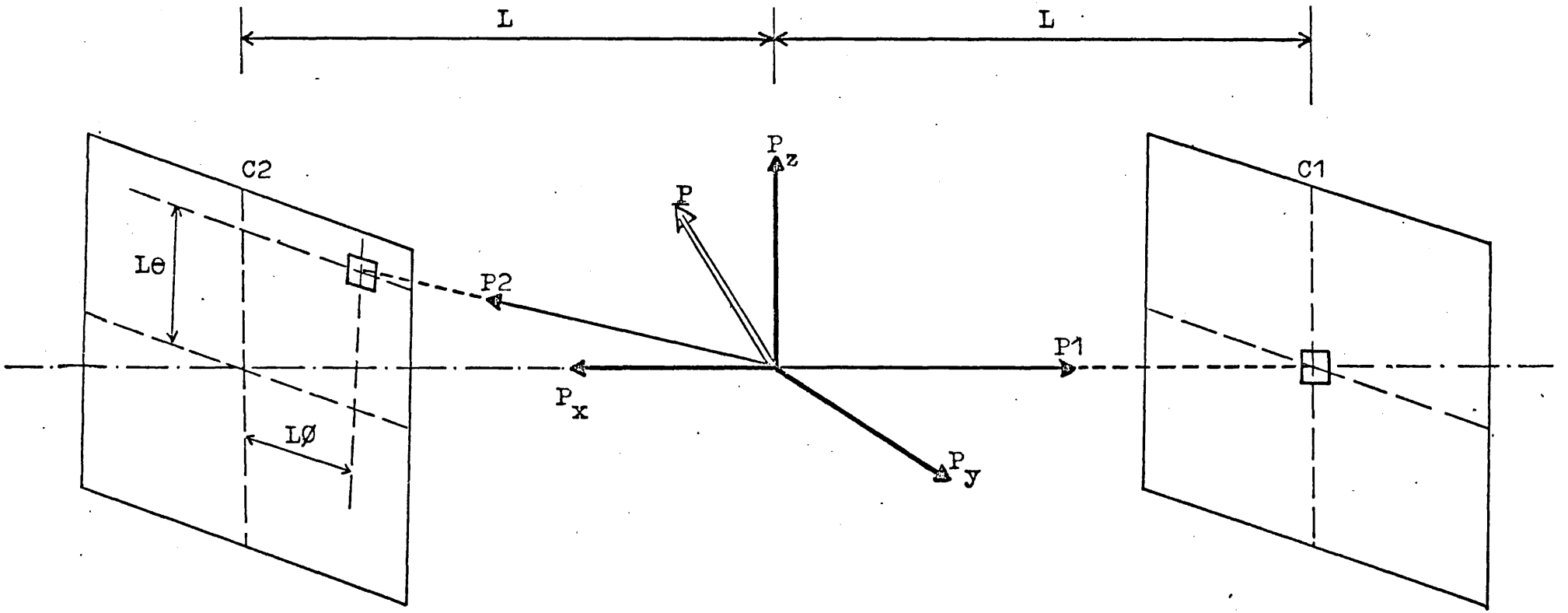

FIG. 1.3 The geometry of a two-photon angular correlation experiment for a typical positron-electron momentum $\underline{P}$ (indicated by the double arrow). L is the distance of the two counter planes from the sample. Typically, angles θ and ϕ are a few milliradians (after Berko and Mader, 1975).

(just before annihilation) the departure of the two photons from collinearity is within a few milliradians. If a counter, C_1, detects one of the photons, the second photon will be detected by a counter, C_2, at coordinates θL and ϕL. Here L is the distance of the counter planes from the annihilation centre. Since the magnitude of the photon momenta is equal to mc to within 1% (Berko and Mader, 1975); $P_z = mc\theta$ and $P_y = mc\phi$.

The momentum component parallel to the direction of photons is not measured. Thus, in an experiment with crossed-slit geometry the distribution of angles θ and ϕ measures the distribution of z and y components, respectivelly, of the momentum of annihilating pair. Given a momentum distribution $\alpha(\underline{P})$, carried by the two photons, the crossed-slit geometry measures a coincidence rate given by

$$N(P_z, P_y) = \int_{-\infty}^{+\infty} \alpha(\underline{P})\, dP_x \qquad (1.9)$$

and the long-slit geometry, integrating the momentum distribution over yet onother component, say P_y, measures a coincidence rate given by

$$N(P_z) = \int_{-\infty}^{+\infty} \alpha(\underline{P})\, dP_x\, dP_y \qquad (1.10)$$

The crossed-slit geometry provides the distribution of two components, P_z and P_y, of the transverse momentum of the photon pair, where, the long-slit geometry does for only one. On the other hand, this piece of extra information of the crossed-slit geometry, in most circumtances, is incompatible with the severe worsening of the counting rate

relative to that obtained with the long-slit geometry.

A multicounter crossed-slit angular correlation apparatus, built by Berko and Mader (1975), has the advantage of rapid data accumulation which aims to compensate the losses due to the low counting rates.

In angular correlation studies ^{64}Cu , ^{22}Na and ^{58}Co are among the currently used positron sources. Strong sources, ranging from 10 millicurie up to 1 Curie , can be employed without actually worsening the true-to-accidental background ratio (West, 1974) . The present day best angular resolutions, reported in the literature with the retention of adequate counting rates, are about 0.2 milliradians .

1.3.4 Measurements of Doppler-broadening of Annihilation Radiation

The departure of the energies of the two annihilation quanta from the nominal value of 511 keV is a result of the Doppler shift, produced by the centre of mass velocity of the positron-electron system along the line of emission.

In principle, the Doppler-broadening of the annihilation gamma-ray lines can give the same information about the electronic properties of the substances, in which the annihilation takes place, as can be obtained by the angular correlation of the two quanta.

Figure 1.4 shows the basic system used in Doppler-broadening studies, consisting of lithium drifted germanium (Ge(Li)) gamma-ray detector in conjunction with a linear amplifier

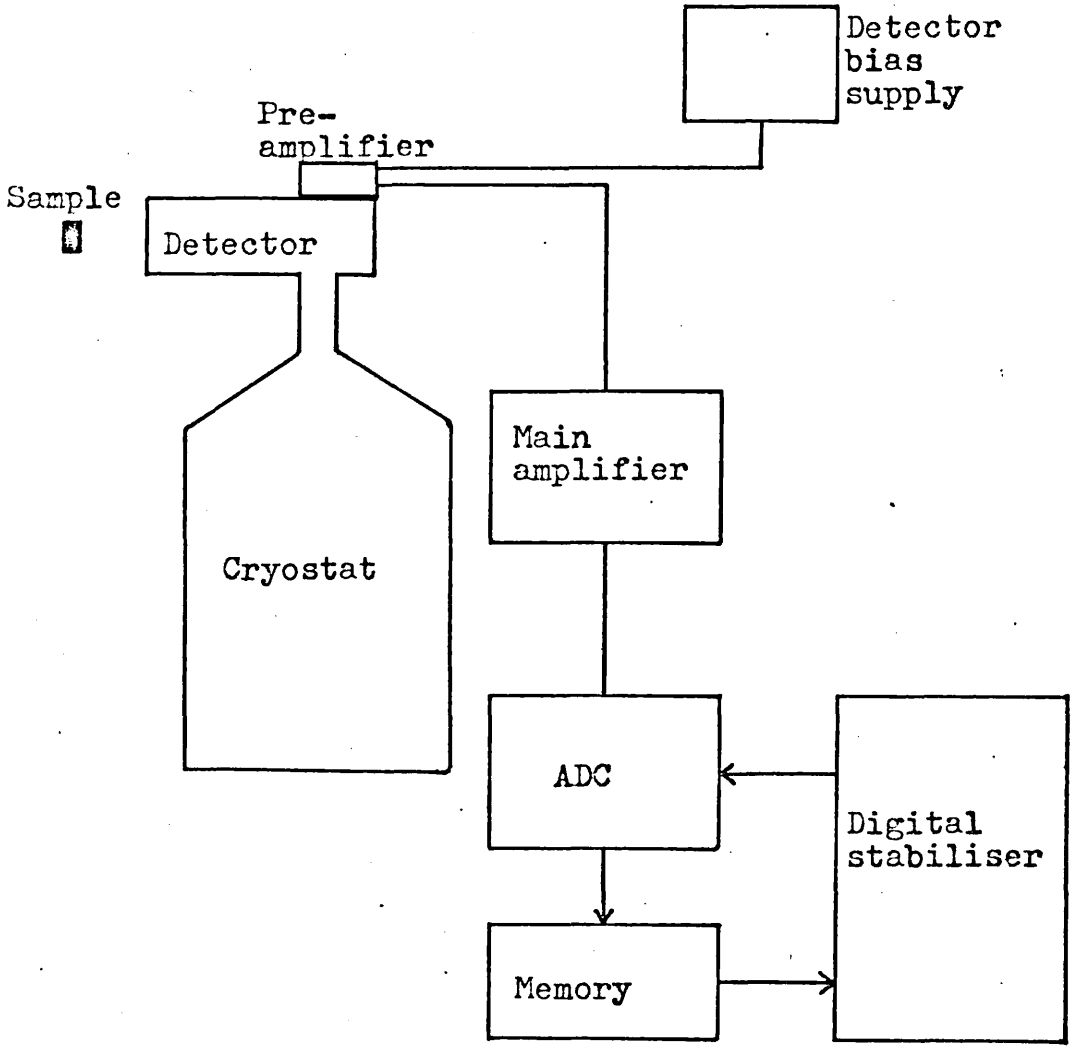

FIG. 1.4 Electronics for Doppler-broadening studies, consisting of a Ge(Li) detector and a pre-amplifier in conjunction with a linear amplifier and a data storage system. The data storage system is a combination of an analog-to-digital converter and a memory unit, complemented with a digital stabiliser.

and data storage system. The data storage system is a combination of an analog-to-digital converter (ADC) and a memory unit, complemented with a digital stabiliser. The cryostat, shown in the figure, is filled with liquid nitrogen and, therefore, maintaines the required cooling for the germanium crystal and field effect transistor (FET) of the preamplifier.

The Doppler-broadening method measures the distribution of the component of momentum along the line of emission. Therefore, it is equivalent to the long-slit angular correlation method. The measured component of momentum along the direction towards the detector, say P_x , is the only one affecting the energy of quanta, to first order (Hotz et al, 1968) . From the conservation of energy and momentum, along the direction of P_x , we have

$$2m_oc^2 = 2h\nu_o = h\nu_1 + h\nu_2 \qquad (1.11)$$

$$P_x = (h\nu_2 - h\nu_1)/c \qquad (1.12)$$

with the condition that $P_x^2/2m_o$ is much smaller than $2m_oc^2$. From equation (1.11)

$$h\nu_1 = 2h\nu_o - h\nu_2 \quad \text{or} \quad h\nu_2 = 2h\nu_o - h\nu_1 \qquad (1.13)$$

Substituting equation (1.13) into (1.12) we obtain

$$P_x = 2h(\nu_2 - \nu_o)/c = 2h(\nu_o - \nu_1)/c \qquad (1.14)$$

Thus, the distribution of the momentum component along the line of emission is identical to the energy distribution of

annihilation quanta. The energy shift is given by $(h\nu_2-h\nu_0)$ or $(h\nu_0-h\nu_1)$. To illustrate the magnitude of effects : a 6 eV Fermi electron can cause a photon shift of up to 1.3 keV . The intrinsic line resolution, at 514 keV, of the recently improved Doppler-broadening measuring systems is approximatelly 1.15 keV (Rice-Evans et al, 1978a), which is just enough to allow the changes in the ratio of annihilations with core and conduction electrons to be detected without appreciable loss of information.

Although this method does not offer the fine resolwing power given by angular correlation technique, its high efficiency practically compensates because it allows faster measurements with better statistics ; the method is therefore suitable for defect studies.

1.4 Electronic Structure Studies in Metals by Positron Annihilation

The early angular correlation experiments, by De Benedetti et al (1950) followed by Farrell (1956) and Stewart (1957), showed the relevance of the positron annihilation technique to the electronic structure studies in metals, particularly the shape of the Fermi surface. This provides direct information on the momentum distributions of valence electrons.

Most of the angular correlation measurements have been performed on polycrystalline samples where only the spherical average of the momentum distributions could be determined.

In addition, the positron annihilation technique is capable of measuring momentum anisotropies in oriented single crystals.

It is known from lifetime and angular correlation measurements that slow positrons reach their lowest energy level, called Bloch state ($\underline{k}=0$) , at the time of annihilation. Thermal excitation is irrelevant (Berko and Plaskett, 1958) .

The observed angular distribution can be classified into two components. Firstly the narrower, nearly parabolic, component with a fairly sharp cut-off at an angle θ given by $k_f h/(2\pi m_o c)$ (k_f is the wavevector corresponding to the Fermi surface) . This is due to the annihilations with the conduction electrons. The second component, which extends way beyond the Fermi cut-off, do not show any prominent break. This approximatelly Gaussian shape is attributed to the annihilations mainly with tightly bound core electrons.

1.4.1 The Positron Wavefunction

In the independent particle model (IPM) , in which the many-body interactions are neglected (West, 1974) , the positron is viewed as existing in a periodic potential. The problem is further simplified with the assumption that the positron annihilates from its ground state ($\underline{k}=0$) .

In the early approach (De Benedetti et al, 1950) the positron wavefunction was represented by a single plane wave, identical to that of the one-electron wavefunction,

$$\psi_+(\underline{r}) = \text{Constant} \qquad (1.15)$$

since $\underline{k}=0$. On the other hand, since positron is excluded from the core region by the Coulomb repulsion of the nucleus, this does not accurately represent the wavefunction in the core region.

Berko and Plaskett (1958) employed the Wigner-Seitz method, which approximates the cell by a sphere, to calculate the positron wavefunction in the core region for aluminium and copper, given by

$$\psi_+(\underline{r}) = R_+(\underline{r})/r \qquad (1.16)$$

where $R_+(\underline{r})$ satisfies the Schroedinger equation

$$\left(\frac{d^2}{dr^2} + E + 2V(r)\right) R_+(\underline{r}) = 0 \qquad (1.17)$$

where $V(r)$ was taken to be the potential of the positive ion, together with the uniform charge distribution potential due to the valence electrons.

1.4.2 Positron Annihilation with Conduction Electrons

One-electron calculations of the positron and electron wavefunctions in simple metals such as aluminium, where nearly all the annihilations take place with conduction electrons, agree well with those measured in angular correlation experiments. In addition, this theory provides a convenient basis for performing detailed calculations for specific many-electron systems. In such calculations, it is usually necessary to introduce many symplifying assumptions

in order to make progress (Herman and Skillman, 1963) . The annihilation rate is simply proportional to the expectation value of the electron density at the positron, averaged over all positron positions.

A free electron wavefunction is given by

$$\psi_{\underline{k}}(\underline{r}) = V^{-\frac{1}{2}} \exp(i\underline{k}.\underline{r}) \qquad (1.18)$$

where V is the volume of normalisation.

Now, the annihilation rate of a positron with wavefunction $\psi_+(\underline{x})$ with an electron with the one-electron wavefunction $\psi_j(\underline{x})$, with the emission of two quanta having momentum in the range $d^3\underline{k}$ at $\underline{k}$, following De Benedetti et al (1950), is given by West (1974) as

$$\Gamma_j(\underline{k})d^3\underline{k} = \frac{\pi r_o^2 c}{(2\pi)^3} \left| \int d^3\underline{x} \exp(-i\underline{k}.\underline{x}) \psi_j(\underline{x}) \psi_+(\underline{x}) \right|^2 d^3\underline{k} \qquad (1.19)$$

The total annihilation rate is obtained by summing over all occupied states and photon momenta

$$\Gamma = \sum_j \int \Gamma_j(\underline{k}) \, d^3k \qquad (1.20)$$

The conventional long-slit apparatus measures the rate of annihilation $N(P_z).dP_z$. But the actual measured distribution is, of course, an arbitrary counting rate. Since $\underline{P}=h\underline{k}/2\pi$, we have

$$N(P_z) \, dP_z \propto \int_{-\infty}^{+\infty} \int_{-\infty}^{+\infty} \Gamma(\underline{P}) \, dP_x \, dP_y \, dP_z \qquad (1.21)$$

For an isotropic distribution of momentum (Stewart, 1957)

$$N(P_z)\, dP_z \propto 2\pi \int_{P_z}^{\infty} \underline{P}\, \Gamma(\underline{P})\, d\underline{P}\, dP_z \qquad (1.22)$$

which provides a parabolic distribution given by

$$\begin{aligned} N(P_z)\, dP_z &= \text{Constant}\ (P_f^2 - P_z^2)\, dP_z \quad \text{when } P_z \leq P_f \\ N(P_z)\, dP_z &= 0 \quad \ldots\ldots\ldots\ldots\ldots \quad \text{when } P_z \geq P_f \end{aligned} \qquad (1.23)$$

In metals, like copper, the fraction of the positrons annihilating with the core electrons is higher, and the simple one-electron model is inadequate to describe them. Furthermore, as noted earlier, the one-electron model is incapable of providing correct litime predictions. To obtain reasonable agreement with experiment electron-positron and electron-electron forces, in other words many-body interactions, have to be considered. Attempts made by Carbotte (1967), to calculate the annihilation rates, taking into account only the positron-conduction electron interactions with uniformly spread ion cores, yielded momentum dependent annihilation rates.

1.4.3 High Momentum Components of Annihilation Radiation

De Benedetti et al (1950), who first observed the wide angular distribution (in gold), attributed it to the sharp cut-off of the positron wave function at the core of the gold ion. A significant, in fact in many metals (with more extended closed d-shells) dominant, broad component of the annihilation photon momentum distribution curve, which

extends way beyond the Fermi cut-off, is an obvious indication of participation of the core electrons in the annihilations. Perhaps some contributions to the broad component arise from the bloch states of the positron and the electron (Mader et al, 1976) .

Using the positron wave function, given in equation (1.16) , in the core region and the tight-binding approximation for the core electrons Berko and Plaskett (1958) calculated the core electron momentum distributions for aluminium and copper. Their result in aluminium agree with experiment. Newertheless, for copper the large angle part of the curve was not correctly reproduced. Attempts by Stroud and Ehrenreich (1968) to modify the positron wave function (due to computational difficulties) resulted without any significant success .

The assumption of a Gaussian form, based on experimental observations, to represent the core electron momentum distribution has been proved fairly valid (Arias-Limota and Varlashkin, 1970 ; West et al, 1967) .

1.5 Positron Annihilation in Defected Metals

1.5.1 Existence and Specification of Lattice Defects

Within the last decade we have witnessed the wide application of the positron annihilation technique to the studies of defects in metals (Seeger, 1973 ; Hautojarvi et al, 1970) .

In defected samples positrons encounter different environments than in the bulk, with a regular array of atoms. Therefore,

the resulting annihilation characteristics are different. Dekhtyar et al (1964) and Mac Kenzie et al (1964) were the first to notify the change in their angular correlation curves as a result of annihilation of positrons in such lattice irregularities, produced by iether cold working or temperature treatment.

The well known lattice defects can be broadly classified into a number of types :

Point defects · (zero-dimensional imperfections)
Line defects (one-dimensional imperfections)
Grain boundaries (two-dimensional imperfections)

(i) Point defects are those involving single lattice points, such as a displaced atom or ion from its equilibrium position. Vacancies, and their complementary defect interstitials, constitute such defects. An interstitial is an extra atom or ion inserted at a lattice site, where normally there is not an atom or ion. If the displaced atom moves to the crystal surface or somewhere within the crystal body the resulting vacancy is called a Schottky defect or Frenkel defect, respectively. The defect with the smaller energy of formation predominates. In metals and alkali halides the most common defects are Schottky defects (Hendersen, 1972) . Point defects can be produced by heat treatment or displacement of atoms from their sites by irradiation, such as gamma-rays, thermal or fast neutrons, electrons, and heavy charged particles.

(ii) Line defects, also called dislocations, occur in all crystals in various forms. An example is an edge dislocation,

consisting of an extra half plane of atoms inserted into the lattice (Hughes and Pooley, 1975) . The neighbouring lattice planes bend to accomodate this half plain of atoms and as a result introduce strain fields into the crystal. A screw dislocation is another version of line defects. In this case a shear distortion is introduced parallel to the dislocation line. Line defects are commonly produced in solids by plastic deformation and influence their mechanical properties.

(iii) Grains or crystallites are known as the individual crystals of polycrystalline solids. The size of grains in a polycrystalline solid can vary widely. Most generally, the grains do not meet together properly. The regions between them are known as grain boundaries, covering several elementary lattice distances. The internal strains in these regions critically depend on the grain size.

1.5.2 Equilibrium and Non-equilibrium Measurements

Defect studies play an important role in determining many of the properties of solids. Positron annihilation studies of defects can broadly be divided into two catagories ; equilibrium and non-equilibrium measurements.

The major advantage of the equilibrium measurements over non-equilibrium measurements is that point defect equilibrium concentration is determined by temperature and pressure whereas non-equilibrium defect concentration depends very much on the pre-history of the sample. In addition the equilibrium theory is much less complecated than that of the

non-equilibrium technique.

One important aspect in which the equilibrium measurements are inferior to non-equilibrium measurements is that they must be carried-out at high temperatures whereas in non-equilibrium measurements, as long as the temperature is not so high that the defects anneal out, the choice of the temperature of measurement is not restricted.

1.5.2.1 Entropies and Formation Energies of Vacancies at Equilibrium Concentrations

Existence of point defects in crystals at finite temperatures are in accordance with that governed by statistical thermodynamics. This is the case, even in the absence of other causes such as, for example radiation, which produces point defects. They may represent a statistical distribution of thermal energy amongst the atoms of the crystal, the energy being concentrated on to a group of atoms to form a defect (Thompson, 1969) .

Existence of defects gives us the concept of entropy since it results from the changes in the vibration spectrum of the crystal associated with the introduction of a vacancy. In other words it represents the disorder in the system. A disordered crystal has a higher potential energy than its perfect form because of the extra energy required to produce the defects. This potential energy difference represents the change, ΔU , in the internal energy U -which is the sum of the knetic and potential energies of the atoms of the system- and corresponds to the change, ΔS , in the entropy S . For

a system at constant volume, and temperature, T , the state of equilibrium is that for which the minimum Helmholtz free energy is given by $F = U - TS$.

In a system containing N atoms and n , say, Schottky defects, and following Hughes and Pooley (1975) one finds that in thermal equilibrium the atomic concentration of vacant sites is given by

$$C_{1v} = n/N = \exp(-G^f_{1v}/kT) \qquad \text{for } n \ll N \qquad (1.24)$$

where k denotes Boltzmann's constent and G^f_{1v} is known as the Gibbs free energy of formation (Thompson,1969), and is defined as

$$G^f_{1v} = E^f_{1v} - T\Delta S^f_{1v} \qquad (1.25)$$

where E_{1v} is the work done in creating a single vacancy in the crystal -the so-called mono-vacancy formation energy. Since, on average, the vibrational frequencies near a vacancy, compared with those of the perfect crystal, are lowered, the entropy of formation, ΔS^f_{1v} , is positive.

The experimental determination of the absolute value of the equilibrium concentration of vacant sites by various techniques (e.g. electrical resistivity measurements) faces two serious problems ; (i) difficulty in subtracting the background effects due to the defect-free crystal and (ii) determination of the contribution per vacancy to the measured quantity.

For an accurate determination of the equilibrium concentration

of point defects an alternative method is to compare dilatometric measurements with x-ray lattice parameter measurements which, in principle, is the only method capable of overcoming the background problems, emphasized above. On the other hand, sensitivity of this method is limited to defect concentrations greater than 10^{-4} .

The observed deviation between the relative change in the specimen length, $\Delta l/l_o$, and the relative change of x-ray lattice parameter, $\Delta a/a_o$, in cubic crystals is due to vacancies as well as interstitials is given by

$$3(\Delta l/l_o - \Delta a/a_o) = C_v - C_I$$

where C_v and C_I denote the atomic concentrations of vacant and interstitial sites, respectively.

In all the metals studied so far, including Al , Pb , Cu , Au , Ag C_I appears to be immeasurably small —i.e., much more smaller than C_v .

In spite of its high sensitivity, even in the presence of minute concentrations of defects ($\sim 10^{-6}$), the positron annihilation technique is not capable of giving the absolute defect concentrations without additional information.

1.5.2.2 Multivacancies

Equation (1.24) gives the concontration of mono-vacancies (implied by the subscript 1v). As the concentration of mono-vacancies increases to high levels, which normally can take place near the melting point of a specimen, vacancies

in neighbouring lattice sites might bind together to form multivacancies ; mainly divacancies. Multivacancies may take up different orientations in the crystal, depending on the coordination number (e.g., in a crystal with coordination number z=12 six different orientations are possible for divacancies) .

When two vacancies are put together to form a divacancy the lattice vibration frequencies will on average be lowered. Following Seeger (1973b) , the equilibrium concentration of divacancies is given by

$$C_{2v} = \frac{z}{2} \exp(\Delta S_{2v}/k).\exp(E^B_{2v}/kT) \; . \; C^2_{1v} \qquad (1.26)$$

where ΔS_{2v} is the association entropy and E^B_{2v} is the binding energy of a divacancy defined as

$$E^B_{2v} = 2E_{1v} - E_{2v} \qquad (1.27)$$

where E_{2v} is the divacancy formation energy.

In the presence of mono and divacancies the total vacancy concentration is given by

$$C_v = C_{1v} + 2C_{2v} \qquad (1.28)$$

1.5.3 The Trapping Model

The trapping model, proposed by Gol'danskii and Prokopev(1965), is based on the rate equations approach of Brandt (1967) which was applied to trapping in metals by Connors and West (1969) and Bergersen and Stott (1969) .

Thermalised positrons diffusing through a metal are assumed to be trapped by various types of traps (labelled j) from which they can annihilate with a decay rate λ_j. Let us assume that there are m different types of traps with atomic concentrations C_j and their trapping rates are given by

$$\sigma_j = \nu_j C_j \qquad (j=1,2,\ldots,m) \tag{1.29}$$

where ν_j are the specific trapping rates. The number and lifetime of trapped or untrapped (free) positrons are given by n_j and $\tau_j=\lambda_j^{-1}$, or n_f and $\tau_f=\lambda_f^{-1}$, respectively.

The rate equations, disregarding detrapping, are given by

$$\begin{aligned} \frac{dn_f(t)}{dt} &= -(\lambda_f + \sum_{j=1}^{m} \nu_j C_j)\, n_f(t) \\ \frac{dn_j(t)}{dt} &= -\lambda_j n_j(t) + \nu_j C_j n_f(t) \qquad (j=1,2,\ldots,m) \end{aligned} \tag{1.30}$$

The general solution of this set of m+1 ordinary linear first order differential equations reads

$$n_f(t) = n_f(o)\, \exp(-t/\tau_o) \quad ; \tau_o^{-1}=\lambda_f+\sum_{j=1}^{m}\nu_j C_j \tag{1.31}$$

$$\begin{aligned} n_j(t) = {} & \tau_o \tau_j \frac{\nu_j C_j}{\tau_o-\tau_j}\, n_f(o)\, \exp(-t/\tau_o) + \\ & \left(n_j(o) - \frac{\nu_j C_j}{\tau_o-\tau_j}\, \tau_o \tau_j\, n_f(o)\right) \exp(-t/\tau_j) \end{aligned} \tag{1.32}$$

$$(j=1,2,\ldots,m)$$

In the analysis of positron lifetimes one should, therefore, find m+1 components, with the assumption that the states

(labelled j) are distinct.

The mean lifetime is defined by

$$\bar{\tau} = \frac{1}{n(o)} \int_o^\infty n(t)\, dt = \frac{1}{n(o)} \int_o^\infty (n_f(t) + \sum_{j=1}^{m} n_j(t))\, dt \qquad (1.33)$$

with the condition that there is not any initial trapping —i.e., $n_j(o) = 0$ for $j=1,2,\ldots,m$.

The mean lifetime is then given by

$$\bar{\tau} = \tau_f \frac{1 + \sum_{j=1}^{m} \tau_j \nu_j c_j}{1 + \tau_f \sum_{j=1}^{m} \nu_j c_j} \qquad (1.34)$$

The important assumption made in the solution of the rate equations, which disregards the detrapping of positrons, is not unjustified since the binding energy of positrons in metal vacancies is so large —of the order of a few electron volts (Tam and Siegel, 1977). This effectively prevents their escape.

An important quantity in the positron experiments is the fraction of positrons which annihilate from any state. For trapping by vacancies the probabilities for annihilation in the free state, P_f , and in a vacancy, P_v , are, respectively

$$P_f = \int_o^\infty \lambda_f \exp(-(\lambda_f + \nu c_v)\, t)\, dt = \lambda_f/(\lambda_f + \nu c_v) \qquad (1.35)$$

and

$$P_v = 1 - P_f = \nu c_v/(\lambda_f + \nu c_v) \qquad (1.36)$$

Application of the trapping model to positron annihilation measurements is usually performed in the following way (Mc Kee et al, 1972a) : Let F denote a feature of the positron annihilation process, which, for example, can be a characteristic of the lifetime or momentum distribution. Positron annihilation data will have the value of the weighted mean of this characteristic in the two different states, i.e.,

$$F = F_f P_f + F_v P_v \qquad (1.37)$$

where F_f and F_v are the values of F when all the positrons annihilate in free states or in traps, respectively.

Substituting equations (1.35) and (1.36) into (1.37), and using the atomic concentration of vacancies given in equation (1.24) the following expression can be obtained.

$$(F - F_f)/(F_v - F) = (\nu/\lambda_f).\exp(\Delta S_v/k).\exp(-E_v/kT) \qquad (1.38)$$

where ΔS_v and E_v are the vacancy formation entropy and energy, respectively.

As has been mentioned earlier, positron annihilation in metals may be studied in the following ways, viz

(i) Lifetime measurements
(ii) Angular correlation of two-photon annihilation radiation
(iii) Dopplr-broadening of annihilation gamma-ray lines .

Let us consider these three techniques :

(i) The two principal methods for analysing the lifetime data are :

(a) A sum of exponential decay functions convoluted with the instrumental time resolution and fitted to the data.

(b) The centroid shift method which measures the time difference between the prompt resolution function and the positron decay function with a single lifetime component.

(ii) The available parameters in angular correlation studies are :

(a) The normalised counts at zero angle or any fixed angle.

(b) The normalised counts in the area within fixed limits under the angular correlation curve.

(iii) In Doppler-broadening studies the most commonly used parameter is analogous to the second method employed in angular correlation studies. A less commonly used parameter (Mac Kenzie, 1969) is the FWHM of the annihilation gamma-ray line. On the other hand, unlike the former, the FWHM is not linearly related to the trapping probability.

1.5.3.1 The Trapping Rate

In order to be able to obtain sensible values of the defect parameters (e.g., vacancy formation energies) from experiments a thorough knowledge of the nature of the trapping rate and, in particular, its temperature dependence, is required.

Thermalised positrons diffuse through the crystal until they annihilate or become trapped. Under these conditions their motion can be characterised by a positron diffusion constant D_+ (Brandt, 1974) . Following Waite (1957), the trapping

rate is related to the capture radius, r_o , of the trapping centre according to

$$\nu = 4\pi r_o D_+ / V_a \qquad (1.39)$$

where V_a denotes the atomic volume.

Equation (1.39) does not take the energy difference between the lowest trapping state and the untrapped positron ground state into account. In other words, any positron that has reached a trap during its diffusive motion falls in it. Frank and Seeger (1974) considered both diffusive motion of the positron and the overcoming of a barrier prior to trapping, and wrote

$$\nu = \frac{4\pi r_o}{V_a} \left(\frac{1}{D_+} + \frac{1}{k_o r_o \, \Delta r_o} \right)^{-1} \qquad (1.40)$$

where Δr_o denotes the width of the potential barrier and k_o is the rate-constant for the capture by the trap.

The temperature dependence of the trapping rate is determined by the following processes ; diffusion, which is characterised by D_+ , or captire, characterised by $k_o r_o \, \Delta r_o$.

Much work has been done on the complicated question of diffusion. Brandt (1974) has combined the effect of positron scattering on electrons, phonons, and crystal imperfections to give, respectively, within the diffusion coefficient

$$D_+ = \frac{\hbar}{\pi m_+} \left[2.5 \times 10^{-5} r_s^2 \left(\frac{T_+}{300\ K} \right) + 5 \times 10^{-2} \left(\frac{T_+}{300\ K} \right)^{\frac{1}{2}} + B C_s \left(\frac{300\ K}{T_+} \right)^b \right]^{-1} \qquad (1.41)$$

where T_+ is the effective positron temperature and

C_s is the concentration of the scattering centres. The constants B and b depend on the properties of crystal imperfections, with $\frac{1}{2} \leqslant b \leqslant \frac{3}{2}$. In a deformed sample, there will be a multitude of imperfections. Brandt (1974) suggests that the first two terms are usually small compared to the third, although, in the expression, this actually depends on the values assumed for B , b and C_s .

Hodges (1970) treated the trap as a potential well and found that the resultant trapping rate was independent of temperature. Bergersen and Taylor (1974) support this view.

The temperature dependence of the trapping rate, including its experimental evidence, will be discussed at length later in chapter 6 .

1.5.3.2 Surface Effects

Surface states and surface energy levels depend on the fact that the atoms involved are bound to the bulk and are not yet completely coordinated.

Since the screening effect of the valence electrons prevents the formation of P_s in metals, only one positron lifetime, determined mainly by the conduction electron density, should be observed. A second component, with an intensity of the order of 1% of all annihilations and a lifetime some two times longer than that of annihilation in the bulk, is measured. This is attributed to positrons annihilating at the surface (Brandt, 1975) .

Positrons in solids diffuse over mean distances 10^2 to 10^3 Å

until they annihilate. Therefore, a small fraction (0.01 - 1% estimated by Brandt (1974)) of all positrons can reach the entrance surface where they encounter a lower electron density and momenta than in the bulk, which results in the low intensity component. When the positron source is imbedded in the bulk no such component is observed.

1.5.4 Anomalous Temperature Dependence of the Annihilation Parameters

The noticeable temperature dependence of the positron annihilation rate at low temperatures, where no vacancy effect should be observable, has been a subject of considerable discussion. This has been the case ever since the importance (Connors et al, 1970) of its accurate subtraction from the main effect, due to annihilation of positrons in vacancies, has been realised in order to obtain accurate values of vacancy formation energies.

To account for the observed temperature dependence in the sub-vacancy region two models have been proposed, and are discussed below.

1.5.4.1 Effect of Thermal Lattice Expansion on Annihilation Characteristics

The observed rise in the annihilation rate, in the region below the vacancy threshold, has been interpreted by Mc Gervey and Triftshauser (1973) as a result of thermal expansion of the lattice. This affects the observed annihilation characteristics in two ways :

(i) by causing a contraction of the Fermi surface

(ii) by decreasing the rate of annihilation with core electrons.

Of these two, the socond is the larger effect.

To support this view, Jamieson et al (1974) suggested that, since the core electron distribution is not a function of the lattice spacing, thermal expansion simply increases the seperation between neighbouring core distributions. Thus, positron-core electron wave function overlapping is reduced.

To justify the observed linear rise in the annihilation rate in the sub-vacancy region, F_f in equation (1.37) is replaced by a temperature dependent variable $F_f = F_f^o(1 + \beta T)$, where β is compared with the coefficient of thermal volume expansion.

1.5.4.2 Self-trapping of Positrons in Metals

The thermal lattice expansion explanation of the sub-vacancy effect has been injured by Lichtenberger et al (1975), who reported a new effect in cadmium. They measured the equilibrium line-shape parameter from 77 K upwards and found non-linear behaviour which, they argued, was due to phonon-assisted trapping of positrons.

Seeger (1975) has given an alternative explanation for the new effect, found by Lichtenberger et al (1975). He shows that the anomalous temperature dependence in positron annihilation properties is a result of the existence of

metastable states with respect to free positron states, in which positrons are self-trapped .

Following Sumi and Toyozawa (1973), Seeger (1975) describes the interaction between the positron wave function and the crystal through a coupling of the elastic dilation, $\theta(r)$, with the positron charge density $|\psi_+(r)|^2$. We have

$$\theta(r) = -\frac{\varepsilon_d}{C_e}|\psi_+(r)|^2 \qquad (1.42)$$

where C_e is a combination of elastic constants and ε_d denotes the positron deformation potential (Seeger, 1972) . He wrote the energy functional as

$$\varepsilon(\psi_+(r))=\frac{\hbar^2}{2m_+}\int(\nabla\psi_+(r))^2 d^3r - \frac{\varepsilon_d^2}{2C_e}\int(\psi_+(r))^4 d^3r \qquad (1.43)$$

Here $\hbar$ denotes Plank's constant divided by 2π, and m_+ is the positron band mass.

Seeger (1975) used the trial function with an adjustable parameter K , which is an adjustable parameter and having the dimension of a wave number, giving

$$\psi_+(r) = (2K^2)^{3/4}\exp(-\pi K^2 r^2) \qquad (1.44)$$

and obtained the energy of the system as a function of K . This is given by

$$E(K) = \frac{3\pi\hbar^2}{2m_+}K^2 - \frac{\varepsilon_d^2}{2C_e}K^3 \qquad (1.45)$$

Equation (1.45) has a minimum at K=0 , representing a free positron state. A second minimum may arise due to the upper

cut-off K_o of K, approximatelly equal to the reciprocal atomic distance. The existence of such a minimum, with energy

$$E(K_o) = \frac{3\pi\hbar^2}{2m_+} K_o^2 - \frac{\varepsilon_d^2}{2C_e} K_o^3 \qquad (1.46)$$

depends on whether the maximum of equation (1.45) occurs at a value

$$K_{max} = \frac{2\pi\hbar^2}{\varepsilon_d^2 m_+} C_e \qquad (1.47)$$

that is smaller than K_o.

This second minimum at, K_o, corresponds to a localised positron which gives rise to the measured annihilation characteristic.

Now, two different situations may arise ;

(i) $E(K_o)$ is positive ; the self-trapped state is metastable with respect to low-lying free positron states

(ii) $E(K_o)$ is negative ; the self-trapped state is stable, but the free positron states are metastable.

According to Seeger (1975) the second case is less likely than the first. Here, at very low temperatures, all the positrons are in Bloch states and as the temperature is increased a fraction of them will be self-trapped.

For the case $E(K_o)$ is positive, Seeger (1975) concluded that the probabilities P_{st} and P_f of annihilation in self-trapped or free states, respectively, was given by

$$P_{st}(T) = \left[1 + B^{-1} T^{3/2} \exp(E(K_o)/kT)\right]^{-1} \qquad (1.48)$$

and

$$P_f(T) = \left[1 + B\, T^{-3/2} \exp(-E(K_o)/kT) \right]^{-1} \qquad (1.49)$$

where

$$B \equiv \prod_j (\nu_j/\nu'_j).\left(\frac{2\pi\hbar^2}{m_+ k}\right)^{3/2}. V_a^{-1} \qquad (1.50)$$

and V_a is the atomic volume, ν_j and ν'_j are the vibrational frequencies of the crystal with free or self-trapped positron. The product $\prod_j$ extends over all vibrational modes of the crystal.

In the temperature range below the vacancy threshold the weighted average of the characteristic annihilation parameter F is given by

$$F(T) = F_f P_f + F_{st} P_{st} \qquad (1.51)$$

Seeger's proposal, that positrons are self-trapped in metals, has been argued upon by Hodges and Trinkaus (1976) and Leung et al (1976) . The former group have employed a lattice theory which avoids the necessity to introduce a wave number cut-off, or upper bound to the degree of localisation. They have concluded that the deformation potential in Seeger's calculations is too large to be realistic in metals, and for most metals positron self-trapping seems to be unlikely. They also added that the time required for the self-trapping of a positron is far longer than the positron lifetime.

1.5.5 Annihilation Characteristics Near Melting Point

An important question is whether or not the annihilation characteristic, say F-parameter, flattens to equal a

saturation value F_v at high temperatures. Published data, even on the same metal, conflict. Mac Kenzie (1972), and Triftshauser and Mc Gervey (1975) observed a plateau in copper where Nanao et al (1973) and Sueoka(1974a) did not. Applying the technique of Nanao et al (1973), which allows for the saturation value itself to be either a constant or a linear function of temperature, Rice-Evans et al (1976a) concluded that a temperature independent value of F_v gives a closer fit to their data for copper.

Nanao et al (1973) and Sueoka (1974a) have also suggested that the variation of the parameter F at high temperatures, approaching the melting point, might be due to the creation of multivacancies, mainly divacancies. Furthermore, for high melting metals, Dlubek et al (1977a) and (1977b) have suggested that thermal detrapping of positrons from monovacancies becomes important, leading to an enhancement of the positron trapping by divacancies. On the other hand, values of positron-vacancy binding energies in metals, calculated by Tam and Siegel (1977), range up to several electron volts. Therefore, it does not seem likely that thermal positrons can overcome this barrier.

CHAPTER 2 INSTRUMENTAL DETAILS AND LINE SHAPE ANALYSIS

2.1 Description of the Spectroscopy System

The schematic illustration of the Doppler-broadening system, employed throughout the experiments, is shown in figure 2.1 .

The intrinsic germanium planar detector with an active volume of 2 cm^3 (16 mm diameter and 10 mm thickness), supplied by Princeton Gamma-Tech Ltd (PGT) , incorporated with an optical feed-back pre-amplifier. The pre-amplifier output pulses were amplified by a Tennelec main amplifier (TC-205). Unipolar output pulses from the main amplifier are then fed directly to a Laben 8215 analog-to-digital convertor (ADC) with a fast conversion time, 4.5 μseconds plus pule rise time. Each pulse was digitised linearly according to its amplitude and subsequently stored in a Nova-2 computer with 8K memory, supplied by Link System.

2.2 Calibration and Energy Resolution of the Spectrometer

The main amplifier output pulses, corresponding to the full energy 511 keV pulses, were about 6 volts amplitude with less than 100 nseconds rise-time and 45 μseconds exponential decay-time. By off-setting the first quarter of the 4096 channels analyser memory we were able to obtain a gamma-ray energy distribution of about 94 eV per channel. An accurate description of a gamma-ray line shape depends on the number of channels across the line. Therefore, the above choice of energy distribution was a good compromise between an accurate line shape description and a good statistical

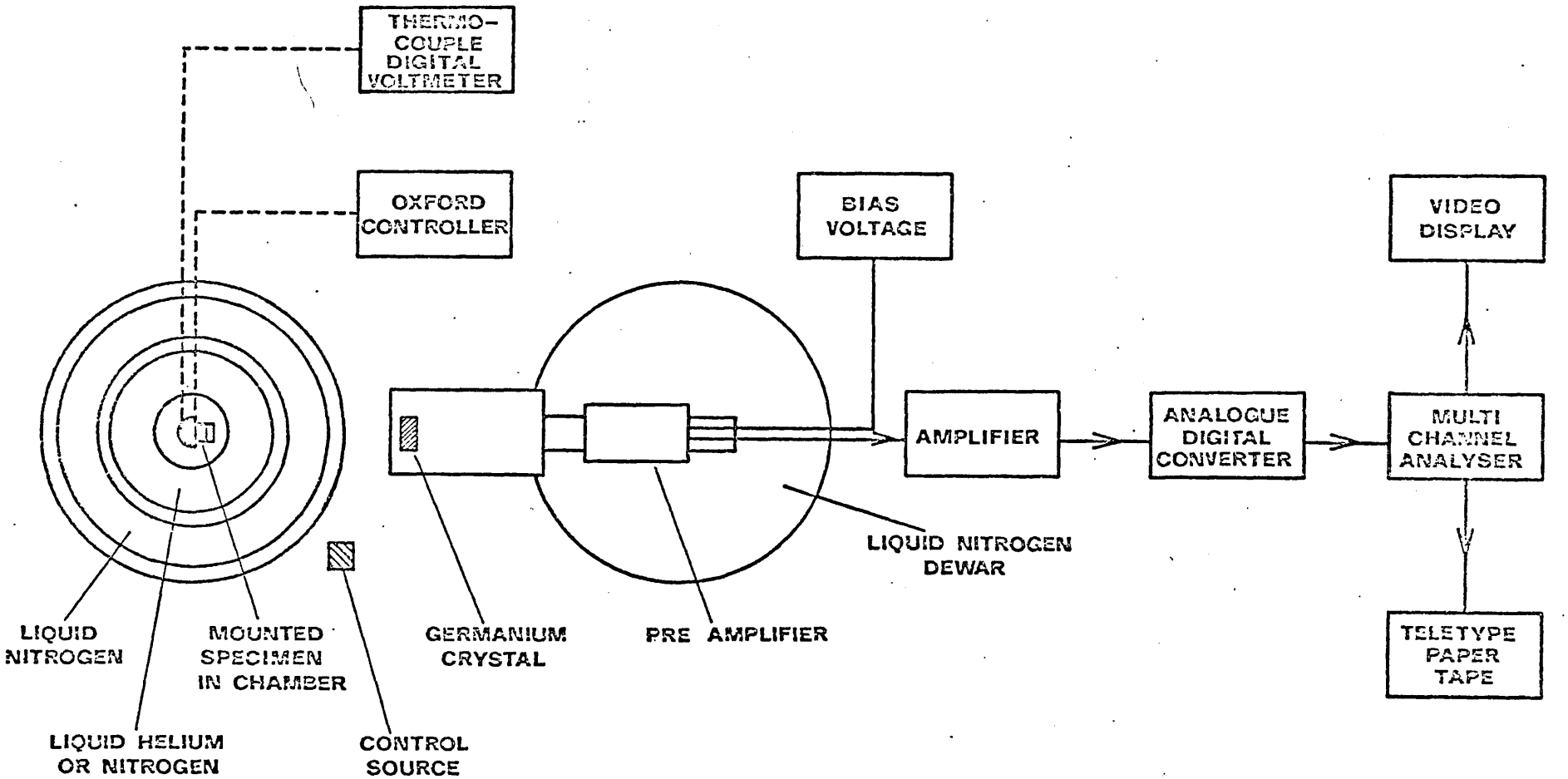

FIG. 2.1 The schematic illustration of the Doppler-broadening system, employed throughout the work.

RADIOACTIVE
DO NOT TOUCH

accuracy. In most of the experiments, each run of two hours accumulated, on average, about 900 000 counts in the 511 keV peak.

Even high resolution Ge(Li) detectors give rather poor energy resolution of Doppler-broadened annihilation lines. Therefore, despite its simplicity, rapid data accumulation and suitability to various experimental arrangements, the Doppler broadening technique is still inferior to the angular correlation method as far as the resolving power is concerned. This resolving power is needed in certain applications, for instance, Fermi surface studies. The contributions to the observed intrinsic resolution of a Doppler-broadening spectroscopy system come from the Ge(Li) detector itself as well as the incorporated electronics.

In semiconductor detectors the incident particle, say photon, produces electron-hole pairs in the solid. Detection of the incident particle is then a problem of collecting the liberated charge by application of an electric field. As far as the efficiency is concerned the crystal purity and perfection is very important, because of the trapping effects.

The major contribution to the observed, finite resolution of a semiconductor detector arises due to the statistical uncertainity involved in the conversion of the incident particle energy into electron-hole pairs. The incomplete charge collection is an additional contribution.

The inevitable noise associated with the chain of electronics, possesing resistances and capacitances through which the signals pass, is an inherent source of the overall resolution.

Ideally, a pre-amplifier output pulse, often called tail pulse, has a very short rise-time (less than 100 nseconds) and an exponential decay-time of about 50 μseconds. Therefore, the typical values of the time constants of the pulse shaping circuitry, in the main amplifier, are choosen to be much shorter than the exponential decay time of the tail pulse, and much longer than their rise-time. This, within certain count-rate limits, effectively prevents the pulse overlapping which causes a consequent error in amplitude interpretation . After careful analysis (to be discussed later) on the gamma-ray line shapes the best value for the time constant of the pulse shaping circuitry, incorporated with the pre-amplifier, was choosen to be 6 μseconds .

Perhaps the counting rate plays a crucial part in the electronics induced resolution. The variation of the resolution, specified as the full width at half maximum (FWHM) , of 514 keV gamma-ray line of ^{85}Sr as a function of total count rate is shown in figure 2.2 . The best compromise between the total count rate and the resolution enabled us to operate the spectrometer at a total count rate of 5000 cps with a resolving power of 1.15 keV (except for 5N indium) . The previous studies (Hlaing, 1976) showed that, by gain shift of the 514 keV gamma-ray line to the

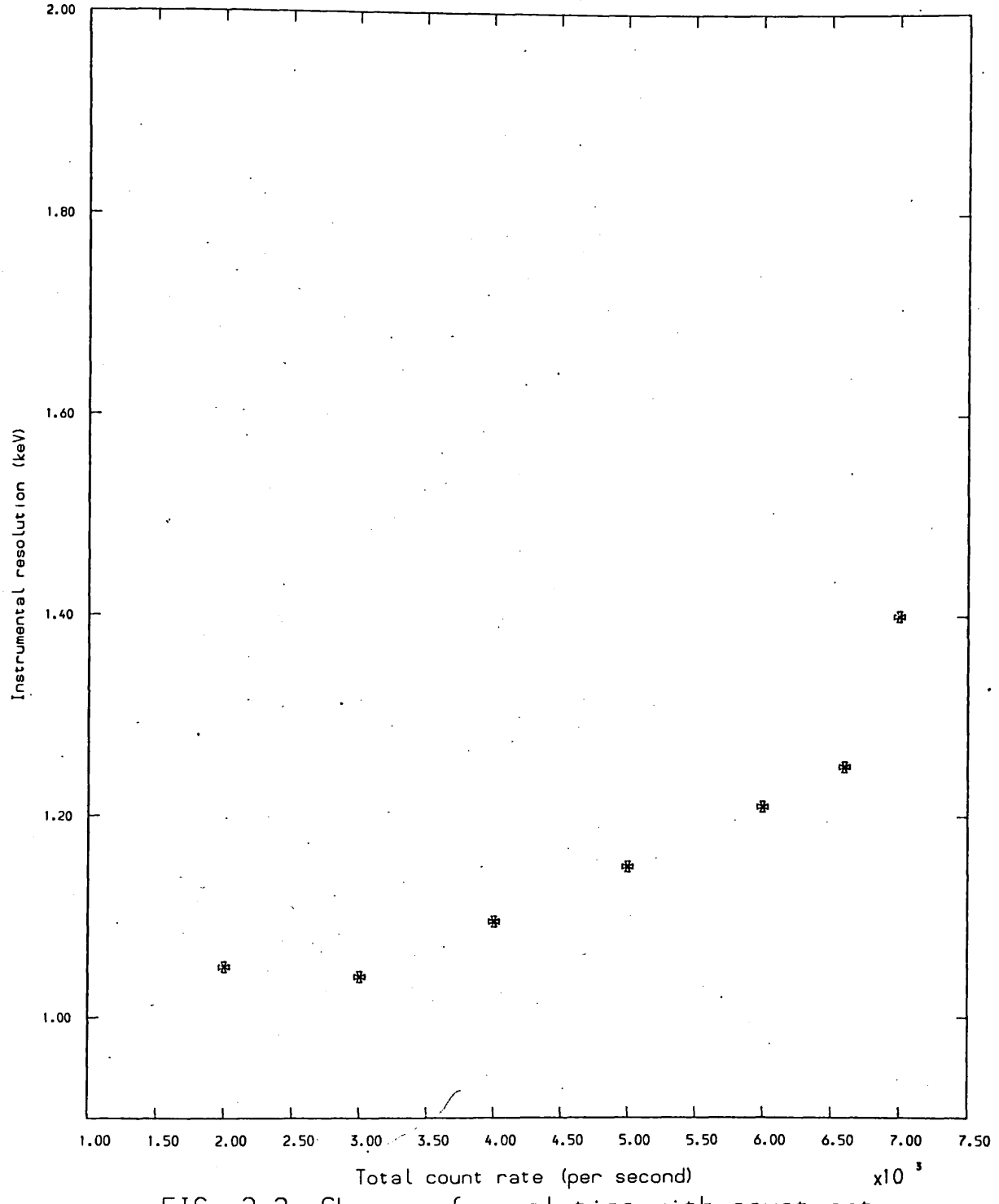

FIG. 2.2 Change of resolution with count rate

position where the annihilation line would normally appear, no noticeable error was introduced into the response function of the spectrometer at 511 keV . Figure 2.3 illustrates the 514 keV gamma-ray line shifted to the position of the Doppler-broadened annihilation line, for annealed lead.

The peak position stability is also very important. Even small zero or gain shifts mean extra broadening of the line shape. Employing a digital spectrum stabiliser would, without a doubt, greatly eliminate the extra blurring of the spectrum.

2.3 Low Temperature Cryostat

Measurements at low temperatures have proved to be very informative in many studies where the positron annihilation technique is one of them. In order to study the positron annihilation line shape parameter below room temperature a cryostat, which enabled us to perform measurements at temperatures down to 4.2 K , was designed and constructed.

A schematic drawing of the low temperature cryostat is shown in figure 2.4 . During the measurements it was immersed into liquid nitrogen or liquid helium in a pyrex dewar, shown in figure 2.5 , which was located at the front of the detector. The sample holder, shown in figure 2.4 , was made of 4N pure copper.

2.3.1 Vacuum Condition

The vacuum chamber, positioned in the inner dewar, was

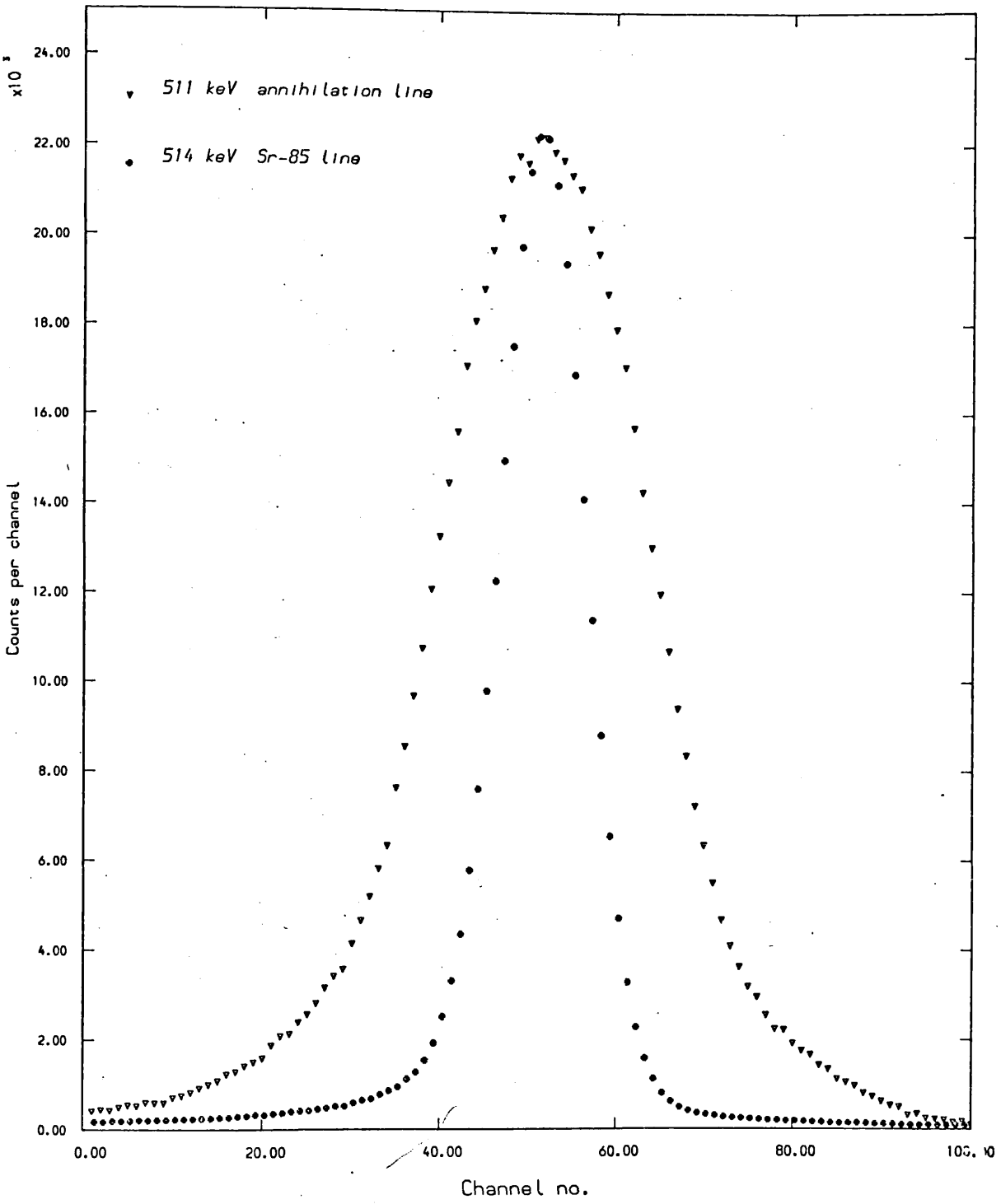

FIG. 2.3 Annihilation line in annealed lead compared to 514 keV gamma-ray line in ^{85}Sr .

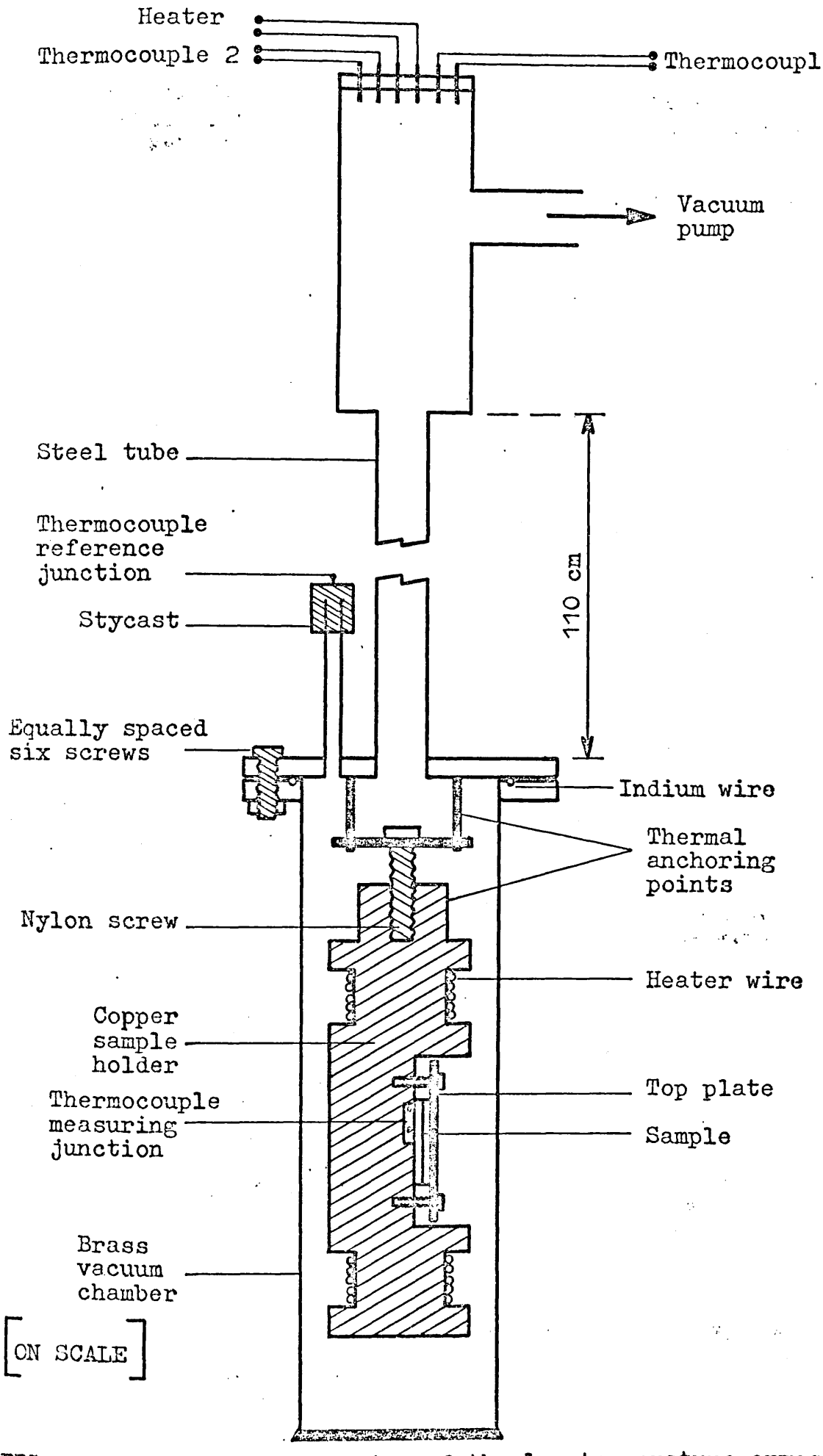

FIG. 2.4 A schematic drawing of the low temperature cryostat.

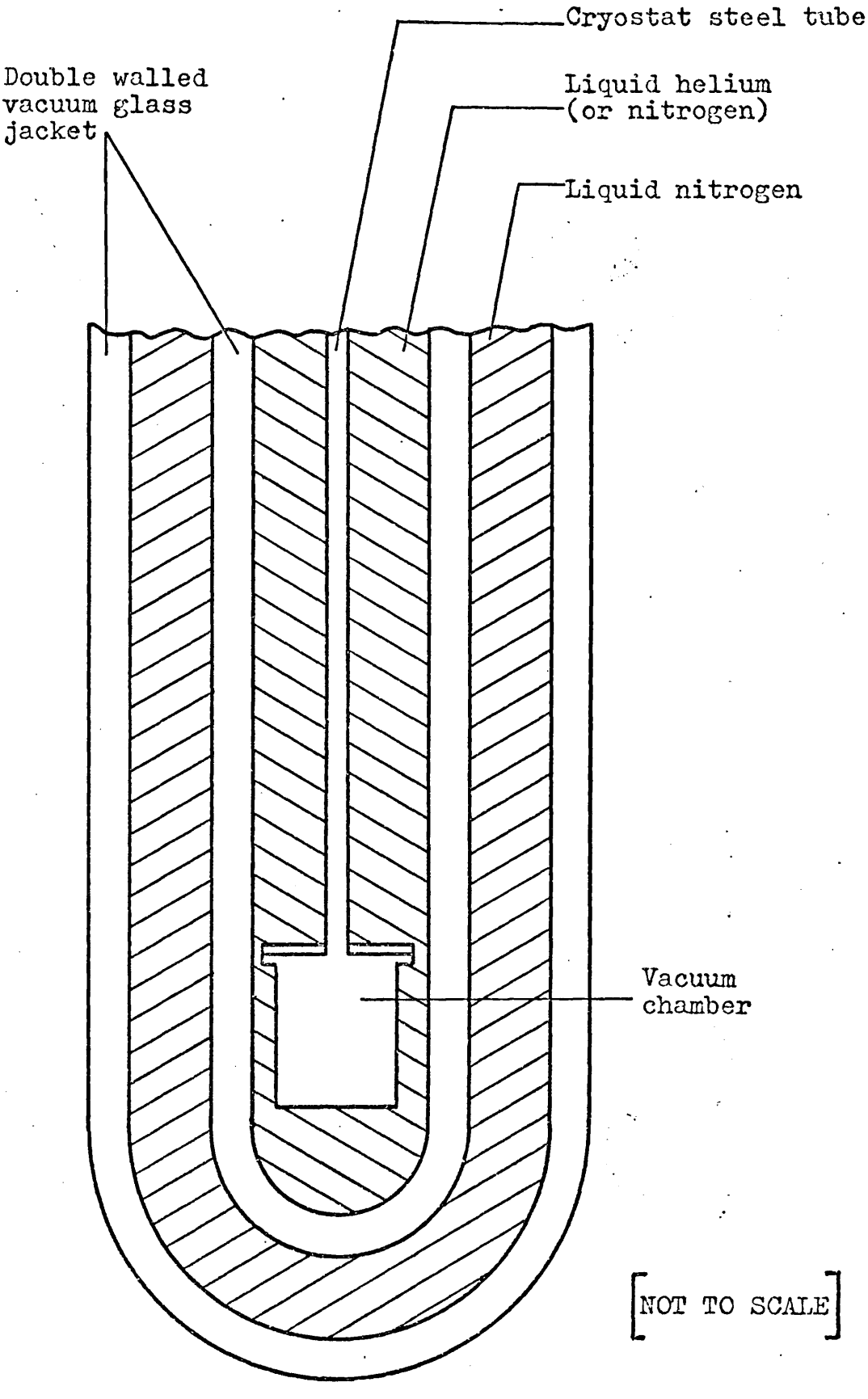

FIG. 2.5 Cross-section of the pyrex liquid nitrogen or liquid helium dewar.

evacuated at romm temperature by an Edwards high power diffusion pump to a pressure lower than 10^{-5} torr and then cooled down. All the joints on the brass vacuum chamber, as well as the steel tube, were hard soldered. 1 mm diameter indium wire which was embedded in a 0.5 mm deep groove made a good vacuum tight seal to the chamber, shown here in figure 2.4 , even at the lowest temperatures.

2.3.2 Cooling Down

During the measurements at 77 K and above, cooling was maintained by liquid nitrogen. For the measurements below 77 K the inner dewar was filled with liquid helium. Unlike liquid nitrogen, liquid helium is difficult to handle. It requires considerable care and knowledge in cryogenics. Pre-cooling the inner dewar, as well as the sample, with liquid nitrogen before liquid helium is transfered is essential. A small amount of innert helium gas was used to speed-up the cooling from 293 K and maintain the sample temperature at 77 K when in liquid nitrogen and at 4.2 K when in liquid helium, prior to the measurements.

Heat leak through the thermocouple and heater wires is a problem. A good temperature stability at the lowest temperatures requires the elimination of this heat injection to the sample, and was best done by thermal anchoring of the wires before they reached the sample holder.

2.3.3 Temperature Control and Measurements

Measurements at temperatures above 4.2 K and 77 K were maintained by the use of a 70 ohm Enamel-Constantan heater wire, which was wound on the sample holder inside the grooves on either side of the sample.

The desired temperatures were maintained automatically by an Oxford Instruments Temperature Controller (DTC-2) with the aid of the thermocouples attached to the sample.

Two different thermocouples were employed. In the region between 4.2 K and 300 K a spec. pure Au + 0.03 at.% Fe versus chromel thermocouple was used. Temperatures between 273 K and 420 K (highest temperature in the cryostat) were measured by a chromel-alumel thermocouple. Throughout the whole range the temperature stability was better than 0.5 K.

2.4 High Temperature Furnace

In order to study positron annihilation in metal samples from room temperature to near their melting point, a tubular high temperature furnace was designed and constructed.

A schematic drawing of the furnace, made of a 60 cm long thermal aluminous porcelain tube with nominal bore 22.5 mm , is shown in figure 2.6 . A heavy piece stainless steel sample holder, attached to the end of a 3 mm dimeter alumina twin bore, was used to maintain a fairly homogeneous temperature distribution on the sample. Using an aluminous porcelain tube has various advantages. First of all it is a good electrical insulator which fits the design, and it can safely go up to 1900 ^{o}C . Another important reason for

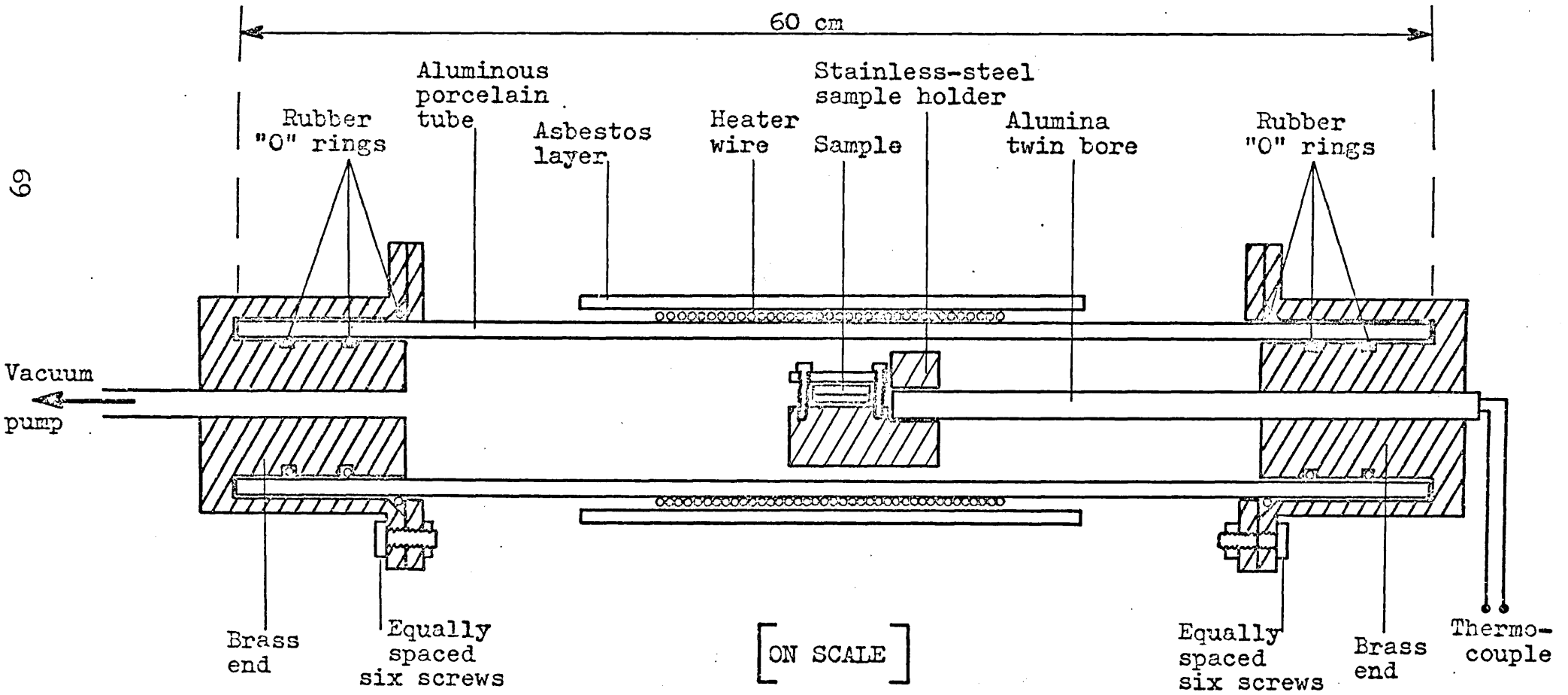

FIG. 2.6 A schematic drawing of the high temperature furnace .

using this material is that it does not outgas appreciably which may contaminate the sample at high temperatures.

The 1 mm thick aluminium enclosure, which covered the heated zone, provides a good thermal insulation to protect the detector at high temperatures and cause a very small scattering of the gamma-rays.

2.4.1 Vacuum Condition

Most metal specimens oxidise absorbing small amounts of oxygen. At high temperatures, due to the increased diffusion rates, the oxcitation process is speeded-up. Therefore, it is essential to heat metal samples under very high vacuum conditions.

As shown on figure 2.6 , one end of the aluminous porcelain tube was connected to the high power vacuum pump, through a brass piece, and the other end of the tube was used for the thermocouple wires, these being passed through the alumina twin bore where one end was open to the atmosphere and sealed with araldite. The brass pices at the each end of the tube were specially made with high precision. The three rubber "o" rings at each end enabled us to support the brass pieces to the tube firmly and to provide a high vacuum inside the tube, better than 10^{-6}torr .

2.4.2 Heating, Temperature Control and Measurements

A high power 40 ohm nichrom heater wire was wound directly on the aluminous porcelain tube, covering, centrally, 20 cm length provided a heat zone at the position of the sample

with a very small heat gradient. Electric power to the heater was supplied and automatic sample temperature control was maintained by the temperature controller DTC-2 , supported by an Oxford Instruments External High Power unit.

Due to the high vacuum inside the tube, the temperature stability was better than 0.25 K . Throughout the whole range of these temperature measurements a chromel-alumel thermocouple was attached to the sample.

Towards the end of the work, an electronic automatic temperature resetting system was designed and constructed in the college electronics workshop. This enabled us to continue the two-hour runs 24 hours a day, when in the furnace.

2.5 Positron Sources

The available positron sources in positron annihilation Doppler-broadening studies have been listed in chapter 1 . Apart from the work on annealed zinc where a ^{64}Cu positron emitter was used, the rest of the positron annihilation studies were carried-out with ^{22}Na positron sources.

The ^{64}Cu positron sources were produced by neutron irradiation of two micron thick 5N pure copper foils, supplied by Johnson-Matthey, in the University of London Reactor Centre. Seven hours irradiation at the core of the reactor, at a flux of about 1.2×10^{12} neutrons. cm^{-2}. sec^{-1} , produces a specific activity approximatelly 270 mCi/gr . Despite its relatively short half-life (12.8 hours) ^{64}Cu is a commonly used positron emitter due to its relatively small

intensity of the 1.340 MeV gamma-ray, which gives rise to a very small background.

Although the thickness of the copper foils was considerably smaller than the calculated, effective range of positrons in copper, Hlaing (1976) estimated the fraction of positrons absorbed in a 2 μm thick copper foil to be about 3% . Therefore, prior to the measurements the irradiated copper foils were annealed for several hours at 600 °C in order to anneale-out the radiation induced defects. This is necessary because some annihilations take place in the foil and, since, the picture of the annihilations in the foil is bound to change at high temperatures, due to annealing of radiation induced defectc, this would —although at a small scale— mask the, small, but genuine, effects in the sub-vacancy region.

The ^{22}Na positron sources were supplied by the Radiochemicals Centre as aqueous solutions of carrier-free sodium chloride. The active samples were prepared by evaporating the $^{22}NaCl$ source directly onto the sample surface so that the nearest distance between the edge of the sample and the evaporated source area, even on the smallest samples were prepared, was not less than 3 mm .

The second round measurements on zinc, over the temperature range from 4.2 to 420 K , using ^{22}Na sources showed no appreciable difference from those using ^{64}Cu . Zinc is known as one of the most interactive metals with weak acids, therefore, any possible contamination on the sample surface,

due to the direct evaporation of the source material, must be irrelevant.

The conventional, maximum range of positrons in matter is given by Segre' (1953) as

$$R(gr/cm^3) = 0.407\ E_{max}^{1.38} \qquad \text{for} \quad 0.15 \leqslant E_{max} \leqslant 0.8 \qquad (2.1)$$

where E_{max}(MeV) is the positron end point energy.

The calculated maximum positron range in the metals studied in this work are given in table 2.1 .

Table 2.1

	Zn	In	Cd	Pb	Au	Ag
Max. range (μm) :	250	240	200	150	90	170

2.6 Gamma-ray Peak Shape Analysis

2.6.1 Nuclear Gamma-rays

An accurate, analytical description of the full energy peaks in the pulse height spectrum, due to monoenergetic photons in Ge(Li) detectors is important.

A variety of functions, among them the function given in program SAMPO by Routti and Prussin (1969), the function given by Dojo (1974) and a third one given by Kern (1970), also cited by Mc Nelles and Campbell (1975), were applied to to the 514 keV line of the ^{85}Sr spectra. They are generally the modifications of a Gaussian distribution to allow for tailing effects on the low energy side of the peak.

The tailing arises from a variety of effects, including incomplete charge collection and electron escape. These distortions in peak symmetry are, of course, different for various other detectors.

Long term and detailed peak shape analysis proved the function given by Kern (1970) to the best fit to the ^{85}Sr line in our detector. Analytical representation of the function is given by

$$C(x) = \frac{S}{(2\pi)^{\frac{1}{2}}\sigma} \exp\left(-\tfrac{1}{2}\left(\frac{x-\bar{x}}{\sigma}\right)^2\right).\left(1+P_3\left(\frac{x-\bar{x}}{\sigma}\right)^4+P_4\left(\frac{x-\bar{x}}{\sigma}\right)^{12}\right)$$

$$+ \frac{S}{\sigma}\left(1- \frac{1}{\left(\frac{x-\bar{x}}{\sigma}\right)^2+1}\right).\left(P_2+P_5 \exp\left(\frac{x-\bar{x}}{\sigma} .P_6\right)\right)$$

$$+ A_o + A_1.x + A_2.x^2 + A_3.x^3 \qquad \text{for } x<\bar{x} \qquad (2.2)$$

$$C(x) = \frac{S}{(2\pi)^{\frac{1}{2}}\sigma} \exp\left(-\tfrac{1}{2}\left(\frac{x-\bar{x}}{\sigma}\right)^2\right) + A_o + A_1.x + A_2.x^2 + A_3.x^3$$

$$\text{for } x\geq\bar{x} \qquad (2.3)$$

where S and σ are the area and the width parameter of the pure Gaussian, and $\bar{x}$ is the peak centroid. The low energy side of the peak is multiplied by a polynomial with terms to 4^{th}, and 12^{th} power whose coefficients are P_3 and P_4, respectively. Two tails are also included on the low energy side of the peak ; a constant tail of amplitude P_2 and an exponential tail of amplitude P_5 and range P_6. A third degree polynomial approximates the background underneath the peak.

The analytical function, given in equations (2.2) and (2.3), was fitted to the 514 keV gamma-ray line of ^{85}Sr by the

program CURFIT (described in appendix 1) . This uses a least-squares minimisation routine.

The resolution of the line, specified as the FWHM , is given by

$$\text{Resolution (FWHM)} = 2.354\ \sigma \qquad (2.4)$$

2.6.2 Annihilation Gamma-rays

An annihilation gamma-ray peak, after the intrinsic resolution is deconvoluted, is postulated to be the sum of two components ; a Gaussian and an inverted parabola. Broadly speaking, these correspond to positrons annihilating with the core and conduction electrons, respectively. The deconvoluted spectrum takes the form

$$F(x) = H_G \exp\left(-\tfrac{1}{2}\left(\frac{x-\bar{x}}{\sigma_G}\right)^2\right) + H_P \left(1-\tfrac{1}{2}\left(\frac{x-\bar{x}}{\sigma_P}\right)^2\right)$$

$$\text{for } |x-\bar{x}| < 2^{\frac{1}{2}}\sigma_P \qquad (2.5)$$

$$F(x) = H_G \exp\left(-\tfrac{1}{2}\left(\frac{x-\bar{x}}{\sigma_G}\right)^2\right) \qquad \text{for } |x-\bar{x}| \geq 2^{\frac{1}{2}}\sigma_P \qquad (2.6)$$

where H_G (H_P) and σ_G (σ_P) are the height and width parameters of the Gaussian (or parabolic) component, respectively. Again, a third degree polynomial approximates the background underneath the peak.

In the deconvolution process the instrumental resolution is removed from the experimental data, leaving an energy spectrum which is identical to the positron-electron pair energy distribution at the time of annihilation. No model

dependence of any kind is assumed.

The convolution technique is a second method of analysis to, effectively, remove the instrumental resolution from the experimental data, and based on a physical model of the annihilation energy spectrum. A spectrum, composed of a Gaussian and an inverted parabola, is generated and smeared with the instrumental resolution, and compared with the observed data .

Throughout the applications of the convolution technique to the various data, by the program CURFIT , the instrumental resolution was ascertained with the 514 keV gamma-ray line of ^{85}Sr . The parameters of the model are adjusted in the least-squares minimisation procedure by successive evaluations, until a minimum is reached. The goodness-of-fit is reflected in the value of the reduced chi-square per degree of freedom.

Figure 2.7 illustrates the application of the convolution technique to seperate the two components of the annihilation gamma-ray line in camium. Error between the fit and the data at individual points are also shown on an enlarged scale within the standard deviation enclosure, which enables us to assess our visual judgement on the goodness of the fit, in addition to the calculated chi-square per degree of freedom value.

The convolution program is described in appendix 2 .

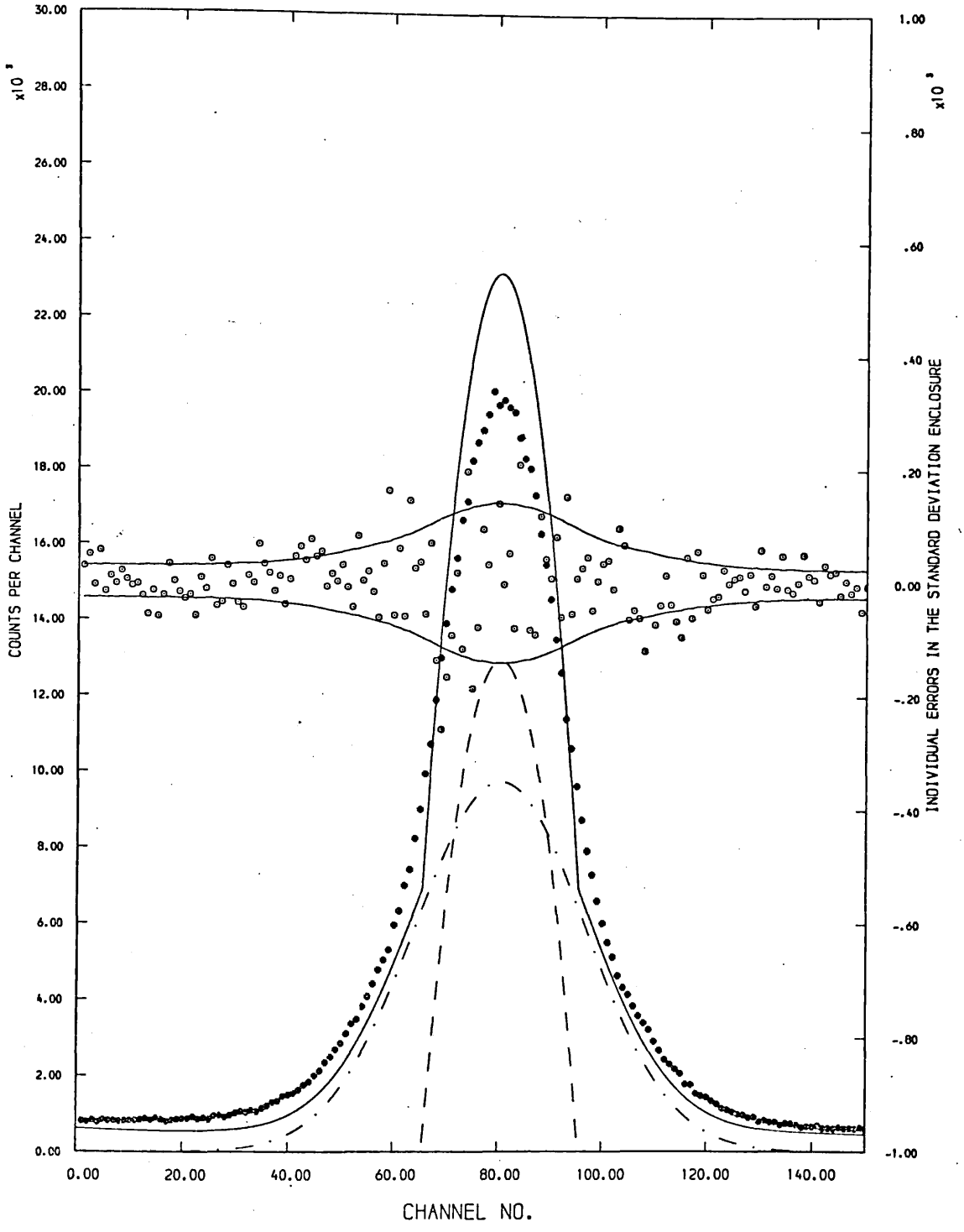

FIG. 2.7 Application of the convolution technique to seperate the two components of the annihilation gamma-ray line in cadmium at 80 K .

CHAPTER 3 POSITRON ANNIHILATION MEASUREMENTS ON ZINC

3.1 Introduction

Zinc crystallises in the hexagonal close-packed (hcp) structure. Apart from cadmium, zinc is one of the most extensively studied metal having this structure.

Angular correlation measurements by Mc Kee et al (1972a) showed a prominent saturation of the normalised peak counts near the melting point. Their simple, two state, trapping model yielded a mono-vacancy formation energy E_{1v}=0.54 ± 0.02 eV , which was later corrected by Doyama and Hasiguti (1973) to 0.56 eV taking detrapping into account. In their lifetime measurements Bergersen and Stott (1969) found a value of 0.71 eV , which contradicts the value given by Schumacher (1968) as 0.44 eV .

Unfortunately, all these measurements were performed above room temperature. Therefore, their fittings could not possibly take the intermediate temperature behaviour of the annihilation characteristic into account. An accurate determination of the value of E_{1v} requires careful subtraction of this background from the vacancy effect (Mantl and Triftshauser, 1978) .

3.2 Experimental Measurements

3.2.1 Using ^{64}Cu Positron Sources

Two 20 x 20 x 1 mm^3 polycrystalline zinc sheets of 99.999 %

purity, supplied by Johnson-Matthey, were etched in dilute hydrochloric acid, and annealed for 8 hours at 633 K in the high vacuum furnace under a vacuum of 10^{-5} torr . These were cooled, slowly, down to room temperature. The annealing period was intended to remove all defects in the sample. Immediatelly after the annealing a neutron irradiated and pre-annealed 2 μm thick pure copper foil was sandwiched between the two zinc sheets.

Measurements over the range 77 to 420 K were performed in the low temperature cryostat and those from room temperature to the melting point in the high temperature furnace. The sequence of measurements involved temperature changes in both directions. Because of the 12.9 hours source half-life, the distance between the detector and the sample was adjusted every 3 hours, so that the detector should operate continuously at the same count rate.

The annihilation spectra were recorded with the spectrocsopy system, described in chapter 2 , whose resolution at a total count rate of 3000 cps was 1.04 keV for the 514 keV line in ^{85}Sr . Each run of three hours accumulated about 850 000 counts in the 511 keV peak. The system stability was about 1 channel in 5000 . For each run a polynomial curve fitting was applied to the central 25 channels to assess the exact position of the peak. The F-parameter, which was defined as the sum of the counts in the 15 central channels divided by the sum of the counts in the 175 channels across the peak, was measured as a function of temperature.

3.2.2 Using ^{22}Na Positron Source

Two pieces of zinc, identical to the previously used samples, were cut from the same sheet and subjected to a similar annealing and cooling treatment. Approximately 90 μCi of carrier-free $^{22}NaCl$ positron source were evaporated directly onto their central regions. These two pieces of zinc were subsequently arranged in a sandwich configuration, wrapped in thin aluminium foil and finally inserted into the low temperature cryostat.

The annealing spectra over the range 4.2 to 420 K were recorded in the same fashion as described earlier for the previous zinc sample. Figure 3.1 shows the variation of the line-shape parameter F as a function of temperature over the range 4.2 to 670 K , obtained from the two different measurements using ^{64}Cu and ^{22}Na positron sources. The normalisation was based on linear curve fittings to the two sets of data in the range 77 to 340 K . Agreement between them in the overlapped region is pleasing.

3.3 Data Analysis

3.3.1 F-parameter Analysis

The simple two-state trapping model has been outlined in chapter 1.5.3 . By substituting the expressions for the probability of annihilation in a free state and at a vacancy into equation (1.37) , and using the mono-vacancy concentration, defined in equation (1.24) , the line-shape parameter may be written as

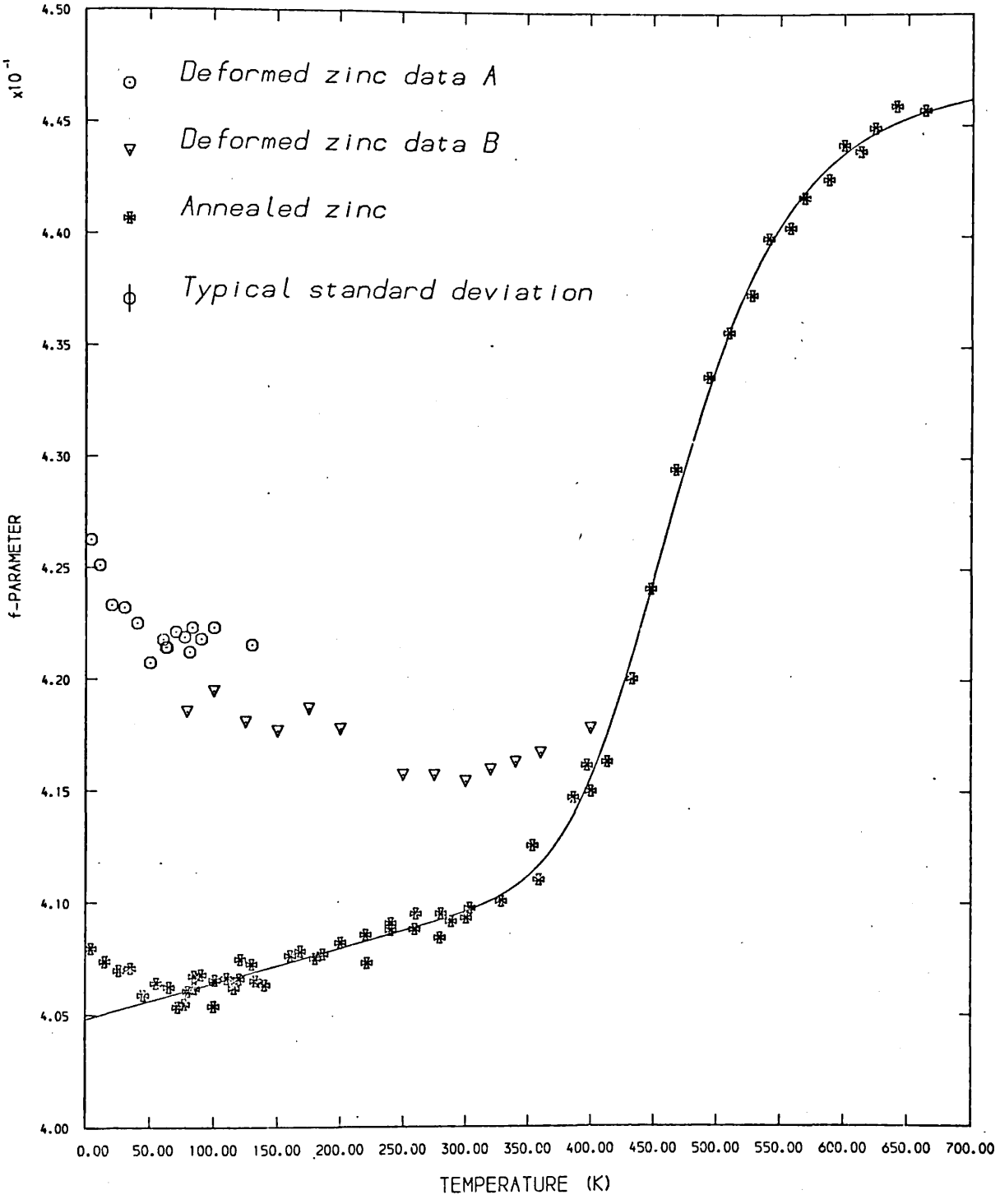

FIG. 3.1 The variation of F-parameter with temperature for annealed and deformed specimens of zinc. The fitted line represents equation (3.2).

$$F = \frac{F_f + F_{1v}\, A \exp(-E_{1v}/kT)}{1 + A \exp(-E_{1v}/kT)} \qquad (3.1)$$

Obviously, this equation, assuming temperature independent value of F_f, cannot possibly give a satisfactory fit to the data shown in figure 3.1 because of the rise in the F-parameter in the region below the vacancy threshold. Jamieson et al (1974) and Triftshauser and Mc Gervey (1975) have suggested that this observed low temperature behaviour is associated with the electron densities as a result of thermal lattice expansion, and it probably continues up into the vacancy region.

Published data on the temperature dependence of F_{1v} conflict. Mac Kenzie (1972) and Triftshauser and Mc Gervey (1975) observed temperature independent values of F_{1v} whereas Nanao et al (1973) did not observe a plateau near the melting point in copper. In our fittings we consider F_{1v} itself to be either a linear function of temperature or a constant.

The use of the variables F_f and F_{1v} in the fitting equation

$$F = \frac{F_f^o(1 + \beta T) + F_{1v}(1 + \alpha T).A \exp(-E_{1v}/kT)}{1 + A \exp(-E_{1v}/kT)} \qquad (3.2)$$

for 3 different cases : $\alpha \neq \beta$, $\alpha = \beta$, and $\alpha = 0$ has resulted in the best fit (above 72 K) for the case $\alpha = 0$ -i.e., temperature independent value of F_{1v} . The best values of the parameters were calculated in the program CURFIT , which is based on a least-squares routine (described in

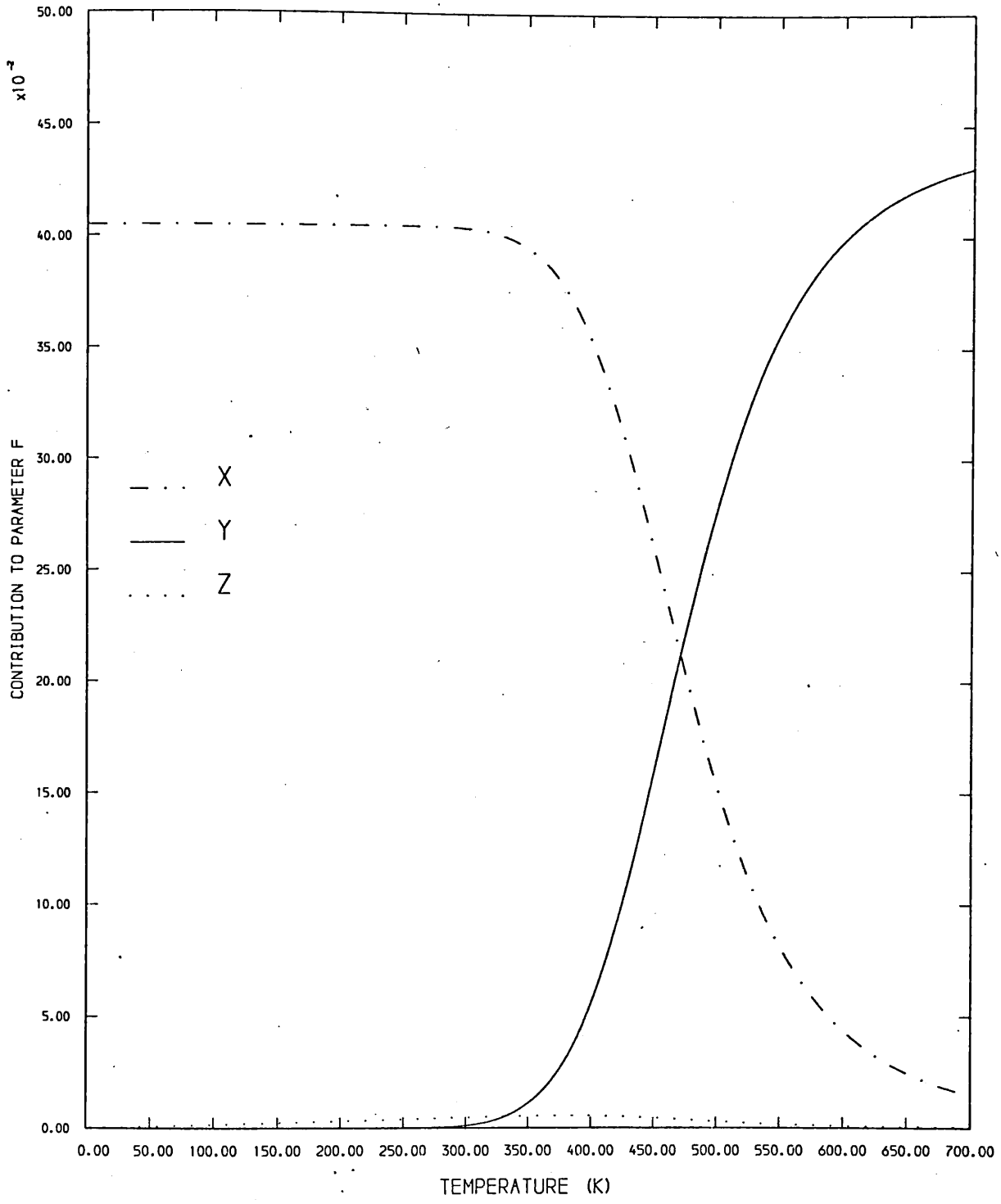

FIG. 3.2 The different contributions to F calculated with the parameters obtained from curve fitting in the case when F_f is taken linearly to rise with temperature. Curves X, Y and Z represent $F_f^o(1-P_{1v})$, $F_{1v}P_{1v}$ and $F_f^o\beta T(1-P_{1v})$, respectively.

Appendix 1) . These gave the values

$E_{1v} = 0.42 \pm 0.02$ eV $\qquad F_f^o = 0.4048$

$F_{1v} = 0.4473$ $\qquad A = 27380.$

$\beta = 39 \times 10^{-6}$

where the goodness of the fit, χ^2/ν gives the value 1.27 .

Figure 3.1 shows the best line obtained by using this fitting. The different contributions to F , calculated with the parameters obtained from this fitting, are shown in figure 3.2 . The slope (β) of the intermediate linear region is slightly higher than the linear thermal expansion coefficient (28×10^{-6} K^{-1}) in this temperature range.

The non-linear change in F-parameter in the intermediate temperature region, in cadmium and other metals, reported by Lichtenberger et al (1975) has injured the hypothesis that the change is due to lattice thermal expansion. Therefore, we applied the self-trapping model proposed by Seeger (1975) to our measurements on zinc (above 72 K) using the assumption, that above the vacancy threshold, annihilation in vacancies predominates.

By substituting the weighted average of the F-parameter below the vacancy threshold, defined in equation (1.51) , into equation (3.1) with $\alpha = 0$ the F-parameter is therefore written as

$$F = \frac{F_f(1 - P_{st}) + F_{st} P_{st} + F_{1v} A \exp(-E_{1v}/kT)}{1 + A \exp(-E_{1v}/kT)} \qquad (3.3)$$

where P_{st} is defined in equation (1.48) and F_{st} is the

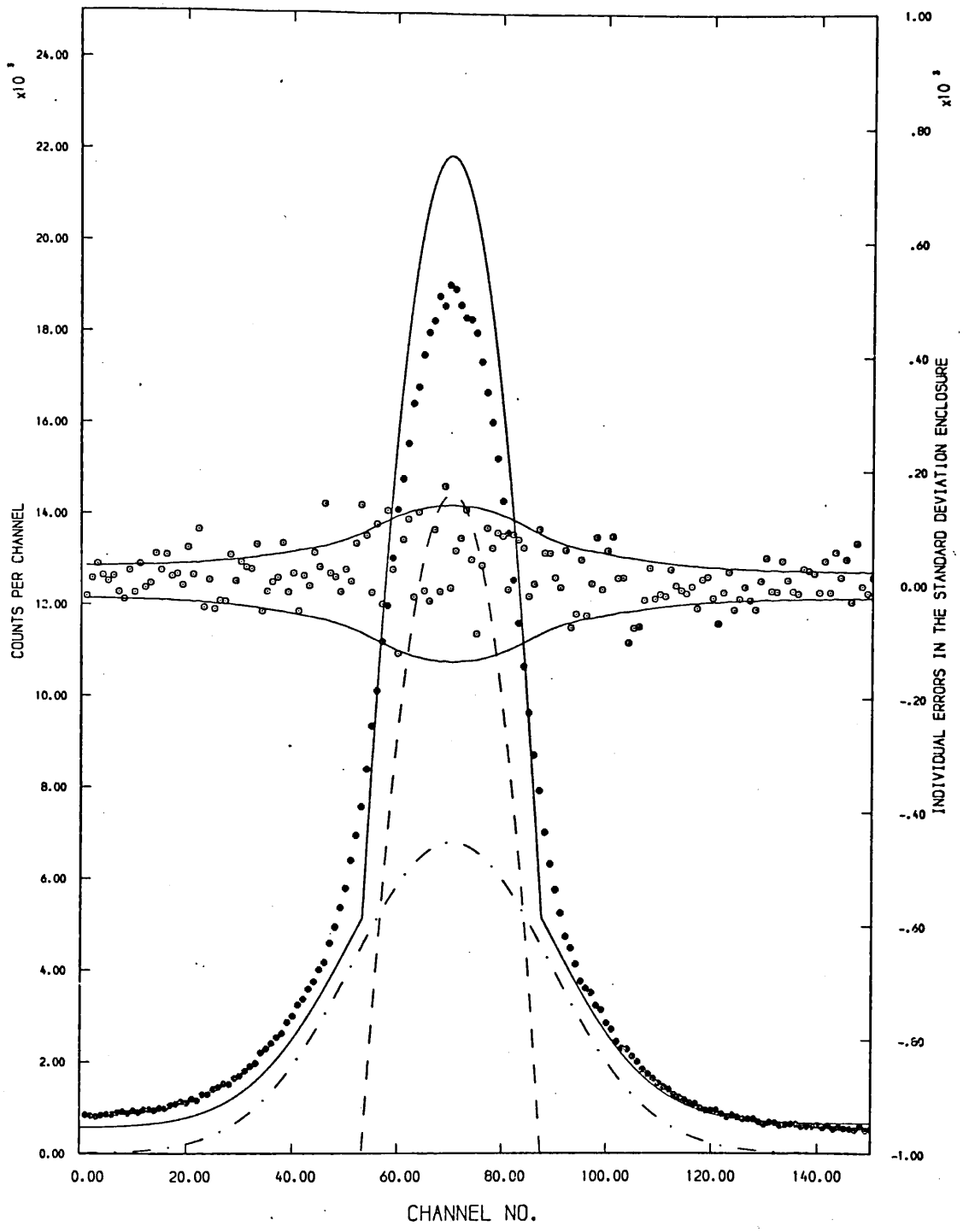

FIG. 3.3 Application of the convolution technique to seperate the two components of the annihilation gamma-ray line in zinc.

value of F when all the positron annihilate in self-trapped states. Fitting equation (3.3) to the data (above 72 K), shown in figure 3.1, by program CURFIT fails to give a minimum. This is apparently due to the linear behaviour of F over the range 72 to the vacancy threshold temperature 350 K.

3.3.2 Convolution

In addition to the use of F-parameter, we analysed the observed Doppler-broadened line shapes in terms of the sum of a Gaussian and a parabolic component, convoluted with the intrinsic resolution function. Figure 3.3 illustrates the sum of the two components as well as the errors at individual points between the convoluted model function and the observed data. The errors are on an enlarged scale, together with the standard deviation on the data points. The proportion of positrons annihilating with conduction electrons, represented by the percentage of parabola, and the line shape width parameters are shown in figures 3.4 a and b as a function of temperature.

3.4 Discussion

The analysis of the annihilation line shapes for zinc has shown that the conduction electrons contribution increases from 51% to approximately 62% near the melting point.

At intermediate temperatures, below the vacancy region, measurements have shown that the annihilation parameter is a function of temperature. Our calculated value of E_{1v}, based on an interpretation of thermal lattice expansion, does not agree with the reported values, outlined in the

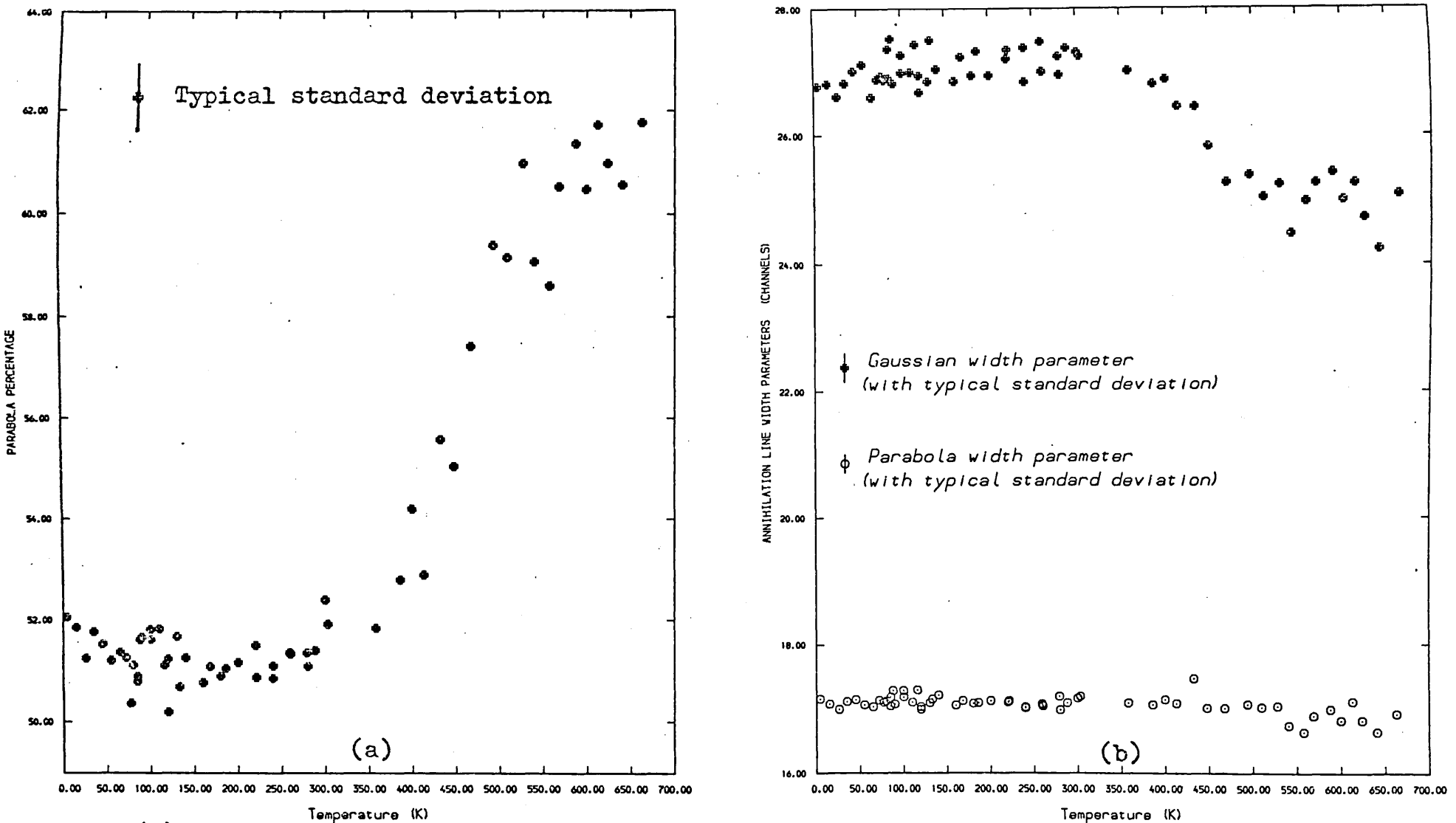

FIG. 3.4 (a) The proportion of annihilations contributing to the parabolic component of the line shape, and (b) the variation of the width parameters of the two components as a function of temperature.

introduction of this chapter, for the data above room temperature. This, no doubt, demonstates the effect of the subtraction of the sub-vacancy effect from the main effect due to annihilation in vacancies.

Due to the apparent linear behaviour of F in the temperature range 77 to 350 K , attempts to interpret the intermediate temperature dependence of the line-shape parameter by the model, based on self-trapping metastable states (Seeger,1975), has resulted in failure.

As liquid helium temperatures have been approached a new effect has appeared. An unexpected rise in F has been seen at low temperatures, but not in copper (Rice-Evans et al,1976b) and lead (Rice-Evans et al, 1978a) .

Even in well-annealed samples grain boundaries exist. In the zinc specimen, micrographs showed the grain diameters to range from 20 to 300 μm , giving an average value of 60 μm . It is known that positrons may be trapped in such boundaries (Lynn et al, 1974 ; Leighly, 1977) , these consisting of complexes of intersecting dislocations. Whether positrons exist in the grain boundaries will depend on the average grain size -i.e., will depend on the surface area of the boundaries. Also, it will depend on whether or not a significant proportion of positrons would encounter the boundaries (Mac Kenzie, 1977) . The increase in the F at the lowest temperatures implies that positrons are captured in shallow grain boundary traps, and that the negative slope (dF/dT) indicates thermal detrapping (Rice-Evans et al,1978b).

A similar low temperature effect, below 50 K , has also been observed by Herlach et al (1977) in their lifetime and Doppler-broadening measurements, on cadmium and gold. On the basis of experimental evidence they suggested that positrons escape from the sample by channeling (Gemmel, 1974) within the grains. These annihilate in the helium gas surrounding the sample, on the walls of the cryostat and on the specimen surface. This, no doubt, is unconvincing if we consider the absence of such channeling in copper (Rice-Evans et al, 1976b and Mantl and Triftshauser, 1976) , in indium (Rice-Evans et al, 1978b) and in lead (Rice-Evans et al, 1978a) .

More convincing evidence and further discussion on the grain boundary trapping of positrons will be presented in chapter 5 , where the single crystal data for cadmium will be considered.

3.5 Annealing Studies in Deformed Zinc

3.5.1 Sample Preparation

To study the annealing of the deformation-induced defects, 1 mm thick specimens of 99.999% pure zinc (from Johnson-Matthey) were sandwiched between two thick steel slabs and hammered to obtain 30% thickness reduction at room temperature. The two sheets were etched in dilute hydrochloric acid both before and after the deformation. Shortly after the final etching approximately 90 μCi of carrier-free $^{22}NaCl$ positron sources were evaporated onto the central region of the two specimen sheets. These were then pressed into a

sandwich configuration, wrapped in thin aluminium foil and cooled down to 77 K in the low temperature cryostat. The whole process took just under 5 hours.

3.5.2 Measurements

Figure 3.1 shows the temperature dependence of the line-shape parameter F in deformed zinc. After the acquisition of data-A, the deformed sample was allowed to worm up to room temperature for 72 hours prior to subsequent cooling and collection of data-B .

Measurements in either case consisted of successive cycles of 2.5 hours, half an hour temperature setting and two hours running, at a total count rate of 5000 cps . Definition of the line-shape parameter F is as in the annealed zinc. Simultaneous measurements of a control ^{103}Ru 497 keV gamma-ray line has also been instituted to assess any electronic drift, and to allow approprite corrections where necessary. A G-parameter, similar in conception to F, has been applied to 497 keV line, and runs corresponding to any significantly low values (rare) were rejected.

3.6 Discussion on Deformed Zinc

It was Berko and Erskine (1968) who discovered that plastically deformed metals trapped positrons prior to their annihilation and that the properties of the annihilation photons were accordingly modified. The exact nature of the defects produced in plastic deformation has been discussed by Dauwe et al (1974) who considered them to be essentially

dislocations.

Perhaps the most striking feature of the deformed zinc data, presented in figure 3.1 , is again the temperature dependence of the line-shape parameter (below 50 K), similar in concept, but not in magnitude, to that in annealed zinc. Reversibility of the temperature dependence in the range between 4.2 and 125 K rules out the annealing involment.

There is no consensus of opinion as to the types of positron traps generated by room temperature deformation (Mac Kenzie, 1977) . In the case of our deformed zinc sample, a simplifying assumption is that only grain boundaries and dislocations are present. Obviously, some annealing occured between deforming and locating the specimen in the sample chamber. The positrons will then annihilate either in free state or become trapped in dislocations or grain boundaries. The proportions are determined primarily by the defect densities and their trapping efficiencies. The effect of an increase of temperature would be to change the balance so that detrapping from shallow grain boundary traps, say edge dislocations, eventually would result in their subsequent annihilation in a jog, or an intersection which acts as a deep trap. Also some annihilations in the bulk may result in line broadening.

The region between 70 and 170 K shows no apparent change due to annealing. A shallow step of annealing is observed over the temperature interval 200-300 K . Above about 300 K a step rise in F-parameter is observed, due to the production of thermal vacancies and the subsequent trapping

trapping of positrons. Occurrence of this rise in F before the completion of annealing suggests that vacancies are more efficient positron traps than the traps produced by plastic deformation.

CHAPTER 4 POSITRON ANNIHILATION MEASUREMENTS IN INDIUM

4.1 Introduction

Positron annihilation studies in annealed indium over the range from room temperature to just below the melting point and in plastically deformed indium, for the first time, were performed by Mac Kenzie (1969) who concluded that indium is one of the several metals to show no sensitivity to the effect of plastic deformation at room temperature. However, these are influenced by vacancies introduced by rising the sample temperature.

Measured values of mono-vacancy formation energy, E_{1v}, in annealed indiun, no doubt, aroused the greatest controversy among all the other metals studied so far by the positron annihilation technique. The reported values of E_{1v} have ranged from 0.55 ± 0.02 eV (Mc Kee et al, 1972a) and 0.48 ± 0.01 eV (Triftshauser, 1975) by angular correlation studies, 0.45 ± 0.03 eV (Seeger, 1973a) as obtained from centroid shift lifetime measurements, to 0.39 ± 0.04 eV (Singh et al, 1975) by simultaneous mean lifetime and Doppler-broadening measurements. Mac Kenzie and Lichtenberger (1976) obtained a value of 0.41 eV from the experimentally observed linear relationship between the mono-vacancy threshold temperature and the diffusion coefficient Q, assuming $Q = 2E_{1v}$.

Doppler-broadening measurements by Segers et al (1977) in the range between 74 K and the melting point (429 K) yielded

a well pronounced, non-linear, anomalous temperature dependence in the sub-vacancy region which was interpreted as an effect of self-trapping of positrons. Based on this model, they obtained a mono-vacancy formation energy 0.48 ± 0.03 eV .

We measured the temperature dependence of the positron annihilation Doppler-broadened line-shape parameter in 5N and 6N indium specimens between 4.2 K and the melting point.

4.2 Temperature Dependence in 5N Annealed Indium

4.2.1 Experimental Measurements

Two $20 \times 20 \times 1$ mm^3 polycrystalline indium sheets of 99.999% purity, supplied by Johnson-Matthey, were etched in dilute nitric acid and then annealed for 40 hours at 125 K in a vacuum of 2×10^{-6} torr . The positron source was 60 μCi of carrier-free ^{22}NaCl evaporated directly on to the central regions of the specimens which were then arranged in a sandwich configuration, sealed around their edges with a high temperature resin and inserted into the low temperature cryostat.

The shape of the 511 keV line was recorded with the spectroscopy system, described in chapter 2 , whose resolution at a total count rate of 3000cps was 1.04 keV for the 514 keV line in ^{85}Sr . Each run of three hours accumulated about 850 000 counts in the 511 keV peak. The system stability was about 1 channel in 5000 . The line-shape parameter F , defined in chapter 3 , was measured as a function of temperature in the range between 77 and 427 K .

Measurements below 77 K , which were also extended up to 400 K , were recorded seperately in the same fashion as earlier.

Figure 4.1 shows the variation of the line-shape parameter F as a function of temperature over the range 4.2 to 427 K .

4.2.2 Line-shape Parameter Analyses

Indium is a rather different to many other metals. There is no indication of the F-parameter showing a tendency to saturate near the melting point. An accurate value of the line-shape parameter when, preassumably, all the positrons are trapped in vacancies cannot be easily determined. This difficulty in finding the best value of F_{1v} led us to the following analysis. The points shown in figure 4.1 were repeatedly fitted to the two-state trapping model for selected values of F_{1v} —with the assumption that the pre-vacancy slope is essentially concerned with the free positrons in the lattice and also due to changing electron densities as a result of thermal lattice expansion— allowing the remaining parameters to be adjusted in a minimisation process. Figure 4.2 illustrates the nature of these fittings by indicating the goodness of the fit, and the respective best value of E_{1v} , as a function of the parameter F_{1v} .

In the sub-vacancy region only a small linear rise in F is apparent. Writting

$$F_f = F_f^o(1 + \beta T) \qquad (4.1)$$

the best fitted value for β is 28×10^{-6} K^{-1}, which may be

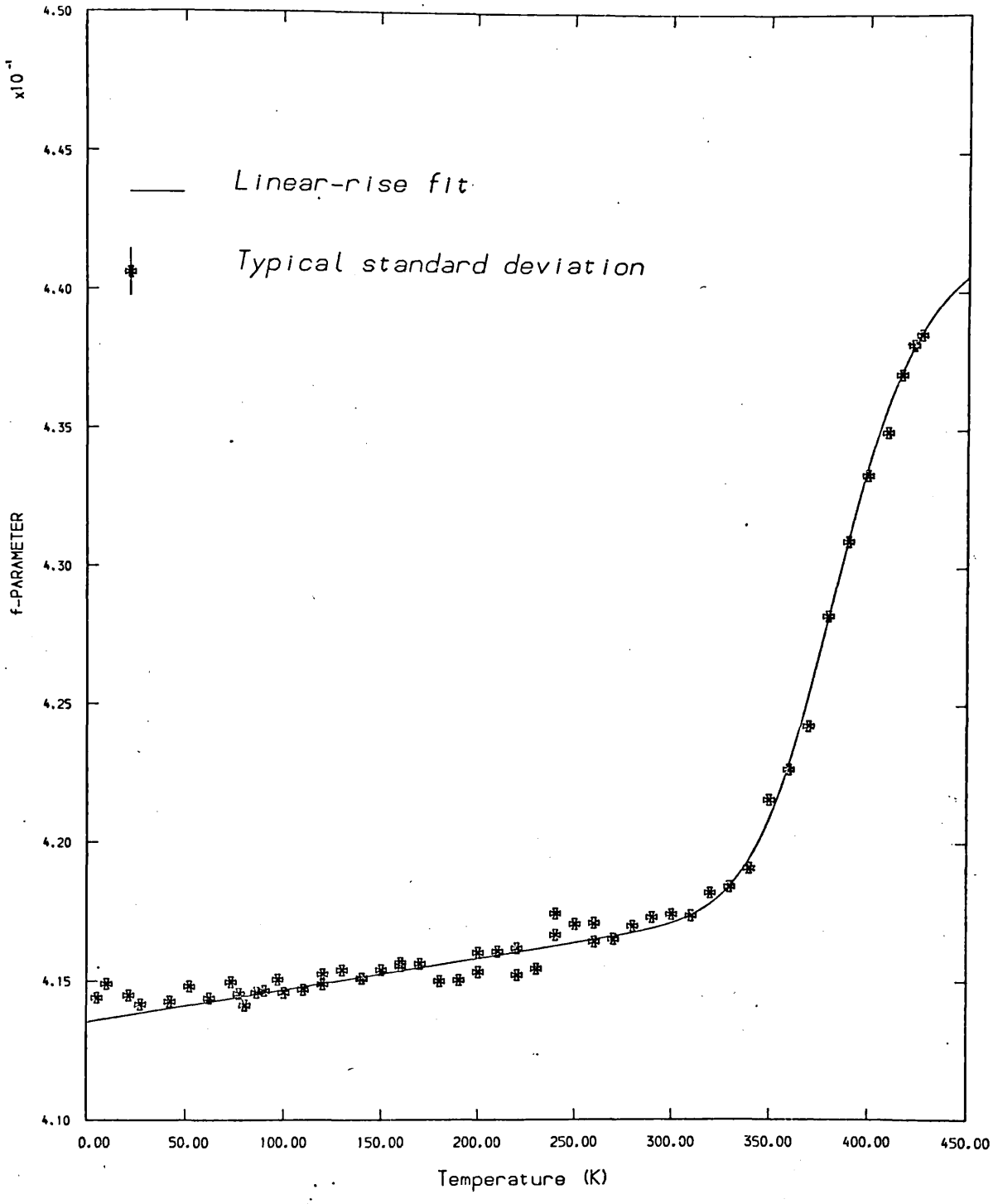

FIG. 4.1 The variation of the line-shape parameter F as a function of temperature for 5N annealed indium. The fitted line corresponds to the case where F_f is taken linearly to rise with temperature.

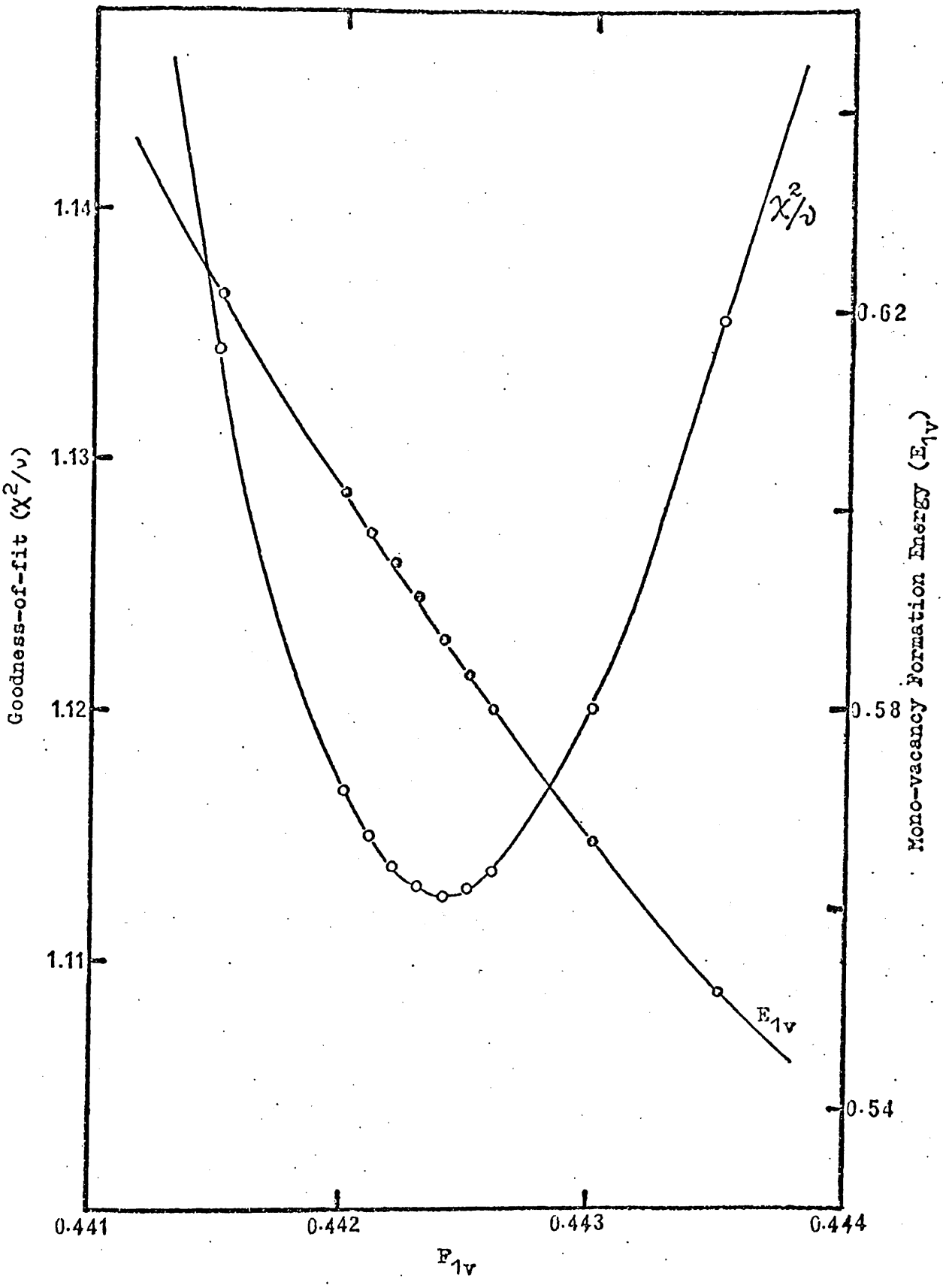

Fig. 4.2 A plot of the goodness-of-fit, and the respective best value of E_{1v}, as a function of the parameter F_{1v}.

compared with the thermal coefficient of the volume of expansion for indium which ranges from 69 to 96 $x10^{-6}$ K^{-1} (Kirby et al, 1972).

Above 300 K the expected step rise in F occurs, due to the production of thermal vacancies and the subsequent trapping of positrons. The least-squares FORTRAN program CURFIT was applied to the data (above 77 K) with allowance for the underlying linear rise in F . The best values of the parameters, given in equation (3.2) with a constant value of the parameter F_{1v} , are

E_{1v} = 0.59 ± 0.02 eV F_f^o = 0.4135

F_{1v} = 0.4424 A = 44138300.

β = 28 $x10^{-6}$

where the goodness of the fit, χ^2/ν gives the value 1.11 . Figure 4.1 shows the best line obtained by this fitting.

We attempted to fit our data with the self-trapping expression, proposed by Seeger (1975), and given in equation (3.3) . The best values of the parameters, which are listed below, were obtained in a series of fittings for selected values of F_{1v} as has been described in the earlier fitting.

E_{1v} = 0.55 ± 0.03 eV F_f = 0.4151

F_{1v} = 0.4430 A = 15.45 $x10^6$

$E(K_o)$ = 0.28 F_{st} = 0.4170

B = 57.2 $x10^8$

where the goodness of the fit, χ^2/ν gives the value 1.20 . We note that the later fit is not as good as the former . Therefore,it does not provide convincing evidence of self-trapping.

4.2.3 Convolution

In addition fitting the F-parameter curve to the trapping model, the actual line shapes have been resolved into their Gaussian and the parabolic components. The intrinsic resolution of the system was ascertained with the analytical function, expressed in equations (2.2) and (2.3), fitted to the 514 keV gamma-ray line of ^{85}Sr . Figure 4.3 shows that the proportion of the annihilations contributing to the parabolic distribution rises from 59% to 65% as the temperature increased from 77 to 427 K .

4.3 Temperature Dependence in 6N Annealed Indium

4.3.1 Experimental Measurements

Two pieces of 99.9999% pure polycrystalline indium (from Koch-Light) were compressed into 1.25 mm thick discs with 22 mm diameter. They were etched in dilute nitric acid before and after the compression. The positron source was a 90 μCi carrier-free $^{22}NaCl$ solution evaporated directly on to the central regions (smaller than 5 mm diameter) of the specimens. These were then pressed in a sandwich configuration. Annealing took place in the low temperature cryostat under a vacuum of 10^{-5} torr for 8 hours at 398 K plus 13 hours at 373 K .

Figure 4.4 shows the line narrowing parameter plotted as a function of temperature for 6N annealed indium over the range covering the melting point down to 4.2 K . Each run of two hours, corresponds to a point in the figure , and

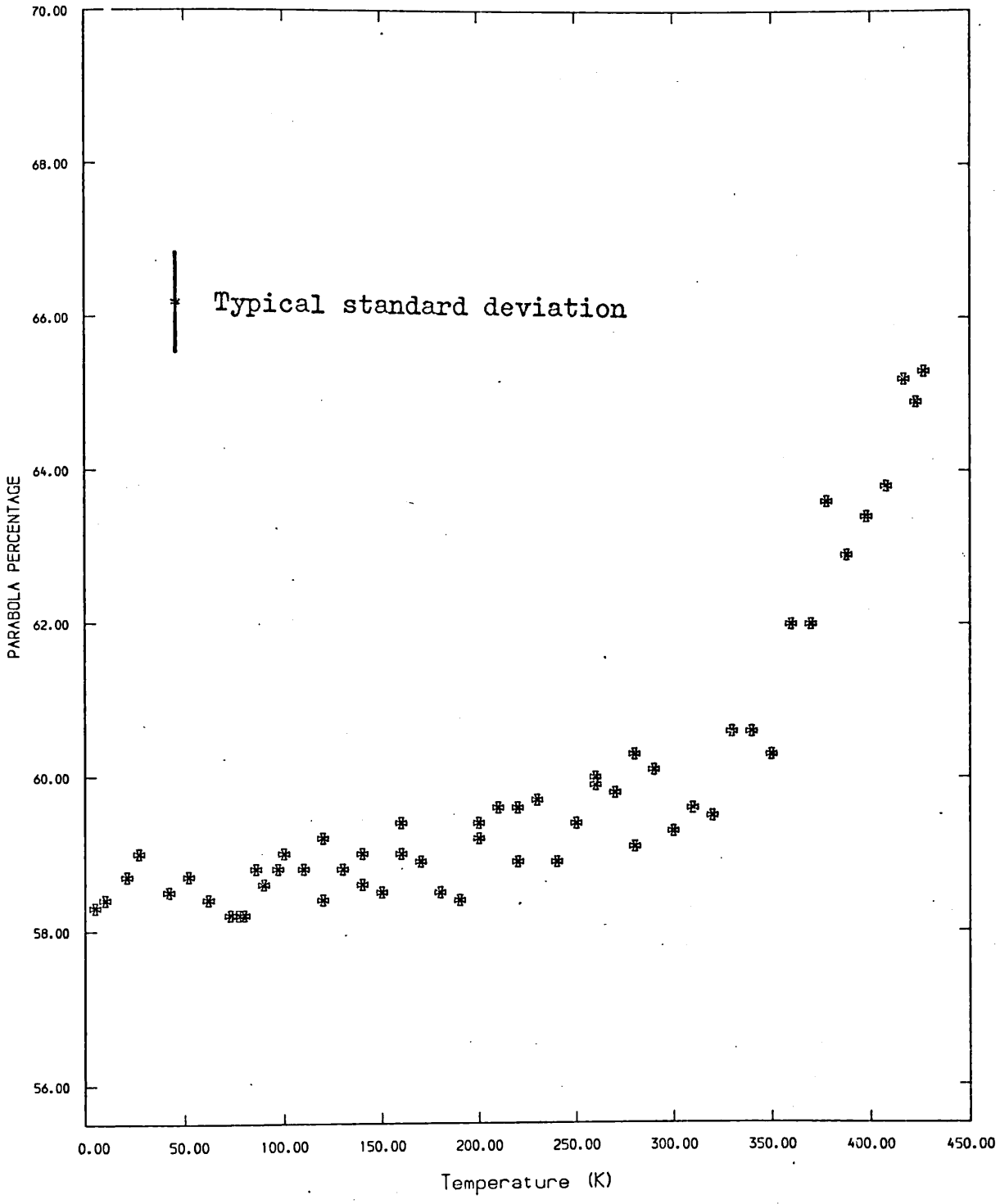

FIG. 4.3 For 5N annealed indium, the proportion of annihilations contributing to the parabolic component of the line shape as a function of temperature. The intrinsic line resolution was represented by an analytical function fitted to the 514 keV gamma-ray line of ^{85}Sr .

accumulated 900 000 counts in the 511 keV peak. Simultaneous measurements of a control ^{103}Ru 497 keV gamma-ray has been instituted to assess any electronic drift and to allow approprite corrections where necessary. The system stability was better than that for 5N indium. Resolution of the system at a total count rate of 5000 cps was 1.15 keV at 514 keV .

4.3.2 Line-shape Parameter Analyses

A G-parameter, similar in conception to F , was applied to the 497 keV line to monitor the electronic stability of the system. Runs corresponding to a significantly low values (rare) were rejected.

The rise in F-parameter above 300 K is associated with the creation of single vacancies. Below this region an apparently linear slope is observed and the graph appears flat over the range 4.2 to 120 K , as was previously found in the case of copper (Rice-Evans et al, 1976b) and lead (Rice-Evans et al, 1978a).

First, we considered the observed rise below 300 K to justify the use of a variable $F_f(=F_f^o(1+\beta T)$ in the fitting (above 120 K) equation (3.2). This has been attempted in the same fashion as has been described earlier for 5N indium. The best values of the parameters are listed in table 4.1 .

We have, also, applied Seeger's self-trapping model, given in equation (3.3), with the assumption that trapping by vacancies always predominates. This has resulted in the following values of the parameters and are given in table 4.1.

Table 4.1 The results of fitting the parameter F with respect to three different thecretical models.

	Two-state trapping model with linear rise of F_f and constant F_{1v} (single vacancies)	Two-state trapping model with self-trapping model and constant F_{1v} (single vacancies)	(single and divacancies)
E_{1v}	0.49 ± 0.02 eV	0.49 ± 0.02 eV	0.49 ± 0.02
F_f^o	0.3876	0.3905	0.3905
F_{1v}	0.4194	0.4194	0.4114
A	30.10 $x10^5$	29.46 $x10^5$	45.36 10^5
β	53.0 $x10^{-6}$	.....	.....
$E(K_o)$	.....	0.18	0.19
F_{st}	.....	0.3943	0.3949
B	.....	39.57 $x10^6$	14.82 $x10^6$
F_{2v}	.....	.....	0.4231
E_{2v}^B	.....	.....	0.18
A_{2v}	.....	.....	23.33 $x10^8$
χ^2/ν	1.15	1.27	1.26

We interpret the worsening of the fit in the later case due to the apparently linear behaviour of F in the intermediate temperature region. Figure 4.4 shows the best lines obtained by these two fittings.

As was noted earlier for 5N indium near the melting point,

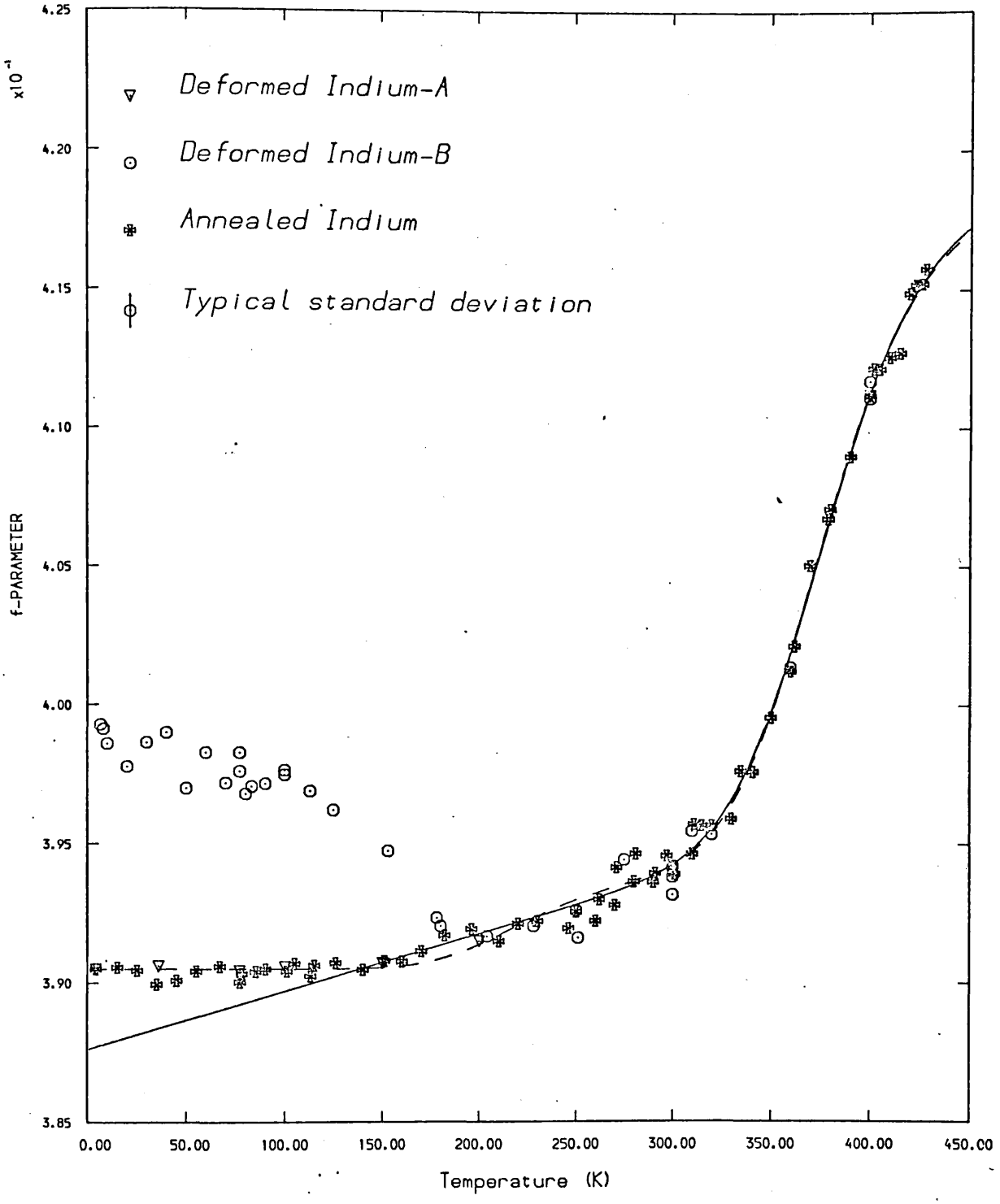

FIG. 4.4 For 6N annealed and deformed specimens of indium, the change in F-parameter as a function of temperature. The solid and the broken lines correspond to the cases where F_f is taken linearly to rise with temperature, and to fit Seeger's self-trapping model, respectively.

the F-parameter still appears to be increasing. Existence of divacancies in various metals have been reported (Dlubek et al, 1977a ; 1977b ; Nanao et al, 1973). Therefore, we decided to serch for divacancies in indium.

Substituting equation (1.35) and (1.36) into equation (1.37) and using the total vacancy concentration —given by

$$C_v = C_{1v} + 2C_{2v} = \exp(-G^f_{1v}/kT).(1 + z.\exp(-(G^f_{1v}-G^B_{2v})/kT)\ )\ ) \tag{4.2}$$

where G^f_{1v} has been defined in equation (1.25) and the free energy of binding of a divacancy of fixed orientation is given by

$$G^B_{2v} = E^B_{2v} + T\ \Delta S_{2v}\ , \tag{4.3}$$

with divacancy binding energy E^B_{2v}— results in the equation

$$F=\frac{F_f + F_{1v}.A.\exp(-E_{1v}/kT) + F_{2v}.A_{2v}\exp(-(2E_{1v}-E^B_{2v})/kT)}{1 + A\ \exp(-E_{1v}/kT) + A_{2v}\ \exp(-(2E_{1v}-E^B_{2v})/kT)} \tag{4.4}$$

Here F_{2v} is the value of F , similar in conception to F_{1v} , for divacancies. Having included Seeger's self-trapping model ($F_f = F^o_f(1 - P_{st}) + F_{st}\ P_{st}$) with the divacancy term in the fitting equation it was found that the goodness of the fit —as evaluated by the program CURFIT — did not improve. The best values of the parameters and the goodness of the fit are listed in table 4.1 .

Near the melting point the calculated ratio of divacancies to monovacancies is approximately 50% .

4.3.3 Convolution

Once again, the convolution technique, outlined in chapter 2, was used in an effort to separate and calculate the proportions of annihilations contributing to the parabolic component.

Figure 4.5 shows the parabola percentage rising from 57.5% to 64% as the temperature is increased from 4.2 K to the melting point. This is expected from the trapping model. The temperature dependence of the annihilation line width parameters are shown in figure 4.6 . The width of the parabolic component represents the Fermi energy. Over the range 4.2 K to 360 K this has an average value of 16 channels, corresponding to 1.504 ± 0.008 keV (94.0 ± 0.5 eV/channel) gamma-ray energy, and a Fermi energy of 8.840 ± 0.095 eV. This is larger than the values quoted by Jackman et al (1974) as 7.5 eV , and by Ashcroft and Mermin (1976) as 8.63 eV .

Our quoted value of error on the Fermi energy is just the error on the energy calibration of the analyser, which is expected to be the largest. Standard deviation on the parabola width parameter and errors entering into the value of this parameter while the remaining parameters involved in the minimisation process are adjusted are, of course, small, but additional sources of errors.

4.4 Discussion of Results

The temperature dependent results in 5N and 6N annealed indium are shown in figures 4.1 and 4.4 , respectively. In both cases, near the melting point, the F-parameter still

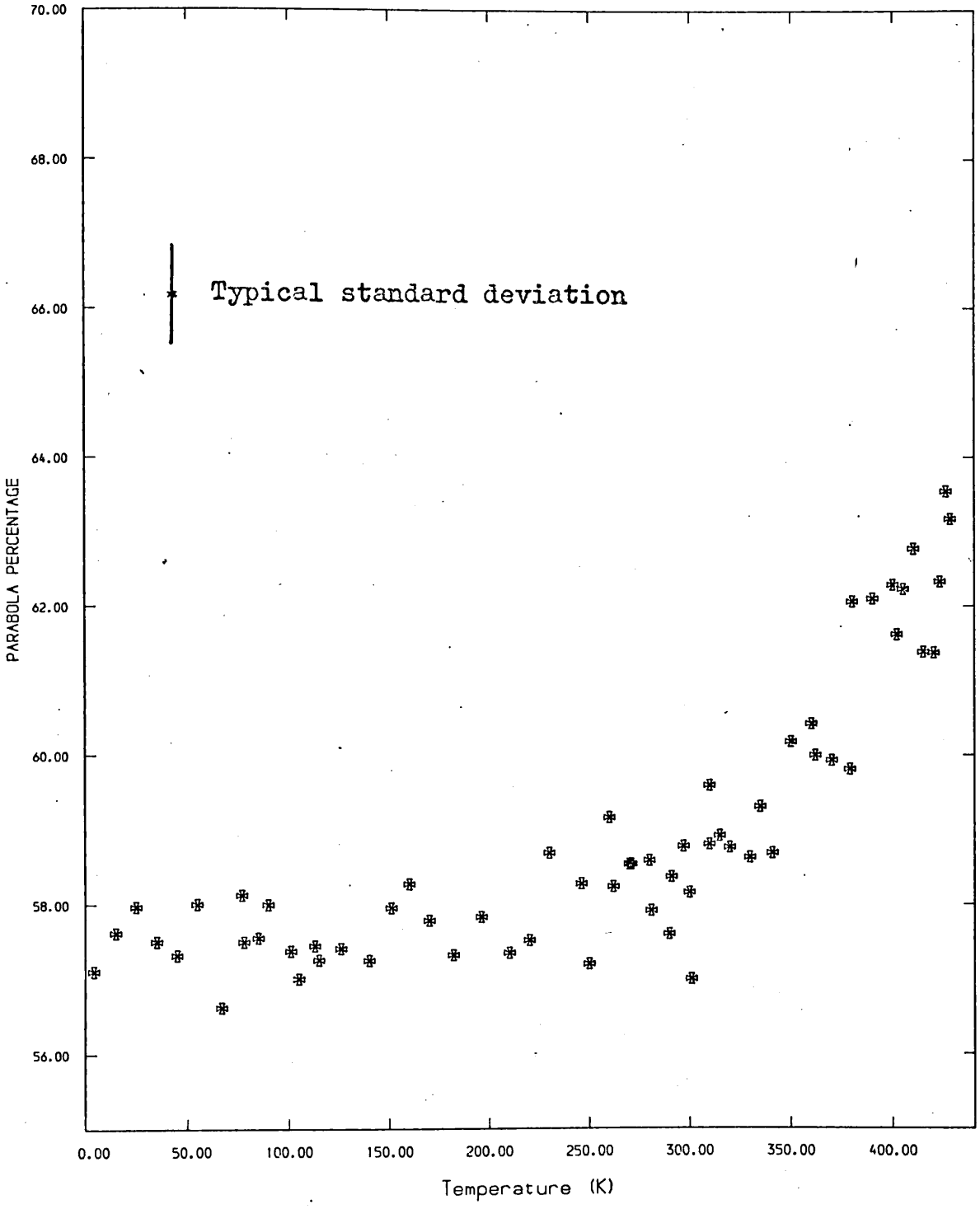

FIG. 4.5 For 6N annealed indium, the parabola percentage as a function of temperature.

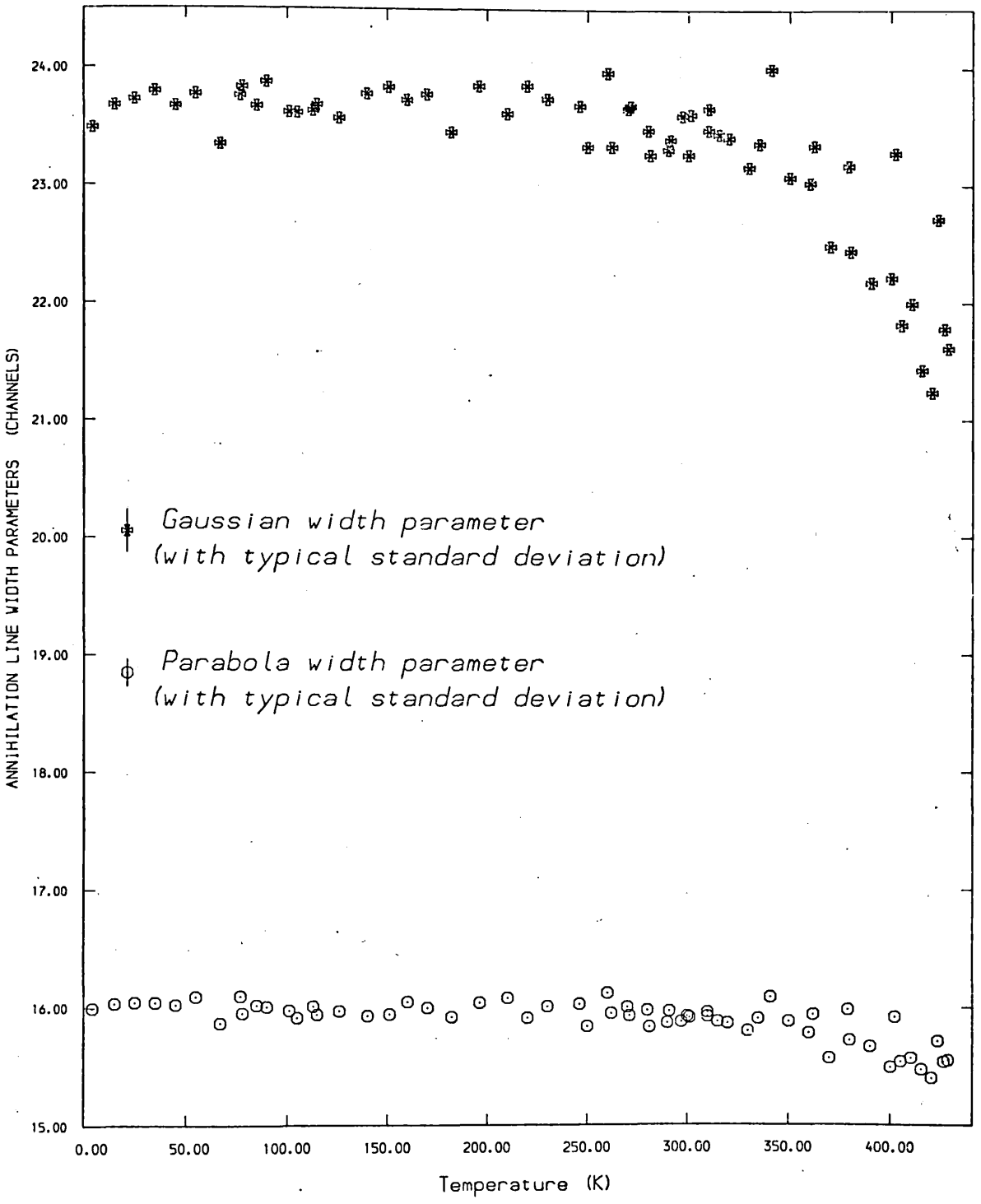

FIG. 4.6 Temperature dependence of the annihilation line width parameters for 6N annealed indium.

appears to be increasing. This makes an accurate determination of the parameter F_{1v} very difficult.

The reported values of E_{1v} on both 5N and 6N indium, outlined in the introductory section of this chapter, including our reported here, show no agreement. Figure 4.2 illustrates the effect of F_{1v} on the value of E_{1v} . Large values of E_{1v} are accompanied by very small changes in the value of F_{1v} , suggesting that the greatest contribution to the error enters into the value of E_{1v} due to the fact that F_{1v} is not accurately determined. Perhaps statistical fluctuations, different sample preparations (Rice-Evans et al, 1977 ; Segers et al, 1977 ; Herlach and Maier,1976) , and different subtruction procedures applied to the intermediate temperature region background play an important role.

Line shapes resolved into their Gaussian and parabolic components yielded approximatelly 1% higher proportion of parabola in 5N indium than that in 6N over the full range. The systematic nature of the error is obvious. In 5N indium the intrinsic resolution was represented by the analytical function, outline in the section 6.1 of chapter 2 , fitted fitted to the 514 keV gamma-ray line in ^{85}Sr . In 6N indium the improved programing enabled us to use the observed 514 keV line for the resolution function, and so does not include any error due to fitting. The reanalysed data in 5N indium, this time convoluted with the observed 514 keV line, is shown in figure 4.7 .

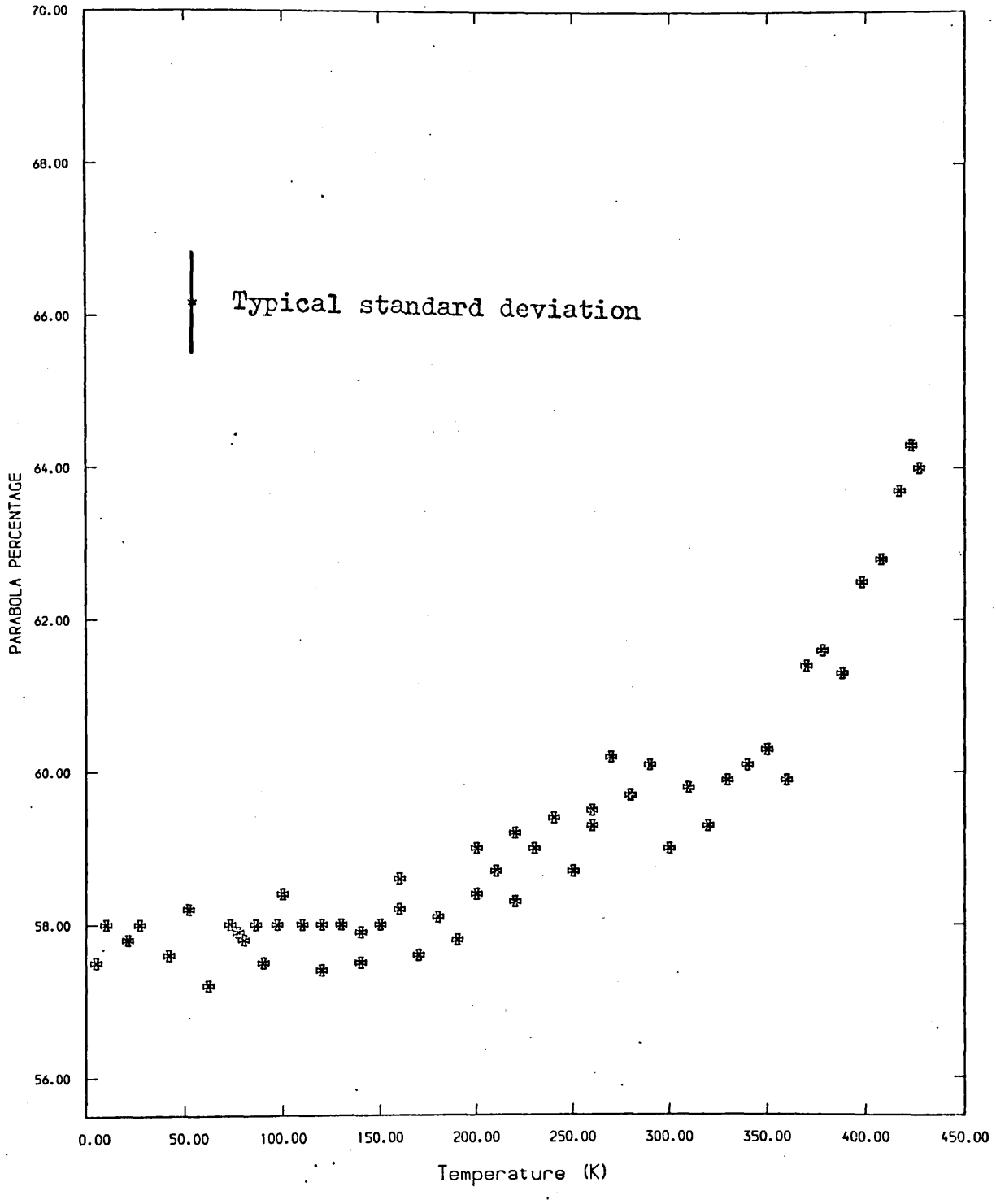

FIG. 4.7 For 5N annealed indium, the parabola percentage as a function of temperature. The intrinsic line resolution was represented by the observed 514 keV gamma-ray line of ^{85}Sr .

The approximately Gaussian distribution of the annihilation gamma-ray line beyond the Fermi cut-off represents, mainly, the core electron energy distribution, and it is a sum of contributions from different core electrons (Lynn et al,1977). Because of the high potential barriers experienced by positrons in the regions close to nuclei, small contributions arise from annihilations with inner bound electrons having higher momentum distributions. We interpret the narrowing of the Gaussian distribution as being due to the increase in the number of positrons annihilating in trapped state, and is a result of reduced overlap between the positron and inner core electron wave functions in such lattice irregularities. A more detailed discussion on the behaviour of the Gaussian width parameter, illustrated in figure 4.6 , will be given in chapter 5 .

The close agreement between the F-parameter curves and the variation of the parabolic percentages as a function of temperature in 5N and 6N , well annealed specimens of indium indicated no detectable influence due to very small (1 ppm) amounts of impurities.

4.5 Annealing Studies in Deformed Indium

4.5.1.1 Deformation at Room Temperature (Deformed Indium-A)

Two pieces of 99.9999% pure indium, supplied by Koch-Light, were compressed at room temperature into 2.5 mm thick discs with 20 mm diameter, They were etched in dilute nitric acid before and after the compression. Shortly after the final etching approximately 90 μCi of a carrier-free $^{22}NaCl$ positron source was evaporated onto the central region of the two specimen discs which were then pressed in a sandwich configuration and inserted into the low temperature cryostat. The time elapsing between the compression at room temperature and the sample temperature reached below 100 K was just under 5 hours.

4.5.1.2 Deformation Under Liquid Nitrogen (Deformed Indium-B)

Deformation was accomplished using a wide jaw vice. Both the vice and the previously deformed and used 6N indium sample (wrapped in thin aluminium foil) were immersed into liquid nitrogen. The aim was to produce deformation-induced defects. An accurate measure of deformation, at this stage, was not required. After the compression the final disc thickness, measured by a slide calliper in liquid nitrogen, was 1.5 mm (each disc). Therefore, the thickness reduction was estimated as 40% .

Sample loading into the holder took place under liquid nitrogen and subsequently transfered into the vacuum chamber, containing liquid nitrogen. Quickly the screws on the chamber

were tightened and evacuation was initiated. During the time the whole process took place and a vacuum of 10^{-5}torr achieved, the sample temperature was continuously monitored. When the sample was transfered to the cryostat, this action taking two minutes, its temperature rose to a maximum of 130 K before it was cooled down to liquid nitrogen temperature again.

4.5.2 Experimental Measurements

Annihilation line shapes, both in deformed indium-A and deformed indium-B, were measured in the low temperature cryostat over the range 4.2 to 400 K . Measurements in the latter followed the annealing of deformed indium-A for two hours at 400 K and several days at room temperature.

Measurements in either case consisted of successive cycles, each of two and a half hours. Each cycle consisted of half an hour temperature setting and two hours for counting at a total count rate of 5000 cps . The definition of the line-shape parameter F is as in annealed indium. Simultaneous measurements of a control ^{103}Ru 497 keV gamma-ray line has also been instituted.

4.5.3 Data Analysis

Temperature dependence of the line-shape parameter, F, both for deformed indium-A and -B are shown in figure 4.4 . Data A is reversible throughout the whole range and has followed the characteristics of the annealed indium specimen.

The reversibility of data B was observed only in the range up to 113 K in which a small negative slope occurred. Annealing commences above 113 K and complete line-shape recovery is achieved at 180 K , above which the results are identical to the well annealed sample.

In an attempt to understand the amount of annihilation with conduction electrons a model consisting of a Gaussian and an inverted parabola was convoluted, as in the annealed data, with the instrumental resolution, and compared with each of the observed spectra. Temperature dependence of the calculated width parameters of the Gaussian and the parabolic distributions and the parabola percentage in deformed indium-B are shown in figures 4.8 and 4.9 , respectively.

Over the range 4.2 to 400 K the reduced chi-square value (goodness-of-fit) in these model fittings, ranging from 1.2 to 1.6 , were no worse than those in annealed indium.

4.5.4 Discussion

The results in deformed indium-A are in good agreement with the observations reported by Mac Kenzie (1969) and Jackman et al (1974) regarding the absence of room temperature plastic deformation-induced-trapping in indium. This results in the rapid recovery of the effect of deformation, no matter how severe, at room temperature.

We are not aware of any studies performed in indium , deformed under liquid nitrogen. The line-shape parameter in deformed indium-B, shown in figure 4.4 as a function of

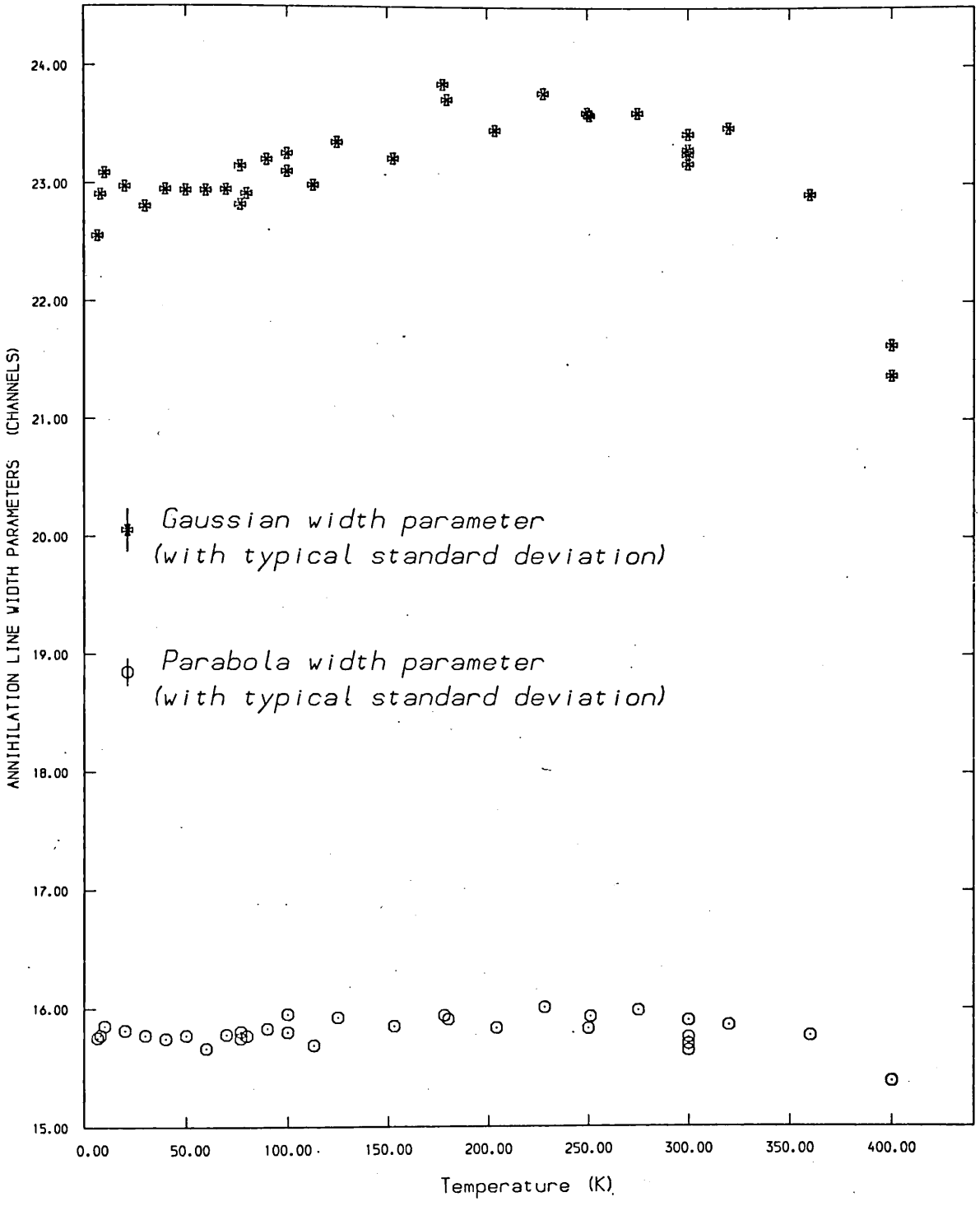

FIG. 4.8 Temperature dependence of the annihilation line width parameters for 6N deformed indium-B .

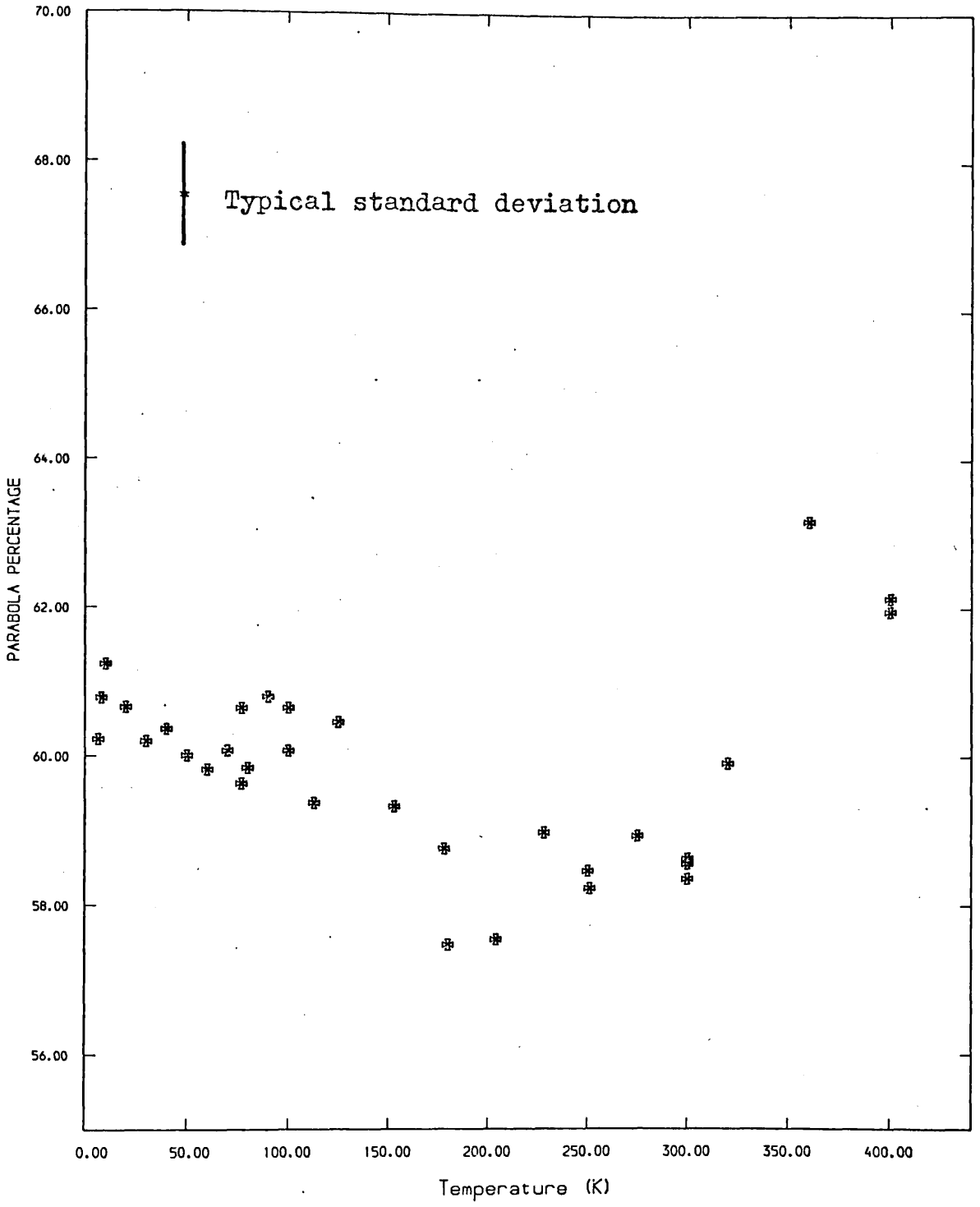

FIG. 4.9 Temperature dependence of the parabola percentage for 6N deformed indium-B .

temperature, illustrates a pronounced effect of deformation. Although 40% deformation in most metals is known to produce high enough concentration of defects to capture all the positrons entering the sample, it is not known whether the saturation trapping occurred because of the transient nature of the sample temperature during evacuation of the cryostat chamber.

Due to the unusual scattering of the points we have not been able to make a satisfactory fit to the data in order to assess the small negative slope over the range 4.2 to 113 K. The absence of a such temperature dependence in the well annealed sample hints at the possibility of annihilation of positrons in the remaining, very small amount of grain boundaries produced by an inadequate annealing of the deformed indium-A specimen. The effect of annihilation of positrons in grain boundaries on the line-shape parameter has been discussed with zinc, will be dealt in detail again in chapter 5 .

Complete recovery (recrystallisation) of the effect of plastic deformation in deformed indium-B occurred below 200 K . Nevertheless, an absolute recrystallisation temperature cannot be determined due to the two-dimensionality of the process. In other words, the time as well as the temperature involvement in the recrystallisation process (Lucke, 1976) .

The model fittings yielded the proportion of annihilations

contributing to the parabolic component of the line shape as a function of temperature, shown in figure 4.9 . As expected, the parabolic percentage diminishes as the deformation-induced defects anneal out. Above 200 K it levels-off at 58% and begins to rise again, following the nature of the annealed sample.

The temperature dependence of the width parameters of the Gaussian and the parabolic components of the annihilation line shapes has been discussed in section 4.3.4 .

CHAPTER 5 POSITRON ANNIHILATION STUDIES IN ANNEALED AND DEFORMED SPECIMENS OF POLYCRYSTALLINE CADMIUM AND IN SINGLE CRYSTAL CADMIUM

5.1 Introduction

Equilibrium measurements of the temperature dependence of the annihilation line shape parameters in many metals show that there are two regions of almost linear slope at temperatures below the vacancy trapping region. This effect is known to vary widely between metals.

In cadmium, measurements extended down to liquid nitrogen temperature and below (Lichtenberger et al, 1975 ; Kim and Buyers, 1976 ; Smedskjaer et al, 1977 ; Herlech et al, 1977 ; Rice-Evans et al, 1978b) have shown the existence of two different slopes, in the pre-vacancy region, exclusively.

Originally, it was thought that (Mc Gervey and Triftshauser, 1973) thermal expansion of lattice might be responsible, but doubt was cast by the discovery in cadmium that the effect disappeared below 200 K . In addition, there are conflicting results as to whether the magnitude of the slope is in agreement with thermal expansion or larger than it (Kim et al, 1974) .

Apart from the value, 0.39 $\pm$ 0.04 eV , reported by Mc Kee et al (1972a) the calculated values of mono-vacancy formation energies in cadmium are not as wide-spread as, for example, in

indium.

Lifetime measurements by Singh and West (1976) yielded a value of 0.47 ± 0.03 eV . Connors et al (1971), who observed an apparent linear temperature dependence of the annihilation parameter between 100 - 300 K in their angular correlation measurements, reported a mono-vacancy formation energy in cadmium as 0.52 ± 0.05 eV .

The positron annihilation technique is valuable in the study of concentration and the nature of lattice defects. For example, Petersen et al (1976) have identified the stages of isochronal annealing in plastically deformed molybdenum on the basis of lifetime and Doppler-broadening data.

The nature of a particular defect will be associated with characteristic values of the parameter F . Hence, the study of changing values of annihilation characteristic parameters in the recovery stages of a defected sample, can indicate the defects involved, and their relative concentrations. For example, Hautojarvi et al (1976) have shown that the traps in deformed iron at room temperature are dislocations.

In principle, one might expect each type of defect to have a characteristic Doppler-broadened line shape ; hence careful analysis of an experimental line into its individual components might reveal the concentrations if more than one type of defect were to be present.

5.2 Positron Annihilation in Polycrystalline Annealed Cadmium

5.2.1 Experimental Measurements

We used polycrystalline samples of 1.6 mm thick and 20 mm diameter cadmium discs of 99.9996% purity (from Johnson-Matthey), which were etched in dilute nitric acid. The annealing consisted of maintaining the specimen discs at 514 K for 23 hours in the high temperature furnace under a vacuum of 10^{-6}torr . These were cooled, slowly, down to room temperature. Following the final etching, approximately 90 μCi of a carrier-free ^{22}NaCl positron source was evaporated directly onto the central regions of the two discs. These two cadmium discs were subsequently arranged in a sandwich configuration, wrapped in a thin aluminium foil and finally inserted into the low temperature cryostat.

Measurements over the range 4.2 to 420 K were performed in the low temperature cryostat and those from room temperature up to the melting point in the high temperature furnace. The sequence of measurements involved temperature changes in both directions. Each run of two hours accumulated about 900 000 counts in the 511 keV peak. The intrinsic resolution at a total count rate of 5000 cps was 1.15 keV for the 514 keV line in ^{85}Sr . The electronic stability was about 1 channel in 8000 . The assessment of the exact position of 511 keV peaks and the definition of the F-parameter were as described in chapter 3 . These, in fact, apply to the other samples as well (except for gold and silver), studied in this work. Simultaneous measurements of a control ^{103}Ru

497 keV gamma-ray line has also been institutad, and a G-parameter (similar in conception to F) has been applied to this line. This has provided an efficient means of electronic stability control.

Figure 5.1 shows the line narrowing parameter F plotted as a function of temperature for the annealed and the two differently deformed specimens of polycrystalline cadmium.

Considering the annealed sample, above 350 K the rise in the parameter F is associated with the creation of vacancies. Below this region an approximately linear slope is observed. At still lower temperatures distinctive behaviour is noticed where the curve flattens at 130 K . At temperatures below 70 K a small but significant, reversible change in the annihilation parameter is observed. A similar but bigger rise than that has been seen in zinc below 50 K .

5.2.2 Line-shape Parameter Analyses

On the basis of several hypotheses, including positron self-trapping, thermal expansion of lattice, and divacancy production, the annealed data points (shown in figure 5.1) have been fitted to the trapping model and the values of the parameters including mono-vacancy formation energies, have been evaluated. Reasonable results were obtained in all cases, and they are shown in table 5.1 .

In the first case above 150 K a linear rise in F was accept: (expressed in equation (3.2) with $\alpha = 0$) .

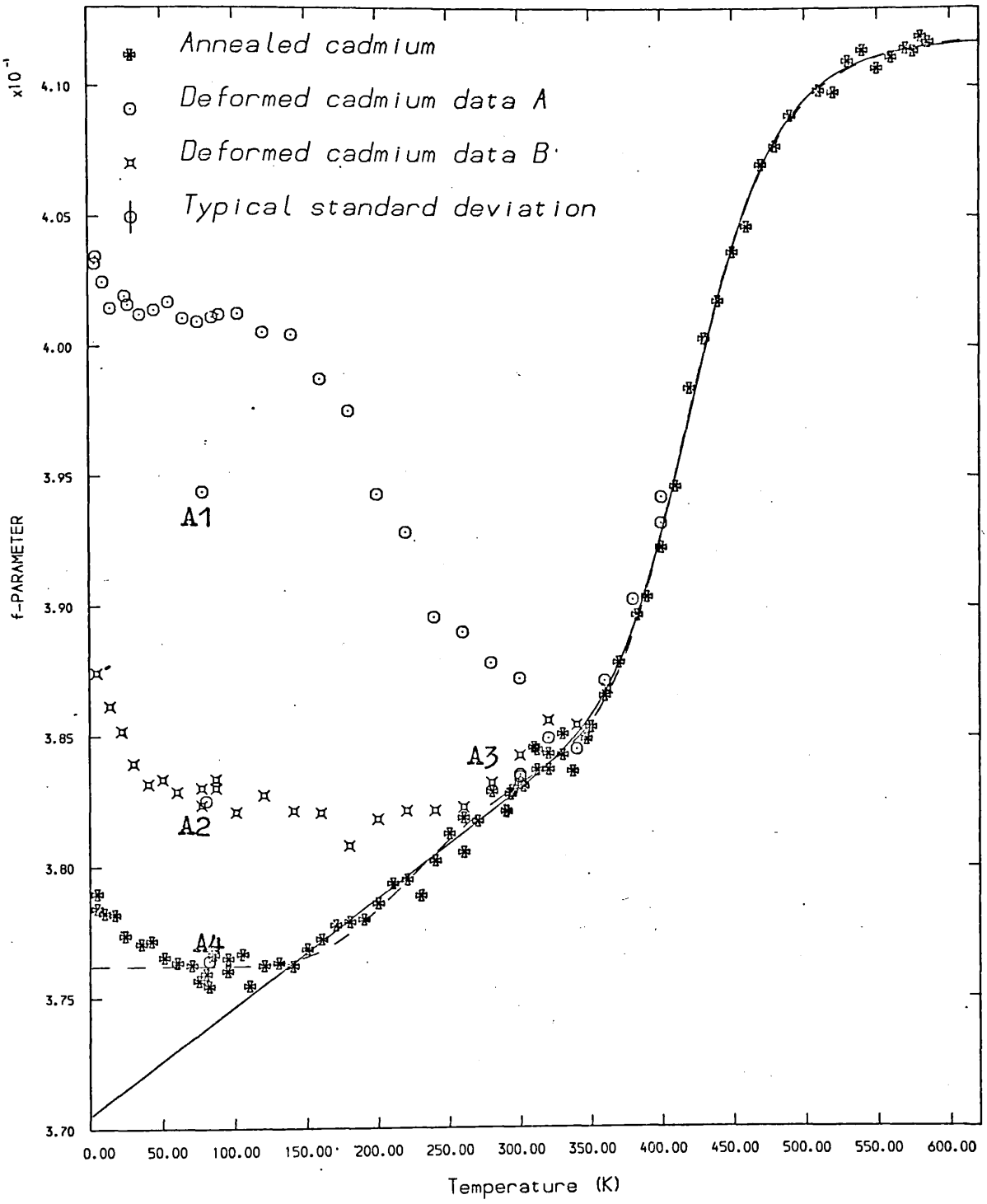

FIG. 5.1 The variation of the line-shape parameter F as a function of temperature for the annealed and the two deformed specimens of polycrystalline cadmium. The solid and the broken lines represent the linear rise and the self-trapping model fittings, respectively, outlined in the text.

	Analysis	E_{1v} (eV) (± 0.02)	F_f^o	F_{1v}	A_{1v} ($x10^5$)	β ($x10^{-5}$)	$E(K_o)$	F_{st}	B ($x10^4$)	χ^2/ν (69 points)
1	Mono-vacancies plus linear rise above 150 K	0.56	0.3705	0.4118	32.9	11.1	....	.....	....	1.40
2	Mono-vacancies plus linear rise plus divacancies above 150 K	0.60	0.3703	0.4108	125.2	11.5	....	.....	....	1.22
3	Mono-vacancies plus self-trapping	0.54	0.3762	0.4120	21.14	...	0.123	0.3886	76.14	1.15
4	Mono-vacancies plus divacancies plus self-trapping	0.56	0.3752	0.4112	52.52	...	0.129	0.3892	66.4	1.16

Additional parameters : For case 2 ; F_{2v}=0.4321 , A_{2v}=156.4 $x10^8$, E^B_{2v}=0.100 eV .
For case 4 ; =0.4163 , =213.6 $x10^8$, =0.064 eV .

TABLE 5.1 The results of fittings the parameter F according to several theoretical models.

The second case was similar to the first, except that divacancies were sought in addition to mono-vacancies (expressed in equation (4.4) with $F_f = F_f^o(1 + \beta T)$) .

In the third case, evidence for self-trapping (equation (3.3)) was sought.

Finally, in the fourth case, both self-trapping and divacancies were allowed for where we consider equation (4.4), with $F_f = (F_f^o + (F_{st}-F_f^o)/(1 + B^{-1} T^{1.5} \exp(E(K_o)/kT))$.

The cases 1 and 3 , i.e.,the linear rise and self-trapping model fittings, respectively, are both illustrated in figure 5.1 . Figures 5.2 and 5.3 illustrate the different contributions to F calculated with the parameters obtained from curve fittings in cases 1 and 3 , respectively.

In cases 2 and 4 , which include provisions for divacancies, the estimated ratios of divacancies to mono-vacancies near the melting point are 7.1% and 24.6% , respectively.

5.3 Annealing of Deformed Cadmium Samples

Two plastically deformed polycrystalline cadmium samples were prepared. First, the previously used annealed cadmium sample received a 30% compression at room temperature to become deformed cadmium-B. The second received an approximately 5% thickness reduction at 77 K to become deformed cadmium-A ; care was taken to ensure the sample did not rise in temperature above 115 K while being swiftly transfered to the cryostat.

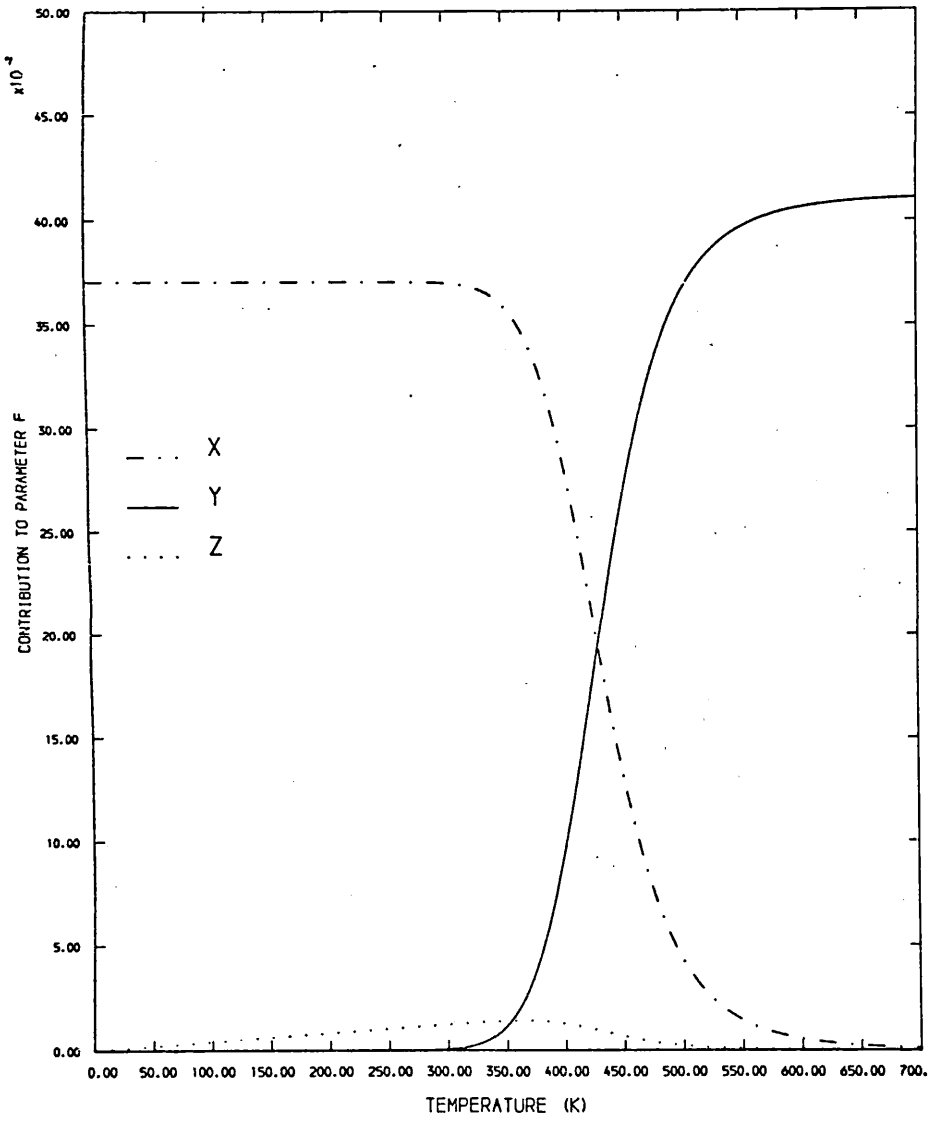

FIG. 5.2 Different contributions to F from linear rise fitting. Curves X, Y, and Z represent $F_f^o P_f$, $F_{1v} P_{1v}$ and $F_f^o \beta T P_f$, respectively.

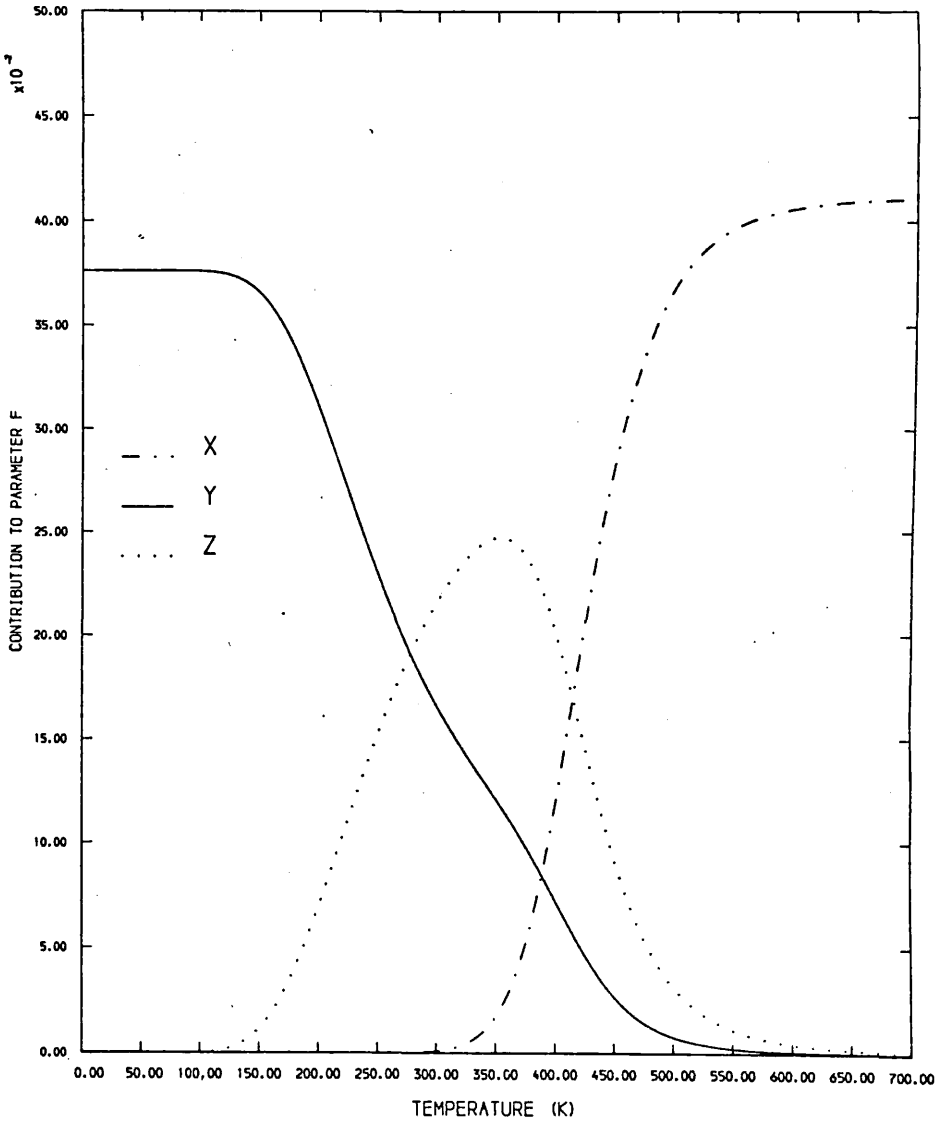

FIG. 5.3 The different contributions to F from the self-trapping fit. Curves X, Y and Z represent $F_{1v} P_{1v}$, $F_f^o (1-P_{st}) P_f$ and $F_{st} P_{st} P_f$, respectively.

At each temperature setting (consisting of half an hour), the analiser accumulated pulses from the detector over a period of two hours. The counting rates, electronic stabilities, assessments of the exact position of 511 keV peaks, and the definition of F-parameters were as described in annealed cadmium.

Figure 5.1 shows the temperature dependence of the line-shape parameter F for the two deformed cadmium specimens. As in the annealed cadmium the deformed samples, as well, show the distinctive, reversible line narrowing as liquid helium temperatures are approached.

In cadmium specimen (A) the region from 40 K to approximately 130 K shows no apparent change due to annealing. At about 150 K a small effect on F , due to annealing, is observed. Above 160 K the rate of annealing increases, and the F curve continues to decline up to 320 K ; thereafter the results are identical to the well annealed sample. Sharp et al (1965), who carried out isochronal annealing electrical resistivity work on deformed cadmium, demonstrated that the stage between 200 K and 300 K involves dislocation rearrangements. They have, also, stated that a full recovery occurs above 70 ^{o}C . Points (A3) and (A4) , shown in figure 5.1 , were taken immediately after the point at 400 K which illustrate a complete annealing of the deformation effect at this temperature.

Looking at the deformed specimen (B) data, it seemed obvious that a partial annealing had taken place prior to inserting it

into the cryostat.

5.4 Line Shape Model Fittings

The line shapes, both for the annealed and the deformed specimens of polycrystalline cadmium, were fitted with the model, consisting of the superposition of a Gaussian and an inverted parabola convoluted with the approprite intrinsic resolution functions. Figure 2.7 illustrates an application of this technique to an annealed cadmium line.

In the annealed cadmium the Gaussian width parameter, shown in figure 5.4 , is constant at low temperatures but at 150 K it starts to decline. This continues over the pre-vacancy region until 330 K when the slope steepens in the vacancy region. At the highest temperatures we have evidence of a flat valley. A very small change in the parabola width occurs at high temperatures. This probably is due to contraction of the Fermi surface as a result of thermal lattice expansion (Kittel, 1971) .

Figure 5.5 shows the parabolic percentage ; it rises from a low point of 38% at 100 K to about 40% at 350 K ; thereafter we see a steeper rise due to vacancies with a plateau of 44% near the melting point.

It is tempting to belive that the width of the Gaussian component characterises the nature of the defect. In figure 5.4 we see that the Gaussian width for the annealed sample in the region of 77 K is 22.8 , and the value drops

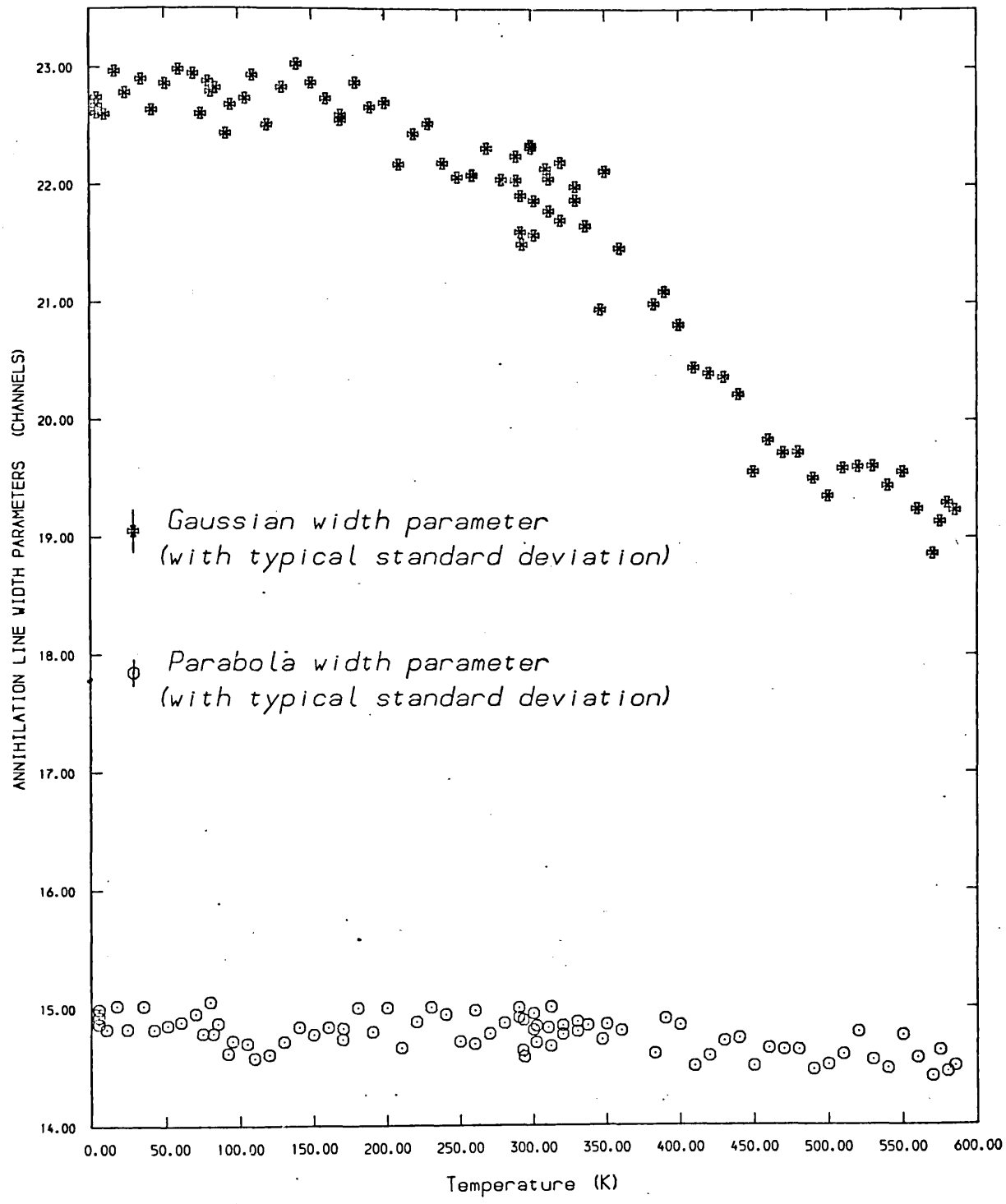

FIG. 5.4 The variation of the width parameters of the Gaussian and the parabolic components of individual lines for polycrystalline annealed cadmium as a function of temperature.

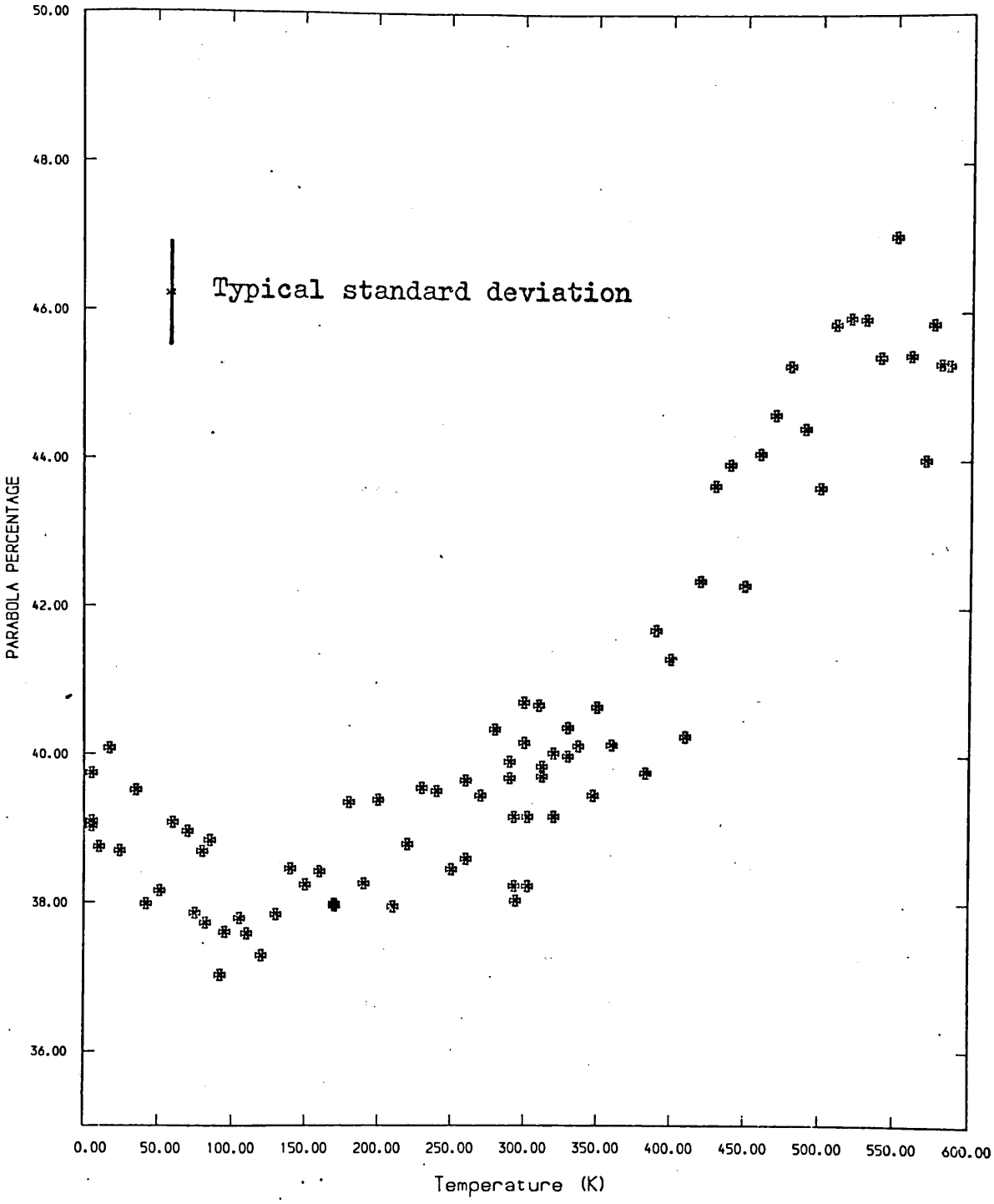

FIG. 5.5 The temperature dependence of the proportion of the annihilations contributing to the parabolic component of the line shape for polycrystalline annealed cadmium.

to about 19.2 corresponding to vacancies near the melting point. In contrast, the defects of the deformed data-A at 77 K give a Gaussian width parameter about 21.2 . The above mentioned Gaussian width parameter σ_G , as expressed in equations (2.5) and (2.6) , actually corresponds to $\sqrt{2}\sigma$ where σ is the known width of a Gaussian distribution.

Rice-Evans et al (1978b) have found that the defects of data-A, shown in figure 5.1 , rapidly annealed out or changed their structure in the region of 250 K , and they argued that majority trapping in a different (second) type of defect began. This conclusion is supported by the data of figure 5.6 : at 250 K a rapid change occurs and the new, dominant defect type exhibits a mean Gaussian width of 22.3 . The argument agrees with the data-B in figure 5.7 . In this sample compression took place at room temperature, and defects of the first type disappeared before the insertion to the cryostat. We suggest defects of the second type then become the major trapping agents ; and indeed in figure 5.7 we see an average Gaussian width of 22.3 up to 250 K .

The goodness of the fits in the deformed specimens were as good as those in the annealed cadmium in the same temperature ranges. Figure 5.8 illustrates the application of the convolution technique to a deformed cadmium-A line at 100 K .

The proportions of the annihilations contributing to the parabolic component of the line shapes for deformed-A and deformed-B specimens of polycrystalline cadmium are shown in

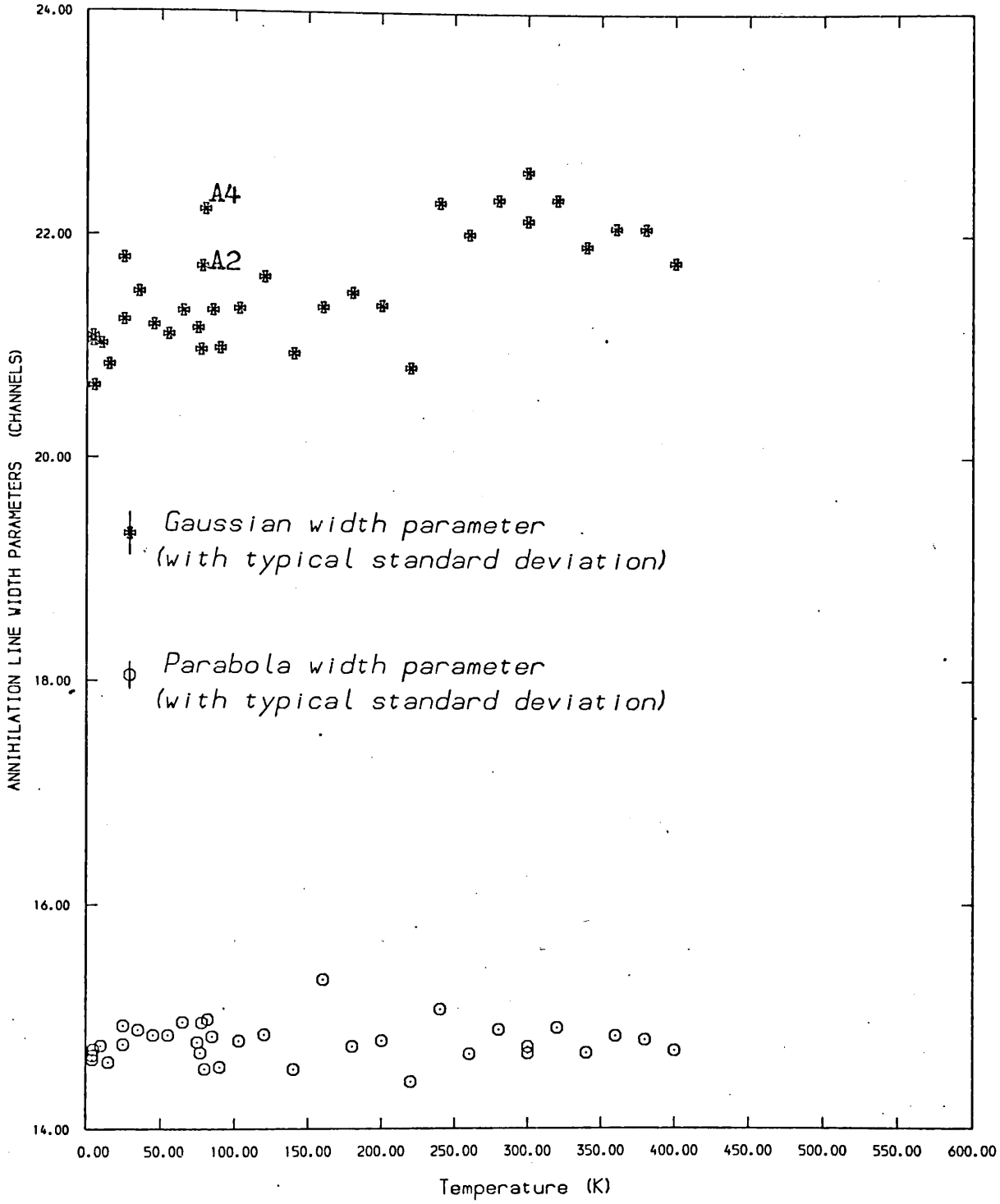

FIG. 5.6 The variation of the width parameters of the Gaussian and the parabolic components of individual lines for deformed cadmium-A as a function of temperature.

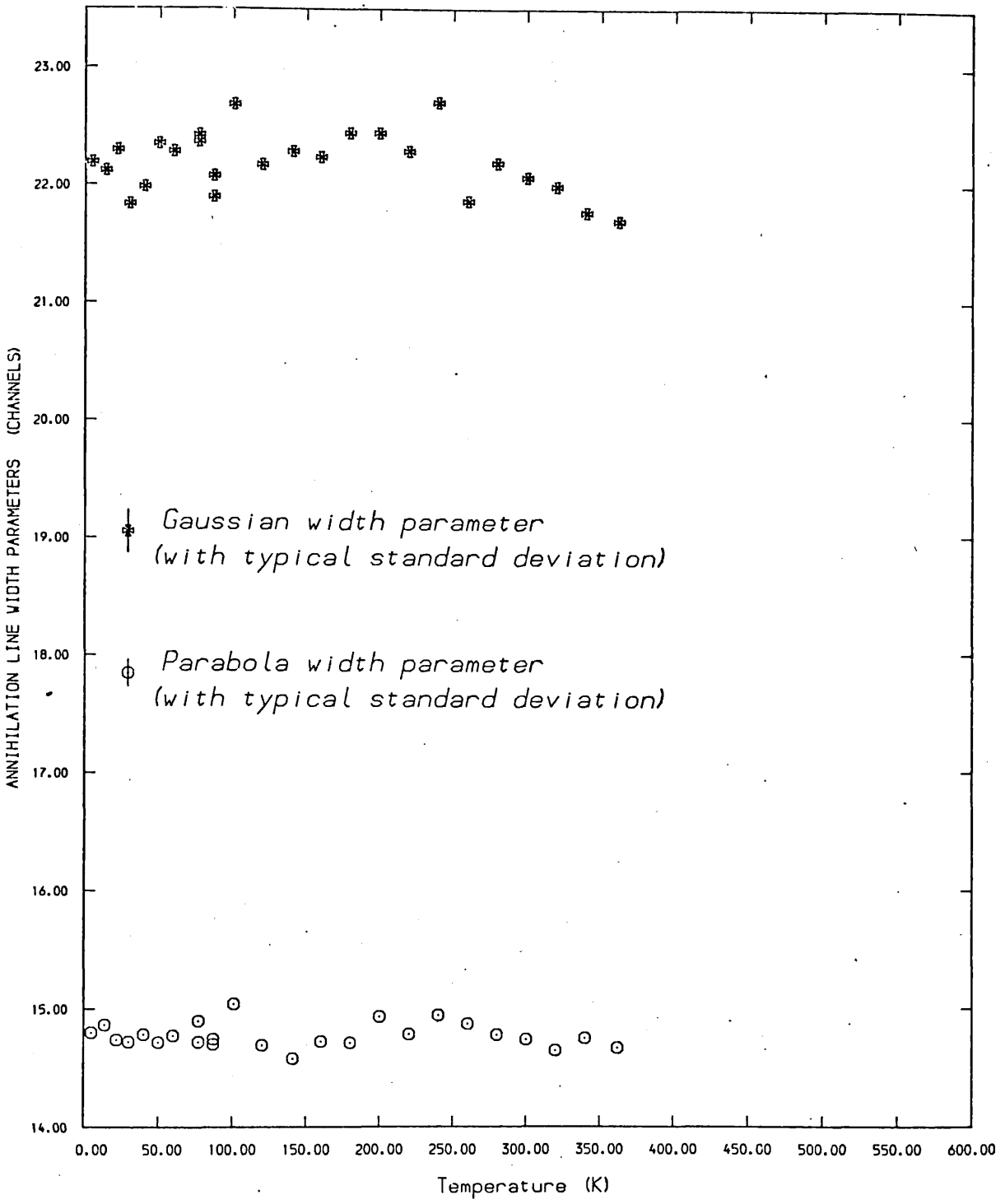

FIG. 5.7 The variation of the width parameters of the Gaussian and the parabolic components of individual lines for deformed cadmium-B as a function of temperature.

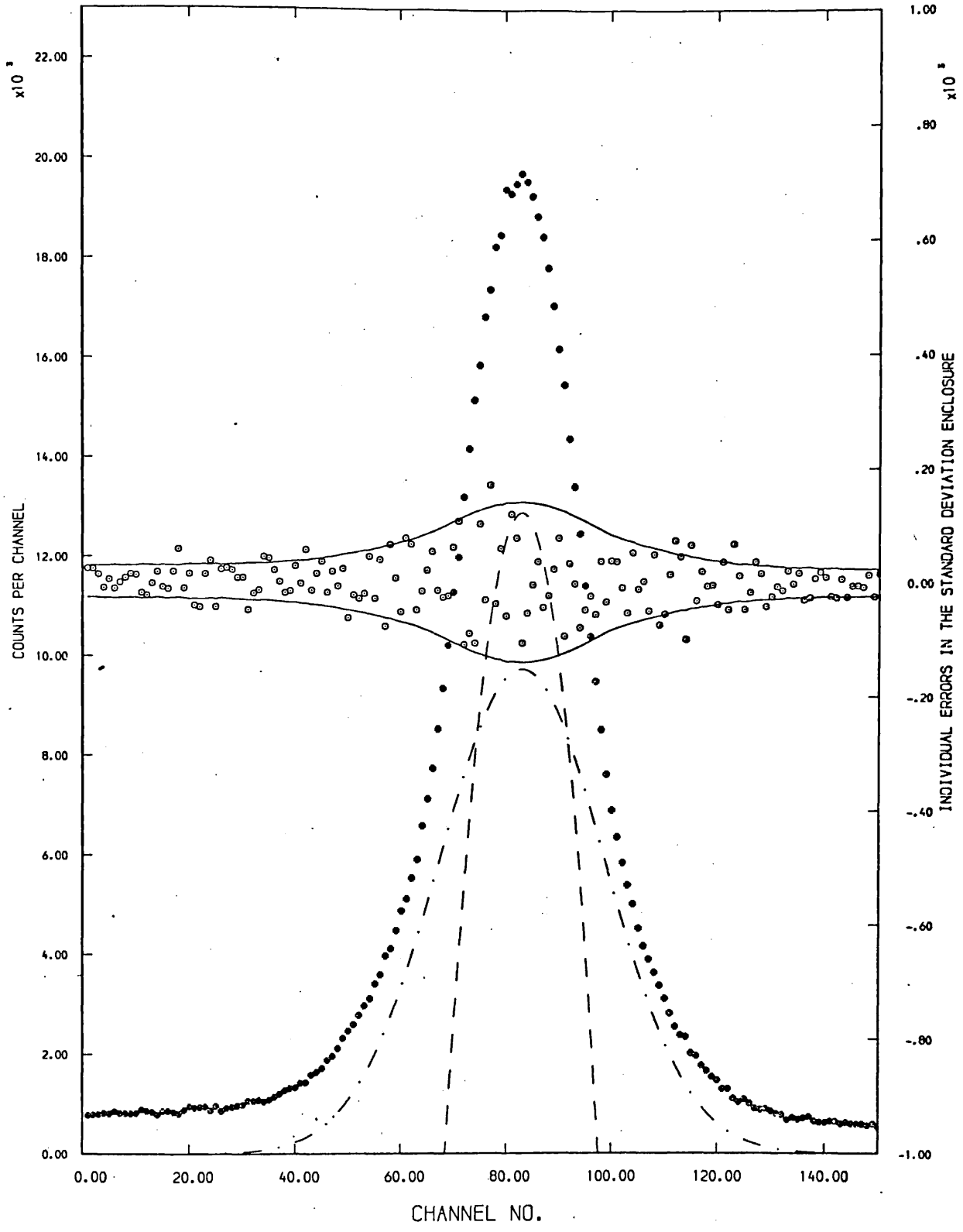

FIG. 5.8 Application of the convolution technique to separate the two components of the annihilation gamma-ray line in deformed cadmium-A at 100 K .

figures 5.9 and 5.10 , respectively. In the specimen (A) the percentage of parabolic component, approximately 47.5% at 50 K , declines to about 40% at 300 K ; thereafter we see it begins to rise again due to annihilation of positrons in thermally generated vacancies. Unlike the specimen (A), in deformed cadmium-B the variation of the parabolic percentage as a function of temperature is gentle. Over the range 50 K to just under 300 K it decreases by less than 1% . The agreement between the annealed and two deformed specimens of cadmium in the region of 300 K is remarkable.

5.5 Discussion of Results

The steep pre-vacancy slope (dF/dT) of annealed cadmium in the range 100 - 350 K is recognised as being extraordinary. Compared with the linear thermal lattice expansion coefficient in this region (30×10^{-6} K^{-1}) the slope (β) , quoted in the cases 1 and 2 in table 5.1 , is huge. This, at least for the case of cadmium, shows the weakness of the hypothesis, which makes the assumption that the pre-vacancy slope is essentially concerned with the free positrons in the lattice and is also due to changing electron densities as a result of thermal lattice expansion.

Among the fittings, based on several hypotheses, the self-trapping model (case 3) has resulted in the best fit. Although, this model seems superior, as far as cadmium is concerned, it still seems inadequate to fulfill all the requirements. These will be discussed in length in section 6.4 of this chapter, when the single crystal cadmium data will be

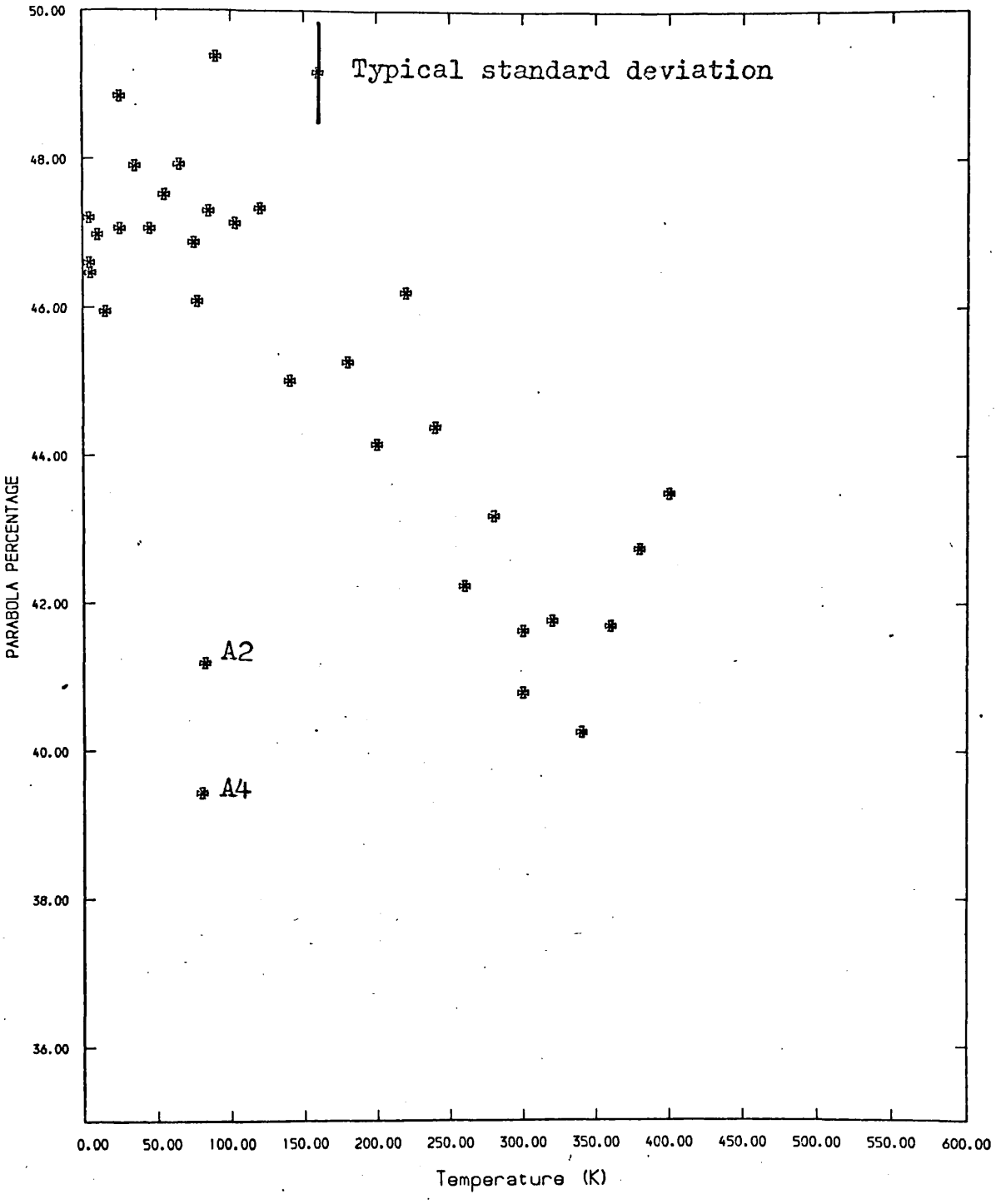

FIG. 5.9 The percentage of parabolic component in deformed cadmium-A .

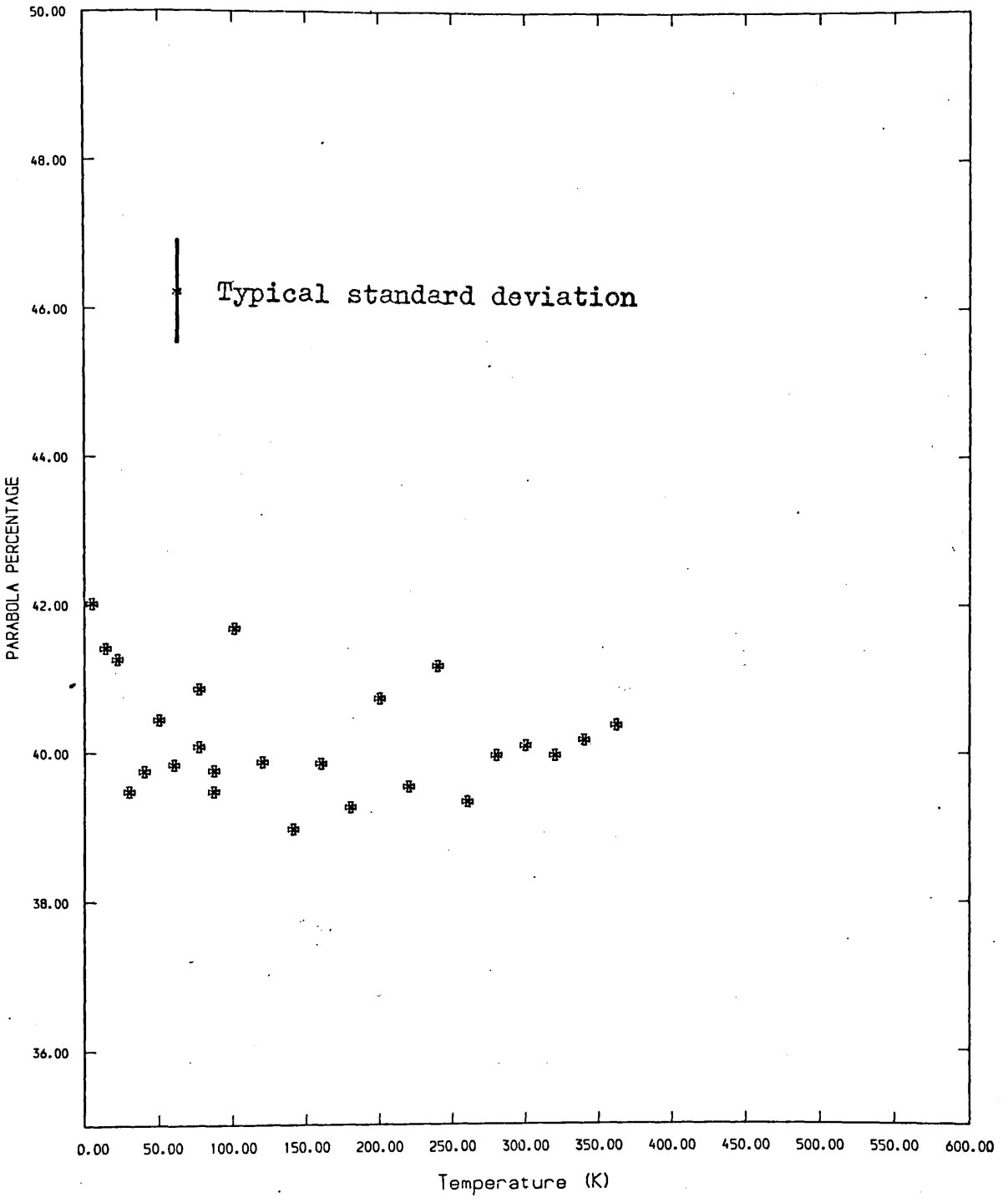

FIG. 5.10 The percentage of parabolic component in deformed cadmium-B .

considered.

The rise in F-parameter in the liquid helium temperature regime, both in the annealed and the deformed specimens of polycrystalline cadmium, is, without a doubt, significant. A similar effect in annealed cadmium and gold specimens have also been observed by Herlach et al (1977) but not in their electron-irradiated gold specimen. The preliminary discussion on this matter have already been presented for the case of zinc (chapter 3) . At this stage there is not much to be added to what has already been said, apart from that which have been extracted from the extended measurements in cadmium: First, the nature of grain boundary defects are very much like those encountered by a detrapped positron and, secondly, their concentrations, especially in the annealed specimens of zinc and cadmium were not as high as those in deformed zinc and deformed cadmium-B specimens, respectively.

An important question, both for zinc and cadmium, is whether or not the low temperature rise in F has the same cause in both annealed and deformed specimens. In this event, one must beware because equations of the type $F=PF_1 + (1-P)F_2$ are normally invoked (Rice-Evans et al, 1976a) . Similar magnitudes of change in F imply quite different trapped proportions.

The temperature dependence of F in the liquid helium temperature regime will be discussed again in section 6.4 of this chapter, when the single crystal cadmium data will be considered.

The deformed cadmium specimen (A) probably was kept below its recrystallisation temperature and, hence, little annealing would be expected. The data of this specimen is specially informative. Apart from the rise in F below 25 K , one sees a flat F for 25 - 130 K implying a temperature independent positron trapping rate. Point A1 in figure 5.1 was taken immediately the point at 200 K ; the fact that they both have the same F suggests again a constant trapping rate for a smaller concentration of defects. Point A2 followed the point at 320 K . This is remarkable. Even though the deformed-A , 320 K F-parameter value virtually equals the annealed 320 K F value, the large value of F(A2) at 77 K indicates that a high proportion (perhaps greater than 70%) of positrons are still trapped in defects. This suggests two distinct types of trap ; one with F=0.401 and the other with F between 0.382 and 0.386 . Perhaps, each type might be a mixture of different traps. It is not possible to say whether, in the annealing process that one type of trap, giving the value F=0.401 , changes into the other, or whether they both present after the deformation, and that the F=0.401 traps dominate.

In figure 5.11 two annihilation lines, one at 80 K and the other 580 K , in annealed cadmium are compared. As expected (from the trapping model) the line at 580 K is considerably narrower than the one at 80 K , and the solid line represents the deviation between these two normalised lines on an enlarged scale. Similar comparisons of the two individual components, i.e., the Gaussian and the parabola of these two

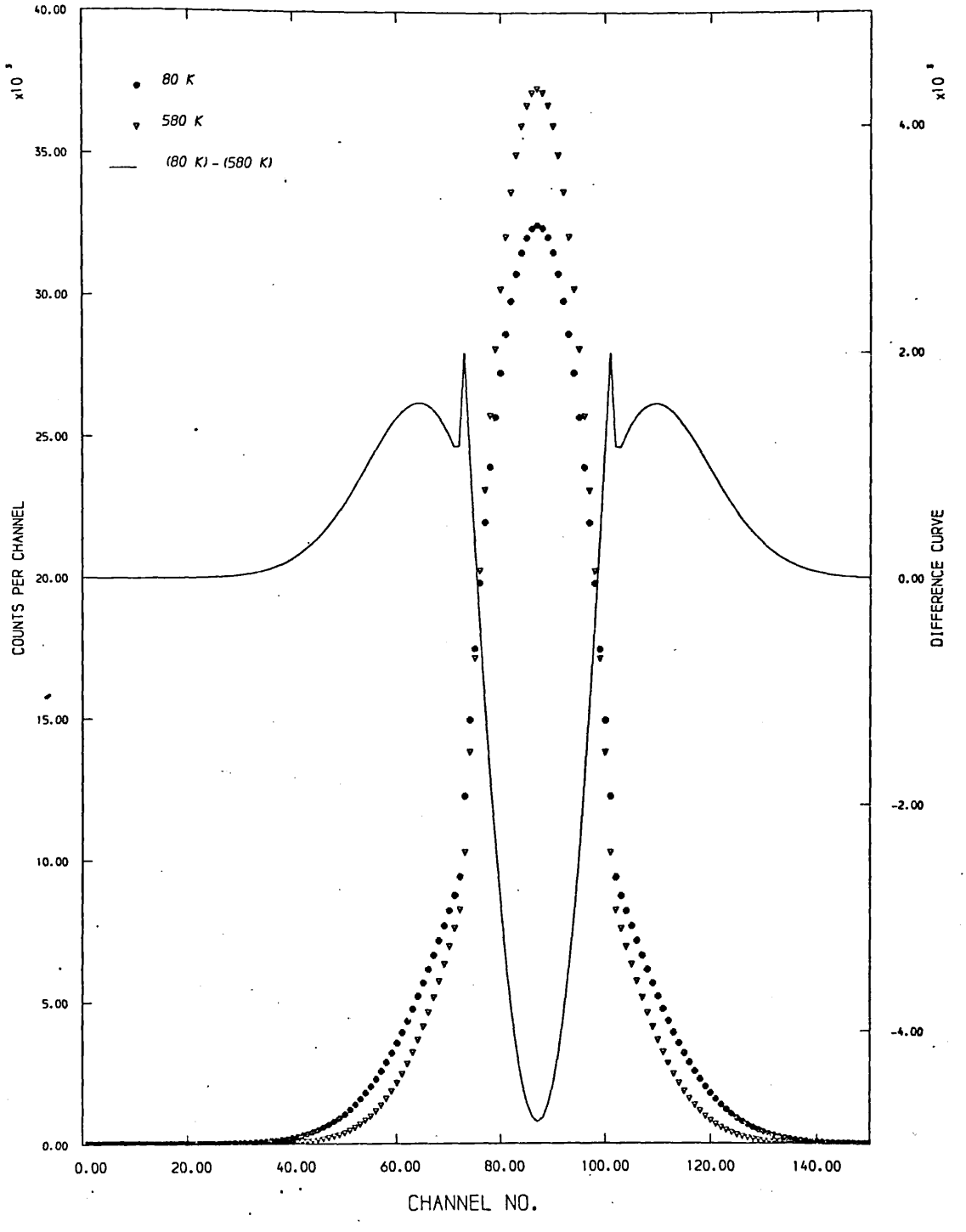

FIG. 5.11 Annihilation line shapes in polycrystalline annealed cadmium at two different temperatures. The solid line represents the deviation between the two lines on an enlarged scale.

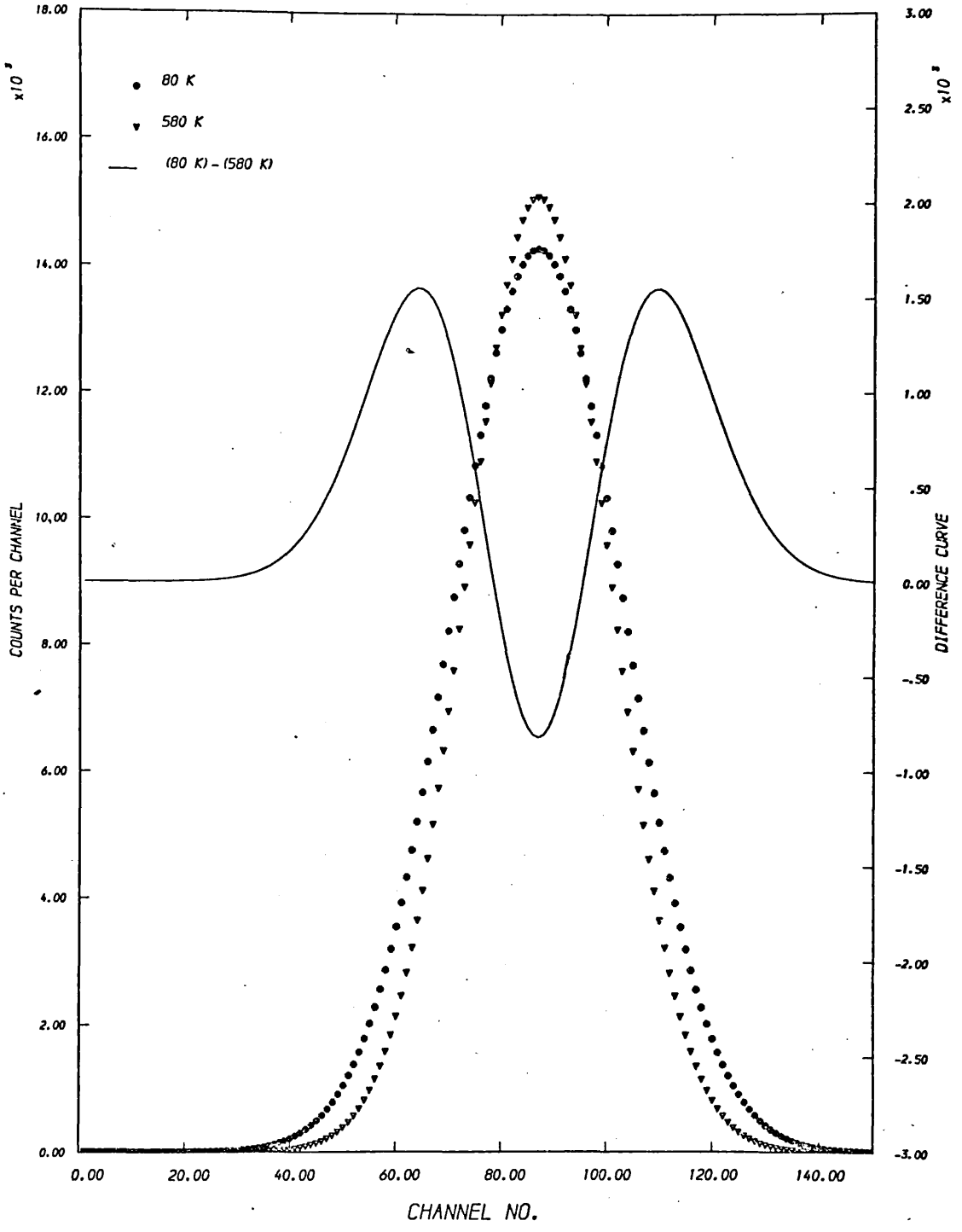

FIG. 5.12 Comparison of the Gaussian components of the two lines showh in figure 5.9 .

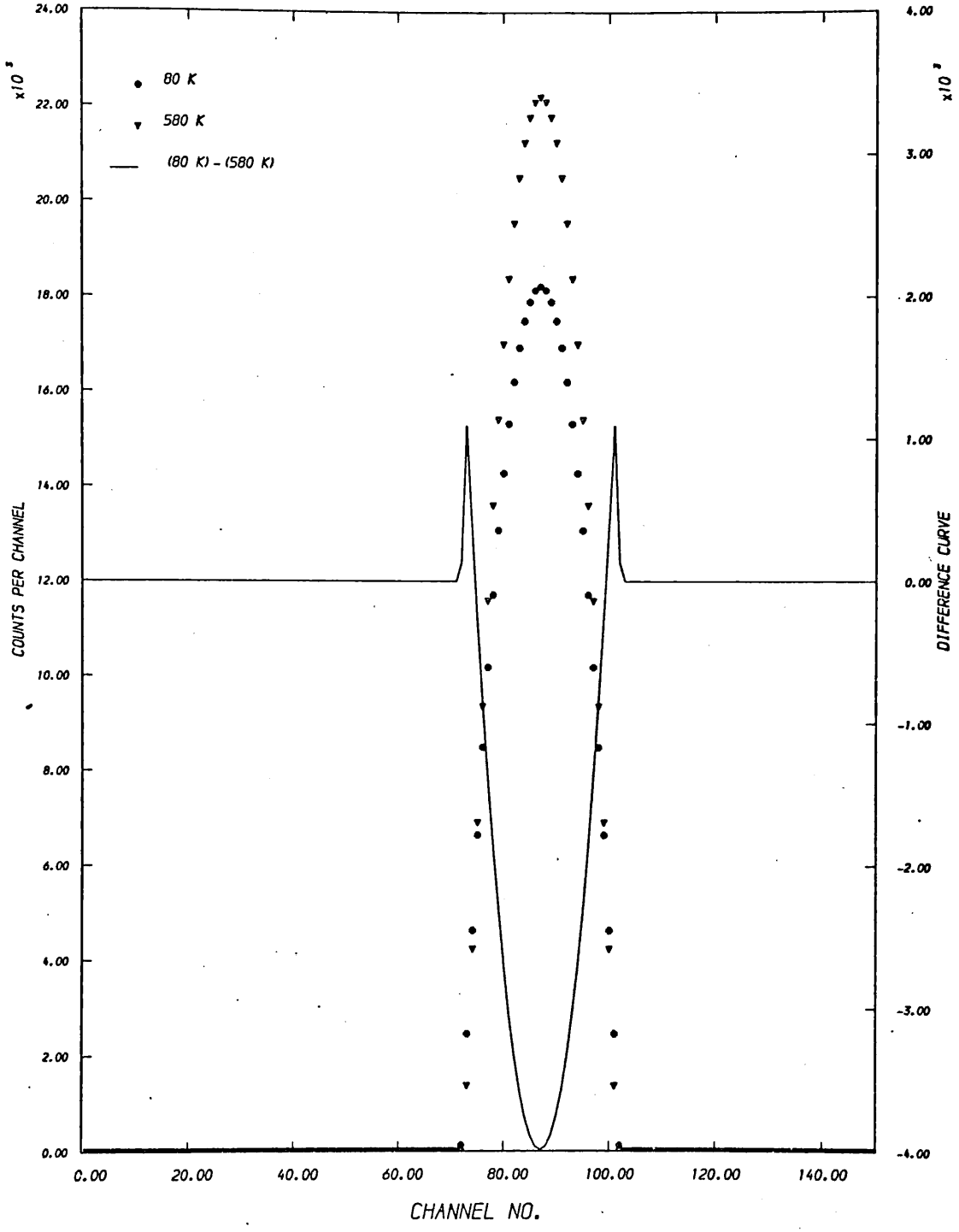

FIG. 5.13 Comparison of the parabolic components of the two lines shown in figure 5.9 .

lines, are shown in figures 5.12 and 5.13 , respectively. These merely strengthen the discussion given in chapter 4 , concerning the effect of reduced overlapping of the positron wave function with the inner core electron wave functions once it gets trapped in a defect. One might assume that this effect depends on the type of defect.

The ability to distinguish different types of defects and their concentrations will, undoubtedly, considerably extend the potential use of the positron annihilation technique in metallurgical studies.

5.6 Positron Annihilation Studies in Single Crystal Cadmium

Two 1.5 mm thick and 10 mm diameter discs of single crystal cadmium were spark cut from a 99.9999% pure rod, supplied by Metals Research Ltd . The main crystallographic axis was along the axis of the rod. The etchant was dilute nitric acid. Immediately after the etching the two discs were electropolished, using 45% concentration orthophosphoric acid as the electrolyte and a carbon rod as the cathode.

After the electropolishing the final sample thickness was 1.1 mm . The positron source, approximately 90 μCi , of a carrier-free ^{22}NaCl solution, was evaporated directly on to a central region, of 1.5 mm diameter, on one side of each of the discs. The sample, in a sandwich configuration, was then wrapped in a thin aluminium foil and mounted in the low temperature cryostat. Throughout the whole process utmost

care was taken to prevent any damage which might be detrimental to the crystal.

5.6.2 Measurements

The line shapes were recorded with the spectroscopy system, described in chapter 2 , in a series of measurements identical to those in the polycrystalline cadmium specimens.

5.6.3 Data Analyses

5.6.3.1 F-parameter Analysis

Analyses, similar to those carried-out in the annealed polycrystalline cadmium for the cases 1 and 3 , were performed on the measurements on single crystal cadmium. The results of these two fittings, based on two different hypotheses, as in the polycrystalline case, are not in agreement. The best values of the parameters are given below.

The linear rise fit :

E_{1v} = 0.46 ± 0.02 eV F_f^o = 0.3721

F_{1v} = 0.4139 A = 22.85 x10^4

β = 15.6 x10^{-5}

where the goodness-of-fit (χ^2/ν) gives the value 1.44 .

The self-trapping fit :

E_{1v} = 0.40 ± 0.02 eV F_f^o = 0.3803

F_{1v} = 0.4147 A = 6.3 x10^4

$E(K_o)$= 0.13 F_{st} = 0.3932 B = 17.87 x10^5

where the goodness-of-fit (χ^2/ν) gives the value 1.16 .

The best fitted lines, derived from the parameters given above, are illustrated in figure 5.14 .

5.6.3.2 Convolution

Although, high precision measurements of the angular correlation of annihilation radiation from single crystals have proved to be capable of showing marked anisotropies (Chiba and Tsuda, 1974 ; Cushner et al, 1970), our instrumental resolution is not precise enough to distinguish between different orientations.

The convoluted model fittings have been described in section 4 of this chapter. Temperature dependence of the resulting line width parameters and the parabolic percentage are shown in figures 5.15 and 5.16 , respectively.

The change in the Gaussian and the parabola width parameters as a function of temperature are comparable with those of polycrystalline annealed cadmium. On the other hand, the variation of the parabolic percentage with temperature is more steeper in single crystal cadmium than the polycrystalline annealed specimen of cadmium. Nevertheless, this difference between the slopes of the single and the polycrystalline specimens of cadmium is more or less along the lines of the F-parameter variations. In addition,it is difficult to understand the enhancement of the parabolic percentage in the single crystal.

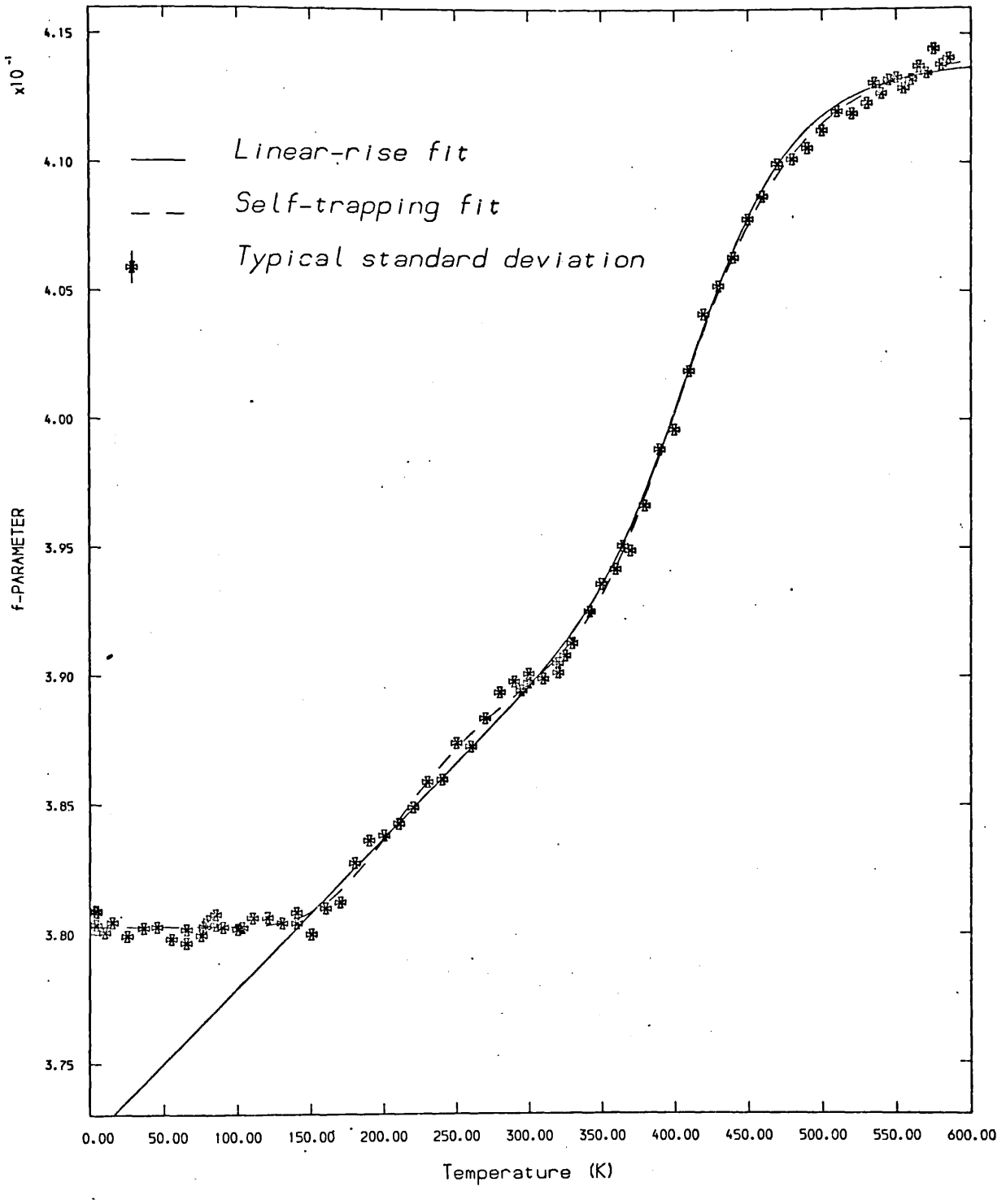

FIG. 5.14 The variation of F-parameter with temperature for single crystal cadmium.

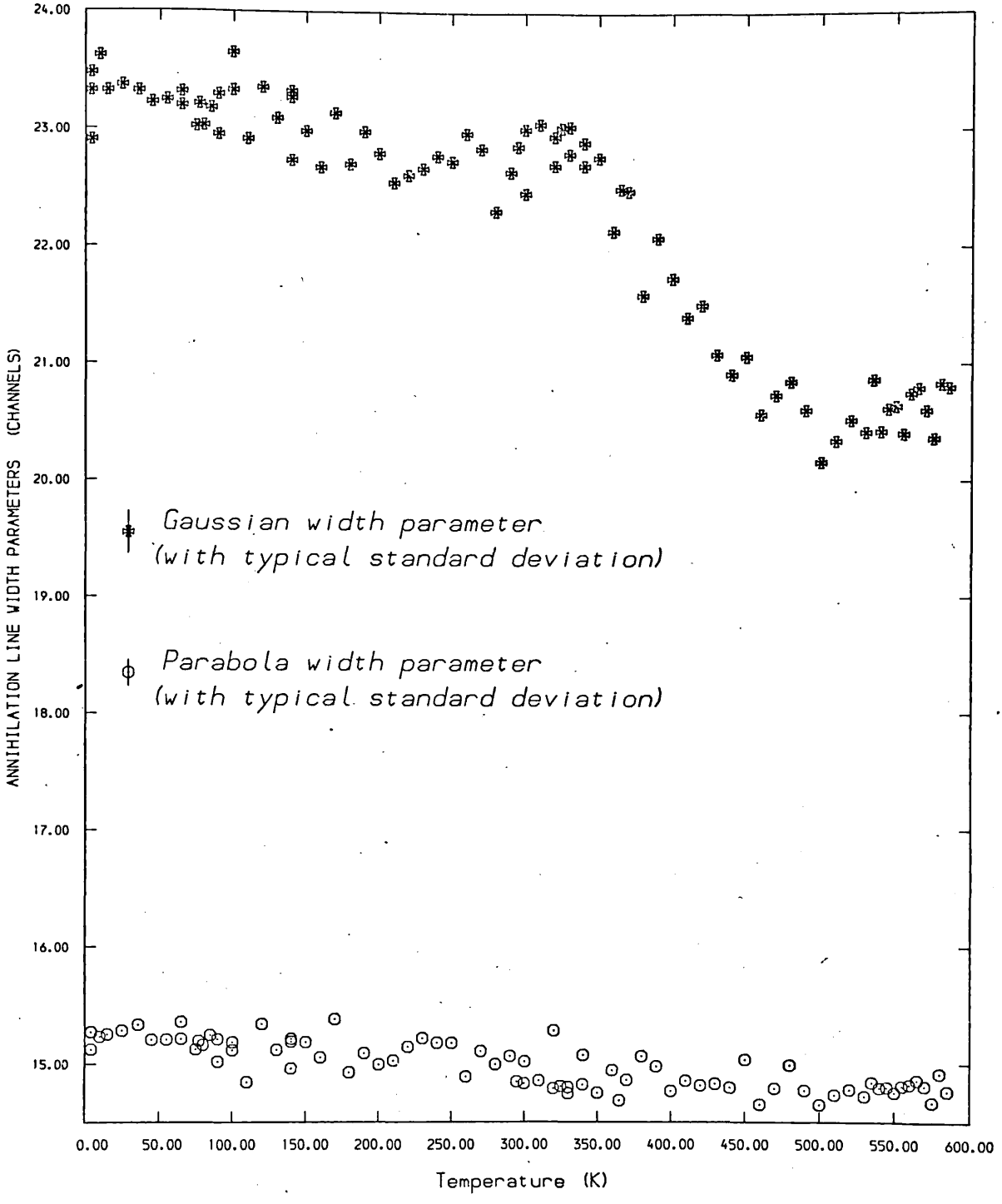

FIG. 5.15 Temperature dependence of the width parameters of the Gaussian and the parabolic components of individual lines for single crystal cadmium.

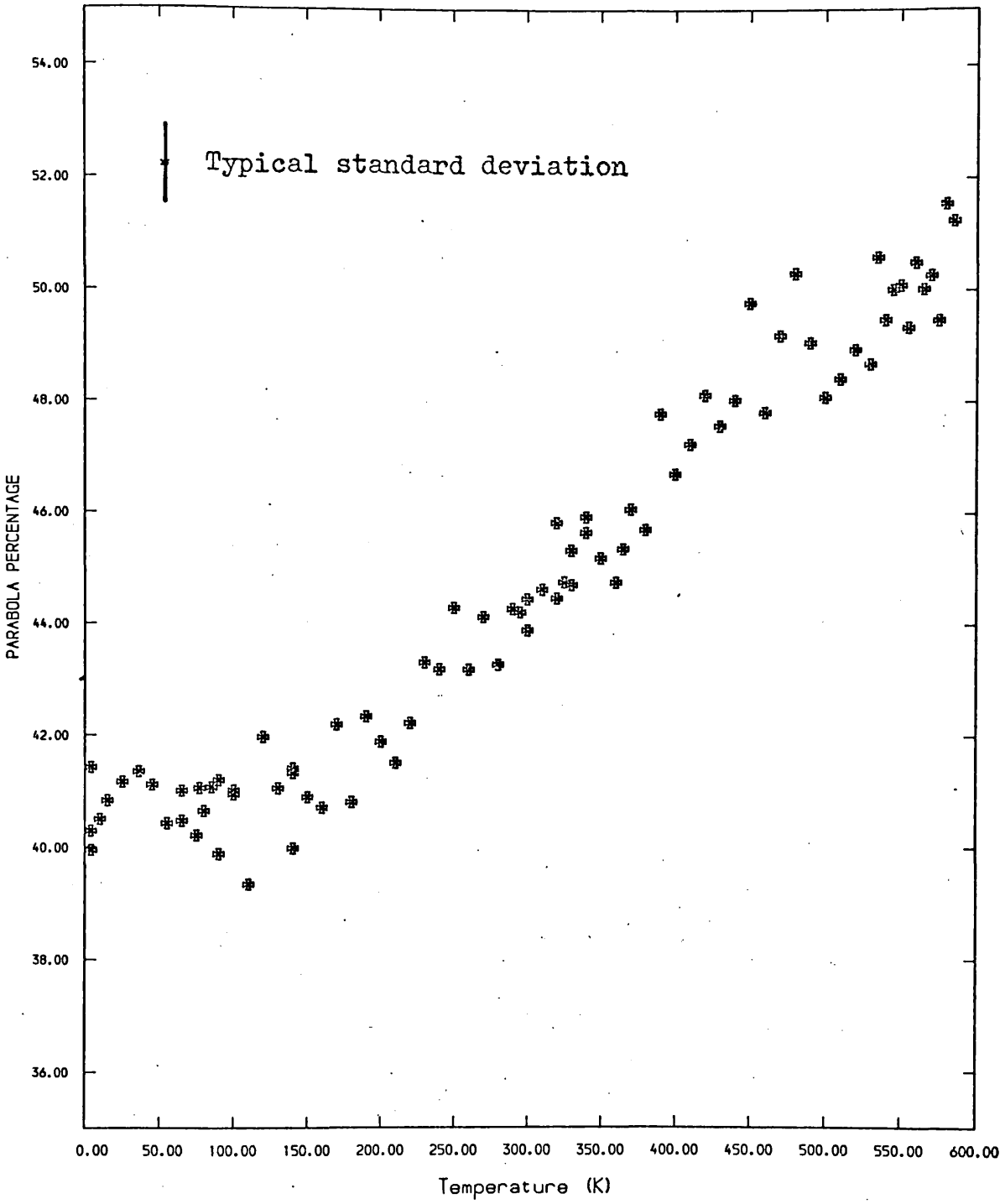

FIG. 5.16 The proportion of the annihilations contributing to the parabolic component of the line shapes for single crystal cadmium, as a function of temperature.

5.6.4 Discussions

Among the six metals studied in this work cadmium is the only one which shows the existence of two prominently different temperature dependencies of the annihilation parameter in the sub-vacancy regime. Indeed is the only one in which the self-trapping model fitting has resulted a distinctively better fit than its alternative fit, the linear rise model. Nevertheless, the inadequacies of the former cannot be escaped, even, by eye. This is seen in figure 5.17 , which shows an enlarged version of the central portion of figure 5.14 with the self-trapping model fit only. The circles in figure 5.17 represent a second set of data points, which were taken on the same sample. The consistency of the plateau between 280 K and 310 K on both sets is remarkable. As positron annihilation data become statistically more reliable it is obvious that a more sophisticated theoretical description to take account of the temperature dependence of the annihilation parameters, observed in the region before the onset of vacancy effect, is needed (for a recent review, see Stott and West, 1978) .

It is belived that the improper definition of the pre-vacancy temperature dependence may be the root of the discrepancies between the values of mono-vacancy formation energies.

The reversibility of the temperature dependence of the line-shape parameter throughout the full range was repeatedly checked to ensure that the single crystal specimen was defect-free within the precision of our measuring technique. Therefore, the argument concerning positron trapping at grain

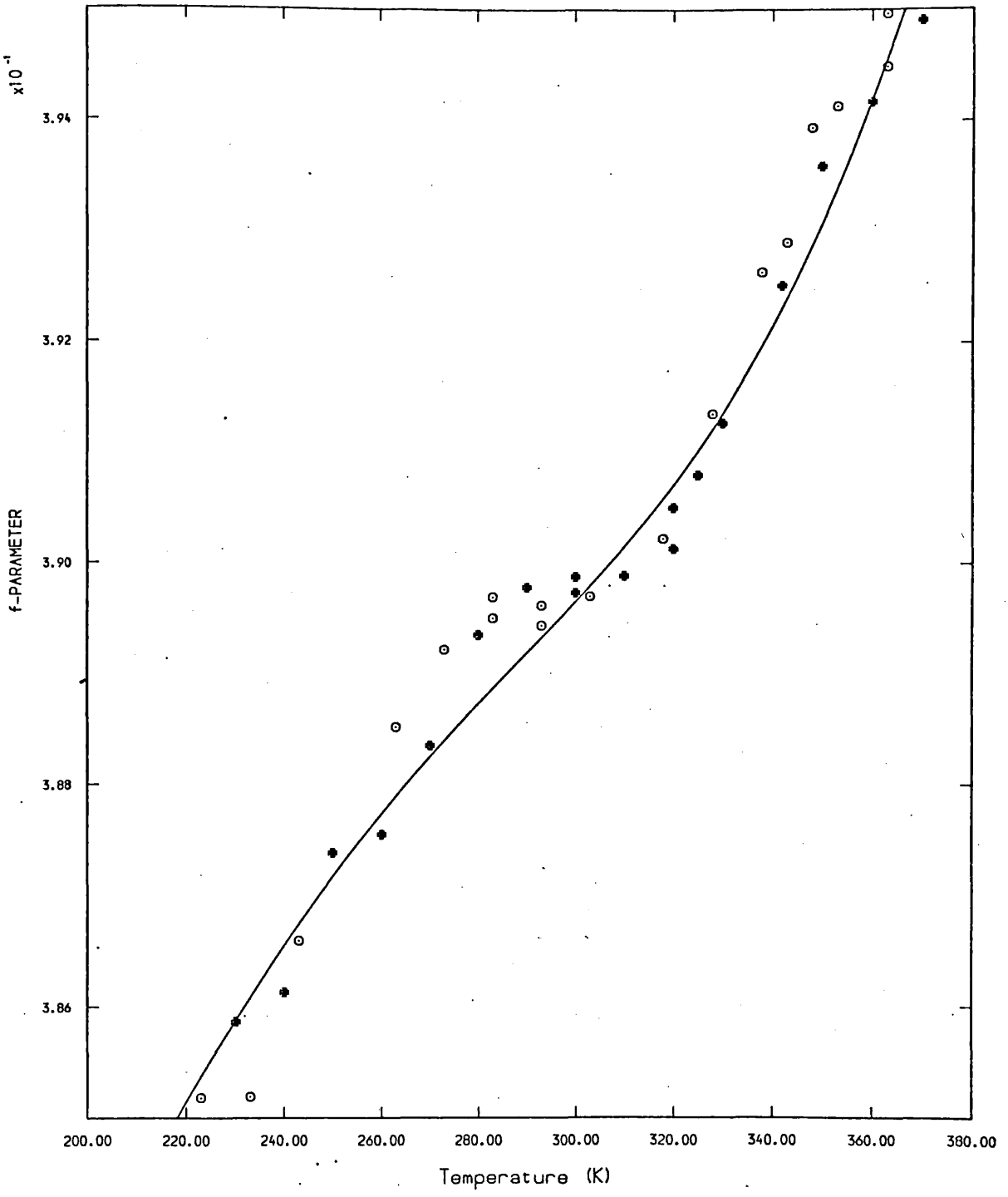

FIG. 5.17 An enlarged version of the central portion of figure 5.14 with the self-trapping model fit only. The circles represent a second set of data points, which were taken on the same sample.

boundaries in the polycrystalline specimen of cadmium has been strengthened by the observation of temperature independence of the line-shape parameter in the liquid helium temperature regime in the single crystal specimen. This is, also, seen in the variation of the parabolic percentage as a function of temperature.

CHAPTER 6 STUDIES OF POSITRON TRAPPING IN LEAD

6.1 Introduction

Most of the positron studies on lead have been concentrated on temperatures above room temperature and below 77 K . The purpose of the measurements extended to liquid helium temperatures were, mainly, to study the annihilation of positrons in superconducting lead compared to normal lead. Lifetime measurements by Shafroth and Marcus (1956) and Green and Madansky (1956) and angular correlation studies by Stump (1955) showed no change near the transition temperature, $T = 7.2$ K .

Mc Kee et al (1972a) reported a mono-vacancy formation energy E_{1v} of 0.50 ± 0.03 eV for lead which is in agreement with 0.49 ± 0.10 eV given by Feder and Nowick (1967). The latter team employed a different technique which compared dilatometric measurements with x-ray lattice parameter measurements. Nevertheless, measurements by Mc Kee et al (1972a) were performed above room temperature and, in their analysis, the prevacancy temperature dependence of the annihilation parameter was not accounted for.

In this experiment the characteristics of positron annihilation in annealed and plastically deformed lead specimens have been investigated. By observing the annihilations in annealed samples up to the melting point the thermal creation of vacancies have been measured, and estimates of the mono-vacancy formation energy have been made.

6.2 Temperature Dependence in Annealed Lead

6.2.1 Experimental Measurements

The sample consisted of two 1.5 mm thick and 20 mm diameter lead discs of 99.9995% purity (from Johnson-Matthey), which were etched in dilute nitric acid. To allow a full nucleation and growth of grains, the annealing consisted of maintaining the specimen at 520 K for 42 hours under a vacuum of 10^{-6}torr . Following the final etching, approximately 90 μCi of a carrier-free ^{22}NaCl positron source was evaporated directly onto the central regions of the two discs. The sample, arranged in a sandwich configuration, was then maunted in the low temperature cryostat.

Figure 6.1 shows the variation of F-parameter as a function of temperature over the range 4.2 to 593 K . The definition of F , together with the electronic stability control and the counting statistics were as for cadmium, which have been outlined in chapter 5 .

The steep rise above 400 K is associated with the thermal creation of mono-vacancies. Below 150 K the graph is flat.

6.2.2 Line-shape Parameter Analysis

In fitting the high temperature data (above 340 K) an important question raised is whether or not the prevacancy slope in F should be assumed to be continuous, and hence whether it should be extrapolated and suitably accounted for.

Fitting the data above 150 K , with the assumption that the

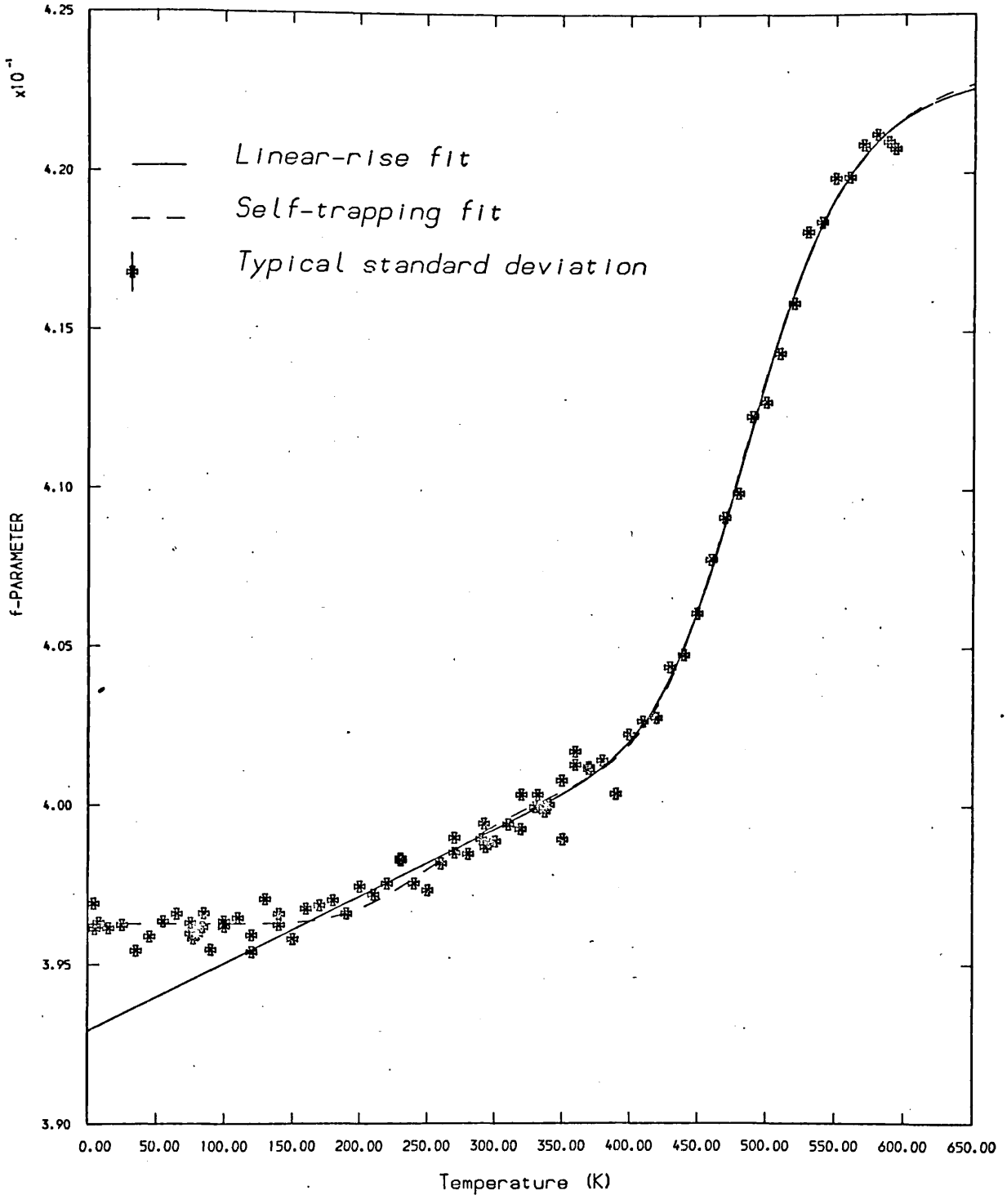

FIG. 6.1 The variation of F-parameter with temperature for the annealed specimen of lead. The steep rise above 400 K is associated with the thermal creation of vacancies.

prevacancy slope is essentially concerned with the free positrons in the lattice and is also due to changing electron densities as a result of thermal lattice expansion, have yielded the values of the parameters displayed in table 6.1 . In the fitting, it was also assumed that F_{1v} was independent of temperature.

We have, also, applied the self-trapping model, expressed in equation (3.3) , to our measurements on lead. This has resulted in the values of parameters and are listed in table 6.1 .

The absence of a plateau at high temperatures in figure 6.1 almost certainly indicates either less than 100% trapping of positrons or, perhaps, increasing divacancy trapping. Although it is conceivable that F_{1v} might vary with temperature, one would normally expect other types of defects to show a similar variation. There is no evidence for this at low temperatures (see figure 6.5) . Having included the divacancy term in the curve fitting to the points above 150 K, with the assumption that the observed prevacancy temperature dependence of F is a result of thermal lattice expansion, or from 4.2 K with the self-trapping model, we have obtained two sets of parameters which are, also, listed in table 6.1 .

Finally, we fitted the simple two-state trapping model, expressed in equation (3.1), to the points above 320 K . These calculated parameters are also listed in table 6.1 .

The thermal expansion (or in other words linear rise) and

	Analysis	E_{1v} (eV) (±0.02)	F_f	F_{1v}	A_{1v} (x10^5)	β (x10^{-6})	$E(K_o)$	F_{st}	B (x10^5)	χ^2/ν (80 points)
1	Monovacancies plus linear rise above 150 K	0.60	0.3929	0.4233	10.9	53	....	.....	....	1.05
2	Monovacancies plus self-trapping	0.56	0.3963	0.4236	6.02	..	0.16	0.4026	21.0	1.16
3	Monovacancies plus divacancies plus linear rise above 150 K	0.61	0.3929	0.4231	14.2	53	....	.....	....	1.07
4	Monovacancies plus divacancies plus self-trapping	0.56	0.3963	0.4237	5.09	...	0.15	0.4026	15.3	1.03
5	Simple model F_f = constant above 320 K	0.51	0.4003	0.4244	1.56	...	....	.....	....	1.18 (34 points)

Additional parameters : For case 3 ; F_{2v}=0.4235 , A_{2v}=70 x10^4 , E^B_{2v}=0.044 eV .
For case 4 ; =0.4230 , =116 x10^4 , =0.21 eV .

TABLE 6.1 The results of fitting the parameter F according to several theoretical models.

the self trapping model fittings are both illustrated in figure 6.1 . Figures 6.2 and 6.3 illustrate the different contributions to F calculated with the parameters obtained from curve fittings in the cases when F_f is taken linearly to rise with temperature or using Seeger's self-trapping model, respectively.

6.3 Annealing of Deformed Lead Specimens

In the experiments the lead specimens were derived from 99.9995% pure rod from Johnson-Matthey. The samples consisted of lead discs, initially 3 mm thick and 10 mm diameter, which were etched in dilute nitric acid. The positron source, 90 μCi , of a carrier-free $^{22}NaCl$ solution, was evaporated directly on to the central region, consisting of a 3 mm diameter drop, on one side of each of the two discs.

Figure 6.4 shows the variation of the line-shape parameter F as a function of temperature for the three deformed lead specimens, and are contrasted with those for the annealed lead. The parameter F is defined as in the case of annealed lead.

The first (deformed lead-A) sample received a 20% thickness reduction at room temperature, and the results show the defects rapidly annealing out at this temperature.

The second sample (deformed lead-B) had undergone 15% compression at 77 K ; care was taken to ensure the sample did not rise in temperature above 120 K in being swiftly (2 minutes) transfered to the cryostat.

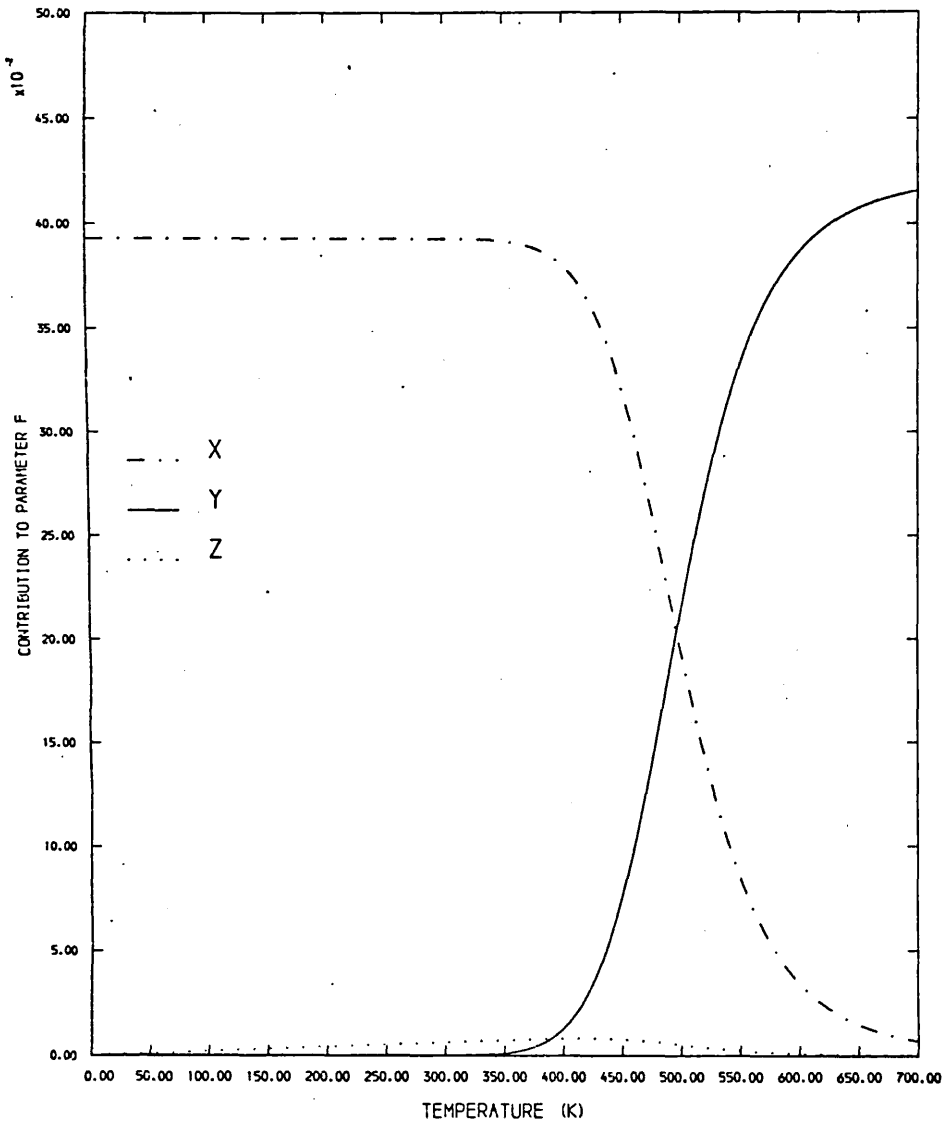

FIG. 6.2 Different contributions to F from linear rise fitting. Curves X , Y and Z represent $F_f^o P_f$, $F_{1v} P_{1v}$ and $F_f^o \beta T P_f$, respectively.

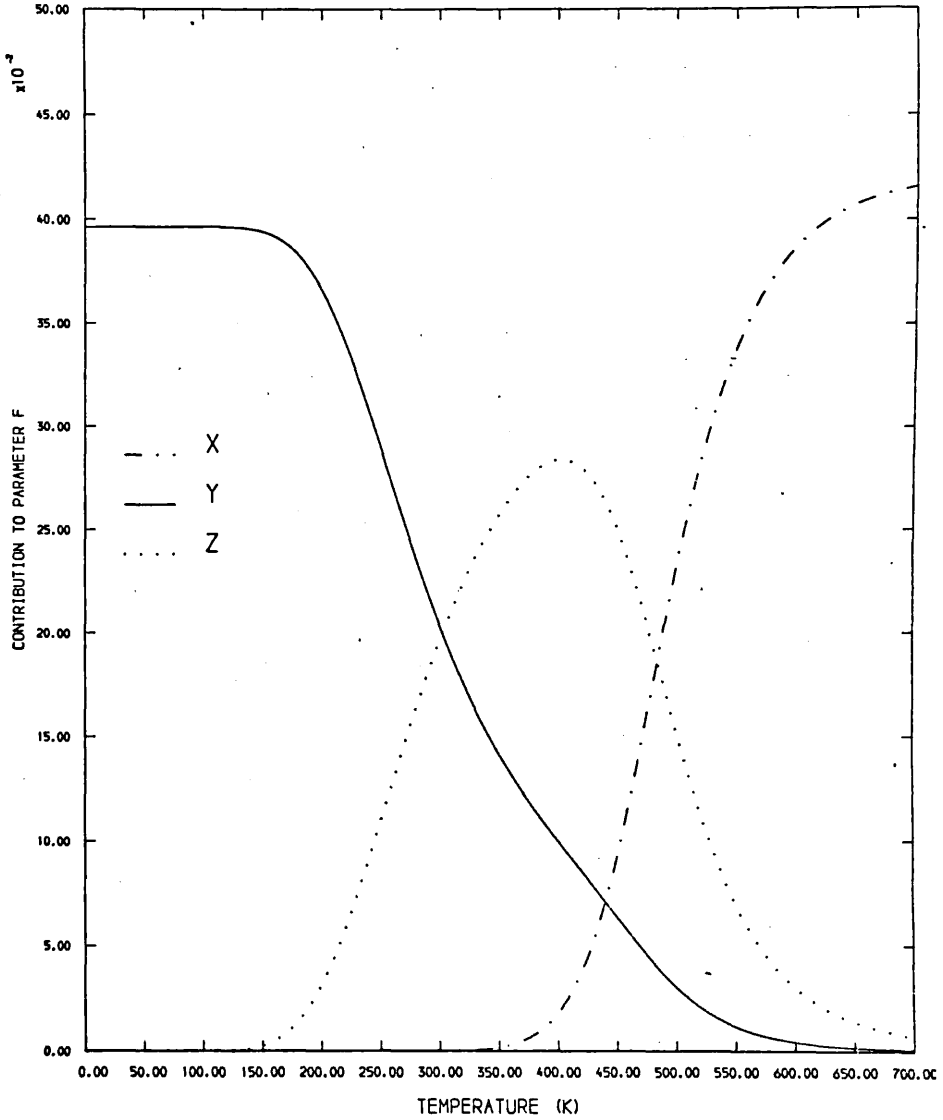

FIG. 6.3 The different contributions to F from the self-trapping fit. Curves X , Y and Z represent $F_{1v} P_{1v}$, $F^o(1-P_{st})P_f$ and $F_{st} P_{st} P_f$, respectively.

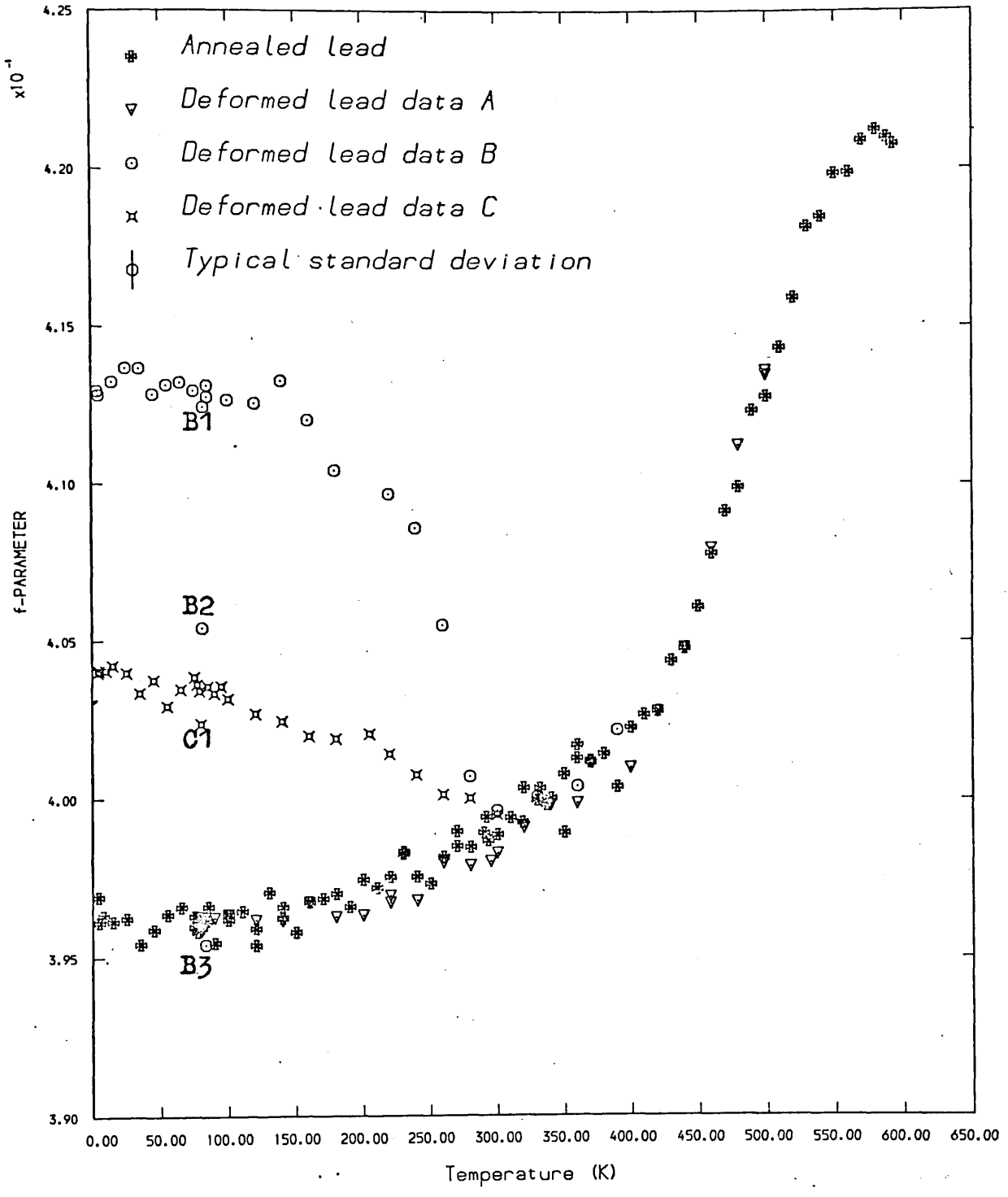

FIG. 6.4 F-parameter values for the three deformed samples of lead, contrasted with those for the annealed sample. In data B , the sharp decline above 160 K shows the annealing of the defects. Some return points are shown : B1 , B2 and B3 were taken immediately after the runs at 140 K , 260 K and 390 K , respectively. In data C the only return point was taken after the run at 200 K .

The third specimen (deformed lead-C) similarly received an intermediate (5%) compression at 77 K .

Measurements were performed in the low temperature cryostat and in all cases consisted of successive cycles, each of two hours and 20 minutes. Each cycle consisted of 20 minutes temperature setting and two hours counting at a total counting rate of 5000 cps . The approach adopted was to, first, reduce the sample temperature down to 4.2 K , and then to accumulate the photon spectrum in a series of increasing temperatures. In this way each 511 keV photopeak contained 900 000 counts. Simultaneous measurements of a control 497 keV gamma-ray line of ^{103}Ru , placed outside the cryostat, also contributed to the spectrum.

Specimen B shows only a slightest annealing in the range up to 130 K ; thereafter the rate increases especially above 200 K . The datum (B2) at 77 K was taken immediately after the run at 260 K ; identically, the equal values of F suggest that our finding (see the following section, also Rice-Evans et al, 1978a), that the positron trapping rate is independent of temperature, is valid up to 260 K . Complete recovery apparently occurs at about 300 K .

The lightly (5%) deformed specimen (C) shows a similar annealing curve for a lower concentration of defects.

6.4 The Trapping Rate of Positrons in Deformed Lead

Figure 6.5 shows the variation of the F-parameter with temperature for annealed, lightly deformed (5%) and severely deformed (15%) specimens of lead.

In the trapping model, the rate ν, at which thermalised positrons are trapped by a unit concentration of defects, is compared with the annihilation rate of positrons. The fraction, P, of positrons annihilating at traps has been given in equation (1.36). As noted earlier, the annihilation line narrows when positrons are trapped in defects and this can be expressed with the linear parameter $F = PF_t + (1 - P)F_f$.

The lower set of points concerns the annealed sample which was assumed to contain an insignificant concentration of defects with $F = F_f$ and $P = 0$. The upper set corresponds to the deformed lead-B specimen. After annealing, the third specimen (deformed lead-C) was, once again, subjected to a comprassion (25%) and the value of F averaged over three points, which were taken at 77 K in this final specimen, was 0.4141 ± 0.0005. Hence, the top set of points virtually corresponds to saturation trapping, i.e. $F = F_t$ and $P = 1$.

The intermediate set points on the 5% deformed sample would not be flat if the positron trapping rate were temperature dependent. To assess the temperature dependence and to allow a comparison with theory, one may write $\nu = \nu_o T^x$.

Several theoretical models have been proposed. Clasically, a dependence given by $x = \frac{1}{2}$ for the trapping rate, was predicted

by Connors and West (1969) for freely propagating positrons. A dependence given by $x=-\frac{1}{2}$ rate was suggested by Seeger (1972) which was governed by the diffusion of positrons arising from frequent scattering with acoustic phonons. This approach was extended by Frank and Seeger (1974) who obtained the expression given in equation (1.40) . Brandt (1974), who considered the effects of positron scattering on electrons, phonons and crystal imperfections, obtained the diffusion coefficient given in equation (1.41) .

An alternative quantum mechanical approach to trapping was initiated by Hodges (1970) who found that the rate was independent of temperature. This result was supported by Bergersen and Taylor (1974) for freely propagating positrons, and by Mc Mullen and Hede (1975) for strongly phonon-scattered positrons in the weak trapping limit. Recently, temperature independence has been reasserted by Bergersen and Mc Mullen (1977) for dislocations with the hypothesis that excess energies are absorbed by electron-hole pair formation ; and by Mc Mullen (1977) on the basis of estimates of positron densities at the defects and their dependence on temperature and phonon scattering.

Our calculated value of x for the intermediate set, shown in figure 6.5 , is given by $x=-0.03 \pm 0.02$, suggesting an insignificant temperature dependence for the positron trapping rate in the range 4 to 100 K .

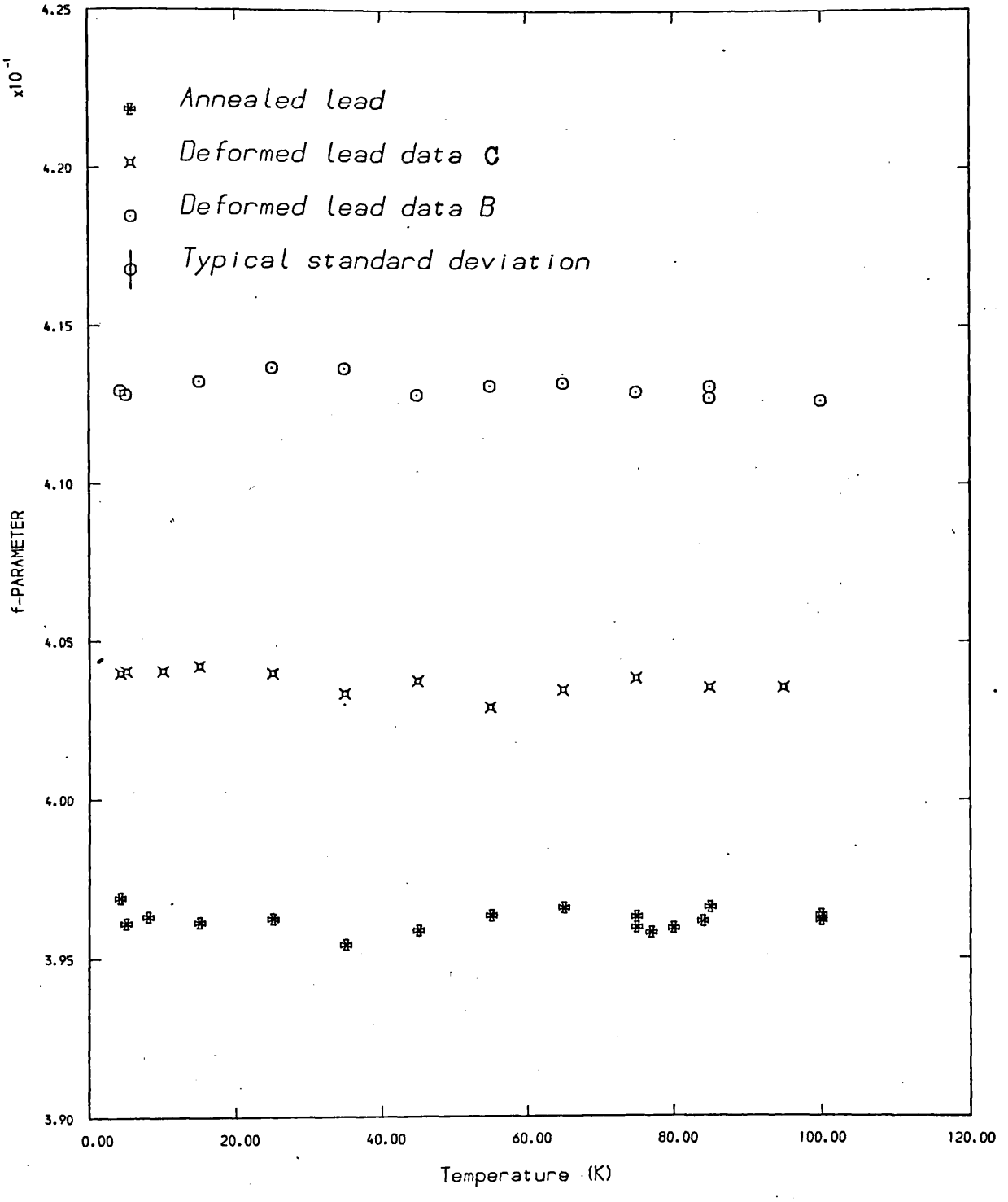

FIG. 6.5 The variation of the F-parameter for annealed, lightly deformed (C), and strongly deformed (B) samples of lead

6.5 Convolution

The line shapes, both for the annealed and the deformed specimens of lead, have been resolved into their Gaussian and parabolic components by the method described in chapter 2, and have employed the appropriate resolution functions.

Figures 6.6 and 6.7 show the variation of the width parameters of the Gaussian and the parabolic components of individual lines for the annealed and the three differently deformed specimens of lead as a function of temperature. The temperature dependence of the proportions of the annihilations contributing to the parabolic component of the line shape (parabola percentage), for the lead specimens, are shown in figures 6.8 and 6.9 .

6.6 Discussion of Results

On the basis of several hypotheses, including positron self-trapping and divacancy production , the calculated values of the monovacancy formation energies, as well as the other parameters involved in the fittings, have been tabulated in table 6.1 .

Our simple analysis of points above 320 K gives a value of the monovacancy formation energy of 0.51 ± 0.02 eV . This is almost identical to the value of 0.50 ± 0.03 eV obtained for lead by Mc Kee et al (1972a) in an angular correlation experiment for a temperature range above 300 K . An alternative method for determining monovacancy formation energies is to compare dilatometric measurements with x-ray lattice parameter measurements. It is striking that both the above given values

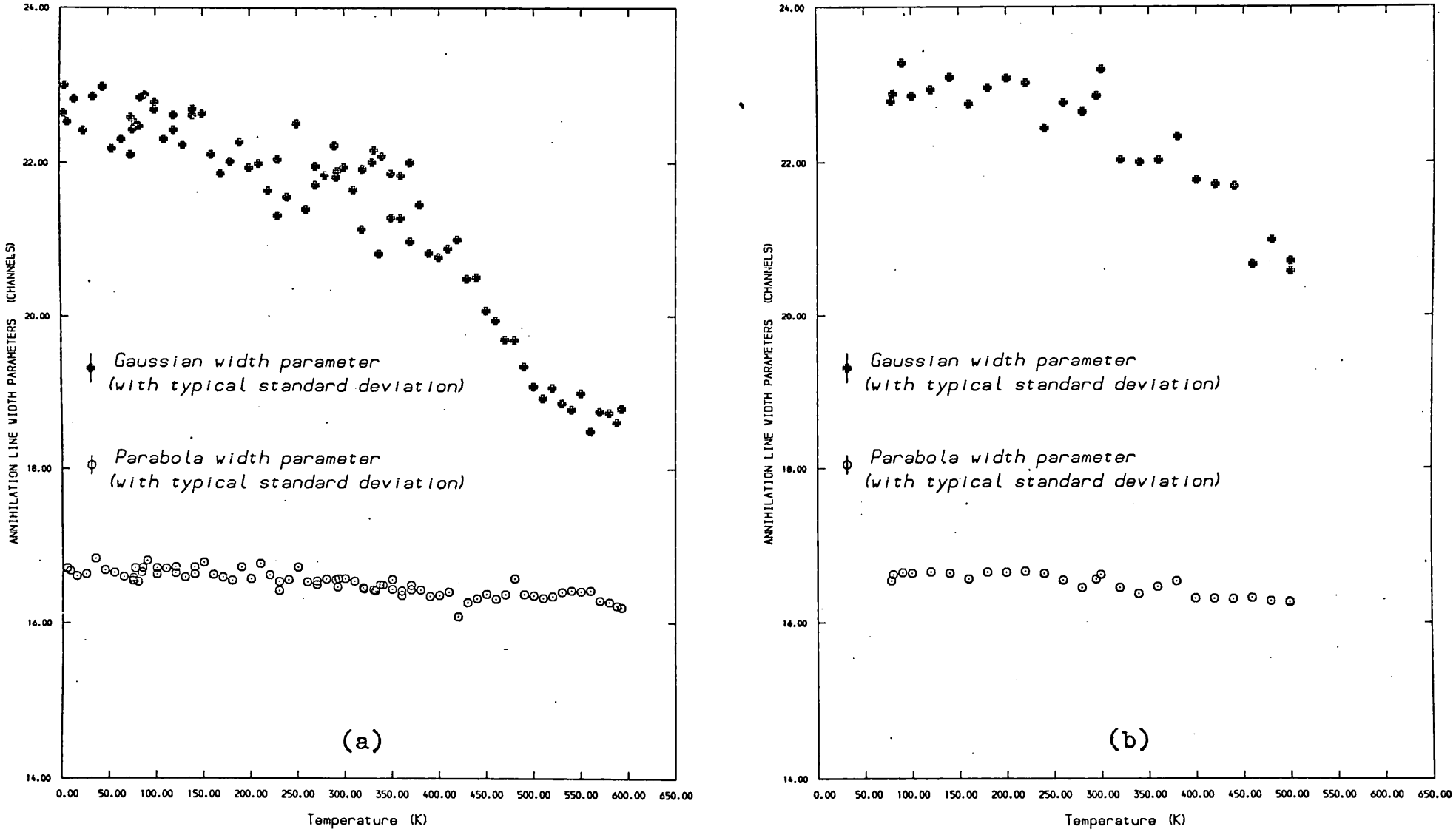

FIG. 6.6 The variation of the width parameters of the Gaussian and the parabolic components of individual lines for :(a) the annealed and (b) deformed-A specimens of lead as a function of temperature.

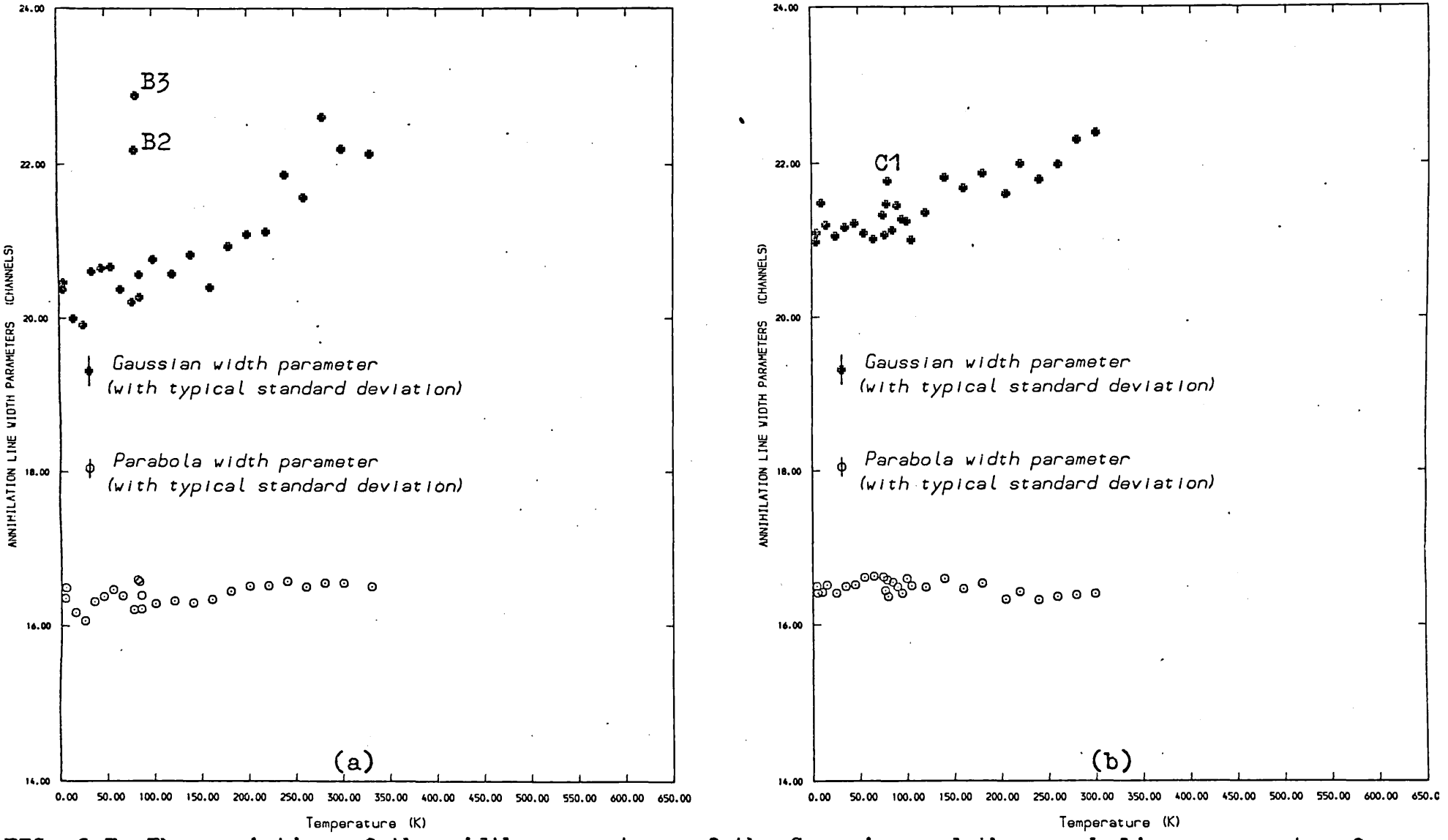

FIG. 6.7 The variation of the width parameters of the Gaussian and the parabolic components of individual lines for :(a) deformed-B and (b) deformed-C specimens of lead as a function of temperature.

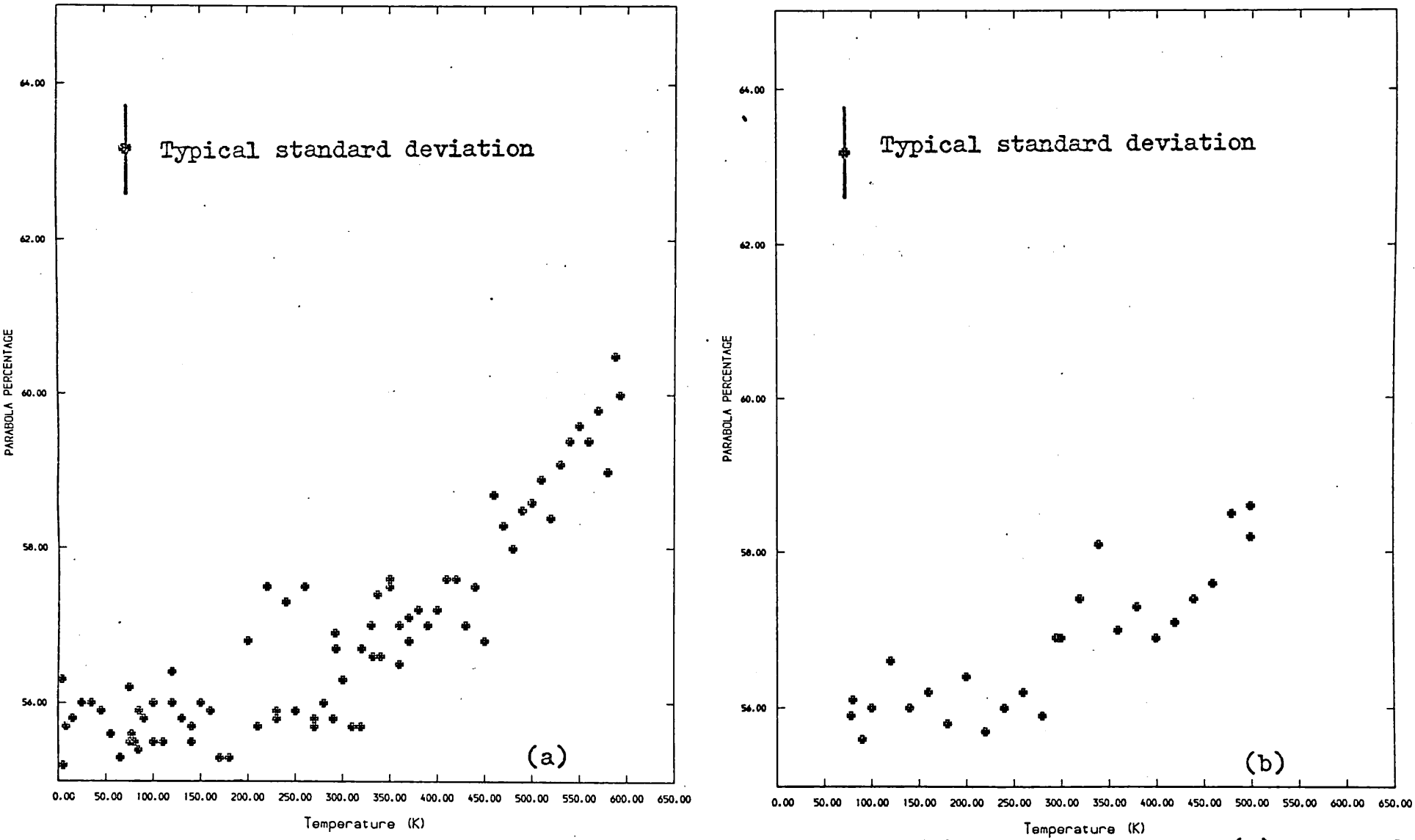

FIG. 6.8 The change in percentage of parabolic component in : (a) the annealed and (b) deformed-A specimens of lead, as a function of temperature.

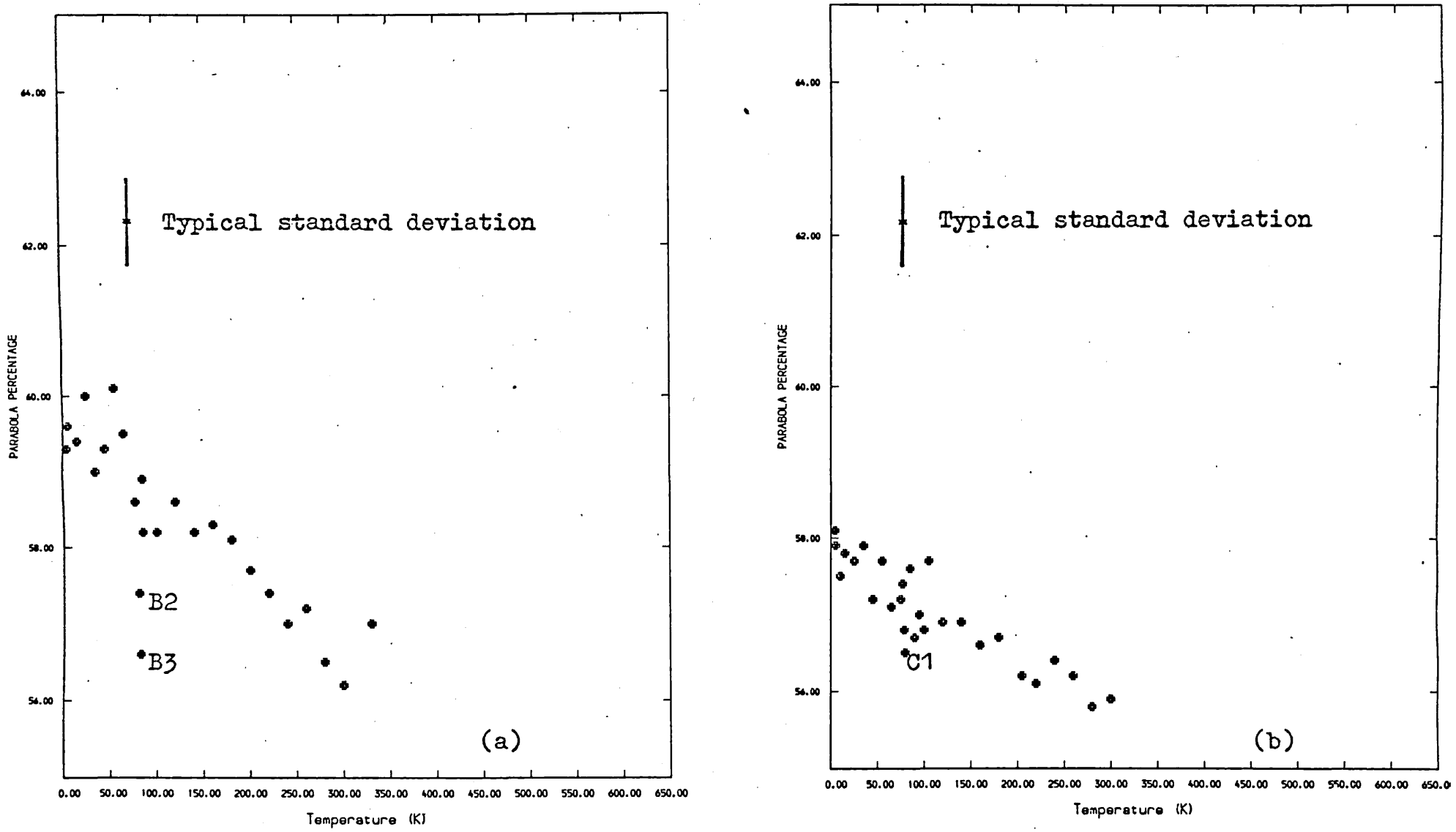

FIG. 6.9 The temperature dependence of the proportion of the annihilations contributing to the parabolic component of the line shape for :(a) deformed-B and (b) deformed-C specimens of lead.

agree with the dilatometric value reported by Feder and Nowick (1967) , although a rather large error (0.1 eV) is quoted for the latter. Unfortunately, the dilatometric measurements were not extended below $20^{o}C$ to observe whether anything analogous to the prevacancy rise is seen. Identically, the dilatometric data for cadmium (Feder ana Nowick, 1972) give little grounds for hope.

In the cases (1) and (3) we have assumed that the underlying linear rise is continued to high temperatures, as one might expect, if thermal expansion were the origin of this rise at intermediate temperatures (bearing in mind that the vacancy effect always predominates). However, the flat graph for F below 150 K creates some cause for concern in this interpretation. We therefore remain sceptical, in spite of the goodness of the fit to the data. One point to note is that the slope (β) is nearly twice the coefficient of linear thermal lattice expansion, $28 \times 10^{-6}\ K^{-1}$. Case (3) includes provision for divacancies. Although a fair fit is obtained, the calculated ratio of divacancies to monovacancies is insignificant.

The self-trapping model is considered in cases (2) and (4) . The resulting E_{1v} , 0.56 eV , is lower than that of case (2) and is higher than the value 0.49 eV found by the dilatometer, but it is within the quoted error of the latter. Of course, positron self-trapping would not be seen in dilatometer experiments. The fit over the full range of 80 points is very reasonable. Hence, on the basis of positron

annihilation alone, we conclude that the self-trapping is the most plausible. After all, it would be absurdly arbitrary just to take points above 320 K with a constant F_f. Inclusion of the divacancy term, in the fitting, yielded the ratio of divacancies to monovacancies as not more than 0.3% at the melting point.

Annealing experiments on electron-irradiated pure lead have been reported by Birtcher et al (1974) and Schroeder and Schilling (1976). With electrical resistivity measurements, the recovery stages I - V , concerning the migration and annihilation of vacancies and interstitials, have been investigated over temperature ranges down to 1.5 K (for review, see Schilling and Sonnenberg, 1973). Schroeder and Schilling (1976) found that up to 50% of the radiation damage annealed out below 5 K . An almost complete recovery of the remaining radiation-induced effect, shown in their isochronal recovery curves for lead below 200 K , verifies that the annealing stage, steepening above 200 K , in our deformed lead-B specimen is not associated with the annealing of vacancies as a result of migration of interstitials. Perhaps the vacancies, if they existed at all, were annealed out soon after the compression at 77 K .

The shape of the recovery curve is dependent on the type of deformation produced. For example, if we consider the electron-irradiated recovery curves reported by Schröeder and Schilling (1976) in lead, we find that the recovery shape is dependent, not only on the different energies of

the ionising electrons, but also on the different irradiation doses as well. This phenomenon has, subsequently, been found to be valid in our experiments performed on lead and cadmium.

CHAPTER 7 POSITRON ANNIHILATION IN GOLD AND SILVER IN THE SUB-VACANCY REGION

7.1 Introduction

The noble metals, chiefly copper, are among the most extensively studied metals by the positron annihilation technique (Mc Gervey and Triftshauser, 1973 ; Triftshauser and Mc Gervey, 1975 ; Jamieson et al, 1974 ; Moya, 1974 ; Dlubek et al, 1977a ; Campbell et al, 1977 ; Herlach et al, 1977).

Lichtenberger et al (1975) reported a non-linear behaviour of the Doppler-broadened line-shape parameter in the absence of vacancy trapping in cadmium and several other metals, including silver. This may be due to phonon assisted trapping of positrons. They also stressed that this effect introduced serious complications into the analysis for vacancy formation energies, hence, suggests a need to investigate the sub-vacancy regime in detail.

In this work we present measurements of line shapes in annealed and deformed specimens of gold over the range 4.2 K to 700 K and in annealed silver from 77 K to 430 K .

7.2 Measurements on Annealed Specimens of Gold and Silver

Gold and silver sheets of 99.999% purity —from Koch-Light and Johnson-Matthey, respectively— were cut into $10x10x0.75\ mm^3$ and $16x16x1\ mm^3$ pieces, respectively. The gold specimens were annealed for 21 hours at 1000 K under

a vacuum of 10^{-6} torr and then slowly cooled down to room temperature. The silver specimens were annealed under the same conditions for 9 hours. Both were etched in dilute nitric acid, and approximately 90 μCi of a carrier-free $^{22}NaCl$ positron source was evaporated directly on to the central region of each specimen which were then composed in a sandwich configuration. The gold sample was wrapped in a thin copper foil and the silver sample was sealed with resin around its edges.

Figure 7.1 and 7.2 show the line-shape parameter F —which was defined as the sum of the counts in the 21 central channels divided by the sum of the counts in the 200 channels across the peak— plotted as a function of temperature for the gold and silver specimens, respectively.

In the gold data each run of two hours, corresponding to a point in the figure, accumulated 900 000 counts in the 511 keV peak. Simultaneous measurements of a control ^{103}Ru 497 keV gamma-ray line, with the annihilation line, has been instituted to assess any electronic drift.

The silver data points correspond to runs of three hours at a total count rate of 3000 cps , accumulating 850 000 counts in the 511 keV peak, and with a slightly poorer electronic stability than in gold data.

Measurements on gold were extended up to the vacancy threshold temperature. Due to technical reasons the measurements on silver were terminated at 430 K ,

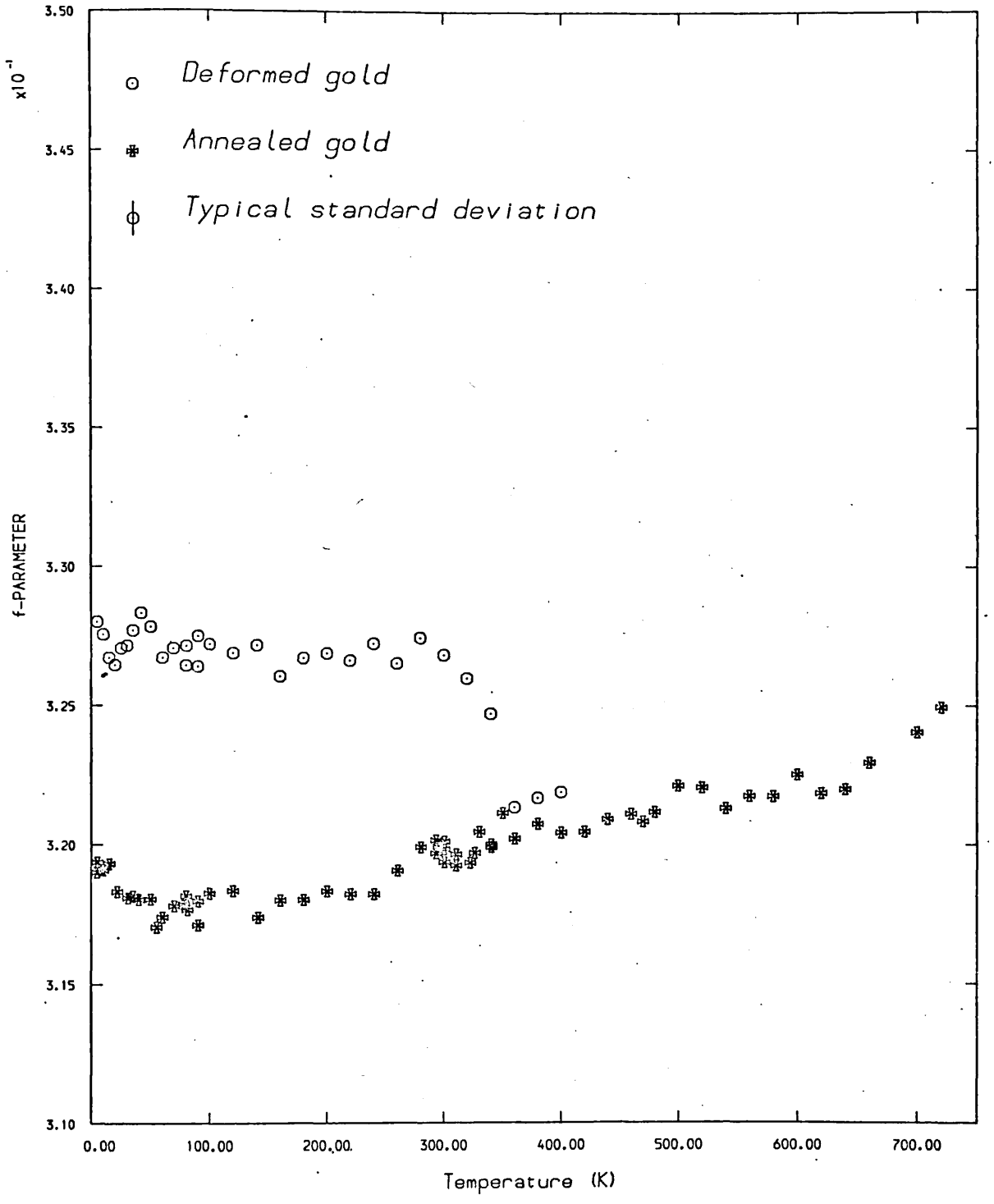

FIG. 7.1 The line-shape parameter F, plotted as a function of temperature for annealed and deformed gold specimens.

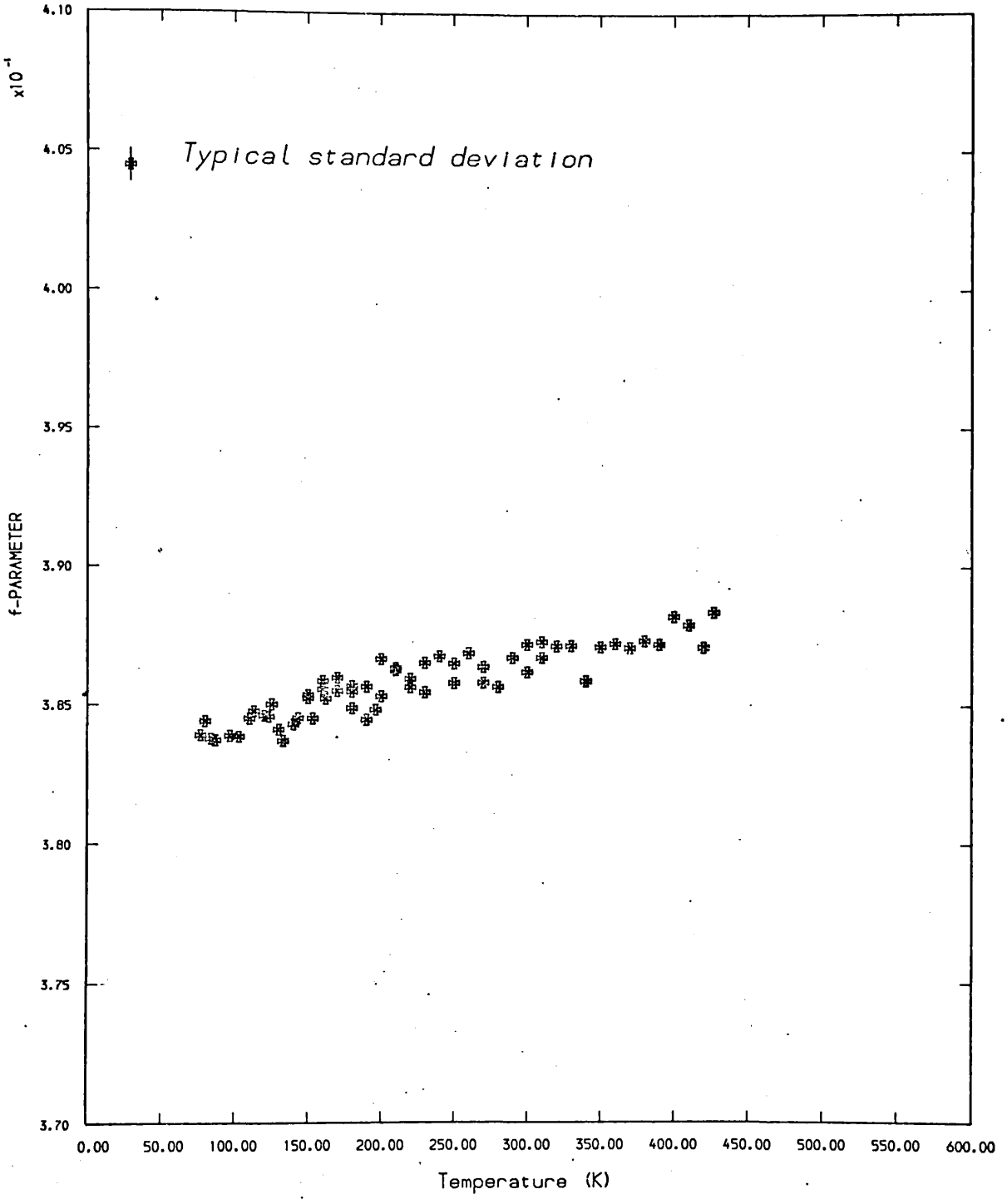

FIG. 7.2 The line-shape parameter F, plotted as a function of temperature for annealed silvre.

approximately 300 K below the onset of vacancy trapping. Nevertheless, both the Doppler-broadening measurements by Campbell et al (1977) and the coincidence counting rates at zero angle by Mc Gervey and Triftshauser (1973) , show an apparent linear behaviour of the measured characteristics of annihilation. This occurs from 300 K to a well defined threshold at which temperature a sharp increase occurs due to thermally generated vacancies.

7.3 Annealing of Deformed Gold

Two 10x10x1 mm^3 sheets of 99.999% pure gold from Koch-Light were deformed in a heavy vice by a 20% reduction in thickness. The deformation was carried-out at room temperature . The source-sample sandwich was wrapped in a thin copper foil to hold it together and to provide good thermal conductivity.

The annihilation line shapes were recorded as has been described for annealed gold. The annealing curve is shown in figure 7.1 . The region up to 320 K shows no apparent change due to annealing. A large step, showing the effect of recovery from the plastic deformation-induced defects as a result of their rearrangements and disappearance, is seen over the temperature interval 320 K to 350 K . The sample was kept for 12 hours at 340 K and the sharp decline above 340 K merely demonsrates the time factor involved in the recrystallisation process.

After the deformation, the sample was kept for nearly 8 hours

at room temperature prior to insertion in the cryostat. Although, in many metals, even 15% deformation is known to result in saturation trapping, it is not known whether this has occurred for our gold specimen.

7.4 Discussion

The correct interpretation of the intermediate temperature dependence of the annihilation characteristics is very important for the analysis of positron trapping by vacancies.

Triftshauser and Mc Gervey (1975) and Campbell et al (1977) reported an apparently linear temperature dependence of the annihilation line shape parameter in the sub-vacancy region in the noble metals, which contradicts the report given by Lichtenberger et al (1975). This led us, initially, to measure the annihilation line shapes in gold and silver from very low temperatures up to the vacancy threshold. Our observations, in these metals, do not confirm the low temperature behaviour of the annihilation parameter F reported by Lichtenberger et al (1975).

Unlike the deformed specimen, the annealed gold shows the distinctive feature at the lowest temperatures which has also been observed in cadmium and zinc but not in indium and lead. Absence of this temperature dependence in the deformed specimen, when the temperature tends to 4.2 K , hints at the possibility of a saturation trapping phenomenon in the deformed gold. Nevertheless, it is also true that the unusually higher order of fluctuations, observed in the

F-parameter in this temperature regime might have masked the small effect of grain boundary trapping.

Herlach et al (1977) has also observed the distinctive behaviour of the line-shape parameter in the temperature range below 50 K for annealed and quenched specimens of gold but not in electron-irradiated gold. On the other hand their suggestion that positrons escape from the sample by channeling within the grains is unconvincing —e.g., the conventional maximum range of positrons, given by the empirical formula $R(gr/cm^2) = 0.407\ E_{max}^{1.38}$, in cadmium and gold are 200 and 90 μm , respectively, which are unlikely to be increased to 1.5 mm in cadmium and to 0.75 mm in the case of gold by channeling.

CHAPTER 8 GENERAL CONCLUSIONS

8.1 Instrumentation

The theme of this thesis has been the studies of positron annihilation in several annealed and plastically deformed metal specimens. Throughout this work the annihilation line shapes were recorded by a high resolution Doppler-broadening spectroscopy system. This consisted of an intrinsic germanium planar detector, incorporated with an optical feedback pre-amplifier, and unipolar output pulses from the main amplifier were fed directly to an analogue-to-digital converter linked to a Nova-2 computer.

8.2 Evaluation of Mono-vacancy Formation Energies

For a clear understanding of metallurgical properties of materials it is important to know the concentrations and the formation energies of point defects. During the last decade, the positron annihilation technique has proved to be very sensitive in studying vacancies, dislocations and voids. Thermal equilibrium measurements of the positron annihilation momentum distribution, in principle, should provide accurate values of vacancy formation energies, providing the underlying sub-vacancy effects are properly accounted for and subtructed from the main effect due to vacancies.

On the basis of several hypotheses, including positron self-trapping, thermal expansion of lattice, and divacancy production, mono-vacancy formation energies have been evaluated.

In many metals the reported values of mono-vacancy formation energies, including ours, do not show a satisfactory agreement. On the basis of our line-shape parameter analysis we have concluded that the improper definition of the pre-vacancy temperature dependence of the annihilation parameters may be the root of the discrepancies between the values of mono-vacancy formation energies. Therefore, it is obvious that a more sophisticated theoretical description is required.

8.3 Temperature Dependence of the Specific Trapping Rate

In the trapping model, the rate ν at which thermal positrons are trapped by a unit concentration of defects is compared with the annihilation rate of positrons. Several theoretical models, concerning the temperature dependence of the positron trapping rate, have been proposed. These have been discussed in chapters 1 and 6 . On the basis of experimental evidence we have found that the rate of trapping of positrons by plastic-deformation-induced defects is independent of temperature. This finding, for lead, is valid up to at least 260 K , and for cadmium up to at least 200 K .

8.4 Liquid Helium Temperature Regime Anomalies

As liquid helium temperatures have been approached a new, reversible effect has appeared. An unexpected rise in the line-shape parameter F has been seen at the lowest temperatures in polycrystalline specimens of zinc, cadmium

and gold but not in indium, lead and single crystal cadmium. Even in well-annealed samples grain boundaries exist. These consist of complexes of intersecting dislocations which are known to trap positrons. Whether positrons exist in the grain boundaries will depend on the average size, i.e., will depend on the surface area of boundaries. Also, it will depend on whether or not a significant proportion of positrons would encounter the boundaries. The increase in F at the lowest temperatures implies that positrons are captured in shallow grain boundary traps, and the negative slope (dF/dT) indicates thermal detrapping. This, eventually, would result in their subsequent annihilation in different states, depending on the concentration of the grain boundary traps.

8.5 Identification of Defects

The positron annihilation technique is valuable in the study of concentration and the nature of lattice defects. The nature of a particular defect will be associated with characteristic values of the line shape parameter, say, F . Hence, the study of changing values of annihilation characteristic parameters in the recovery stages of a defected sample can indicate the defects involved, and their relative concentrations.

In principle, one might expect each type of defect to have a characteristic Doppler-broadened line shape. For example, in cadmium we can conclude that there are at least four characteristic values of the Gaussian widths corresponding to

positrons annihilating in the free state, or trapped in vacancies, or in two different types of plastic-deformation-induced traps. At this stage, it is obvious that much work has to be done in singling out individual defects and identifying them. Having singled out different types of defects, careful analysis of an experimental line into its individual components might reveal the relative concentrations if more than one type of defect were to be present.

There can be little doubt that positron annihilation and, especially, the Doppler broadening technique, will in future be refined to allow for an identification of defect catagories and a close examination of their behaviour with rising temperatures.

APPENDIX 1

Program CURFIT

This program employes the NAG subroutine E04FBF (based on a Harwell routine) or a similar sum of squares minimiser to make a least squares fit of a function non-linear in certain parameters to data, especially that expected to have Gaussian errors. For the convenience of experimenters who wish to derive quotable results estimates of confidence limits for the parameters are also derived.

The Function Required

The user has to supply a FORTRAN function VALUE to calculate the Y value on the curve for a given X. This should have the form :-

```
      REAL FUNCTION VALUE(N,PAR,X)
      DIMENSION PAR(N)
C  THE ARRAY PAR HOLDS THE N PARAMETERS
..... Calculation of VALUE from X and parameters .....
      VALUE=.....
      RETURN
      END
```

The Input Data :

(1) Number of parameters (N)
Number of data points (M) FORMAT(2I20)

(2) The accuracy required for the final sum of squares
The proportion by which the variable should be changed to get a nearby point.
A limit to the number of evaluations of the sum of squares during the iterative minimisation for each data set.

An integer to control the reporting of the movement of the parameters during minimisation. If zero reporting is supressed. FORMAT(2E20.10,2I20)

(3) (A set of cards ONE for EACH parameter

Name of the parameter

Order of magnitude for this parameter

Initial guess for that parameter

Generous estimate of the possible difference of the final result from the initial guess. Used in the termination criterion for the minimisation FORMAT(A10,3E20.10)

(4) Variable format card (should contain a Format of 3 real variables ; X, Y and Weight for each data point. If all the Weights are zero they are assigned value 1).

(5) Identification card —e.g., the program title.

(6) The data as specified in (4)

Output :

The program writes out all the data after reading it in, though it may be in a different format. It reads in X, Y and WEIGHT values for the data and prints them out again. Then it repeats the guesses for the parameters and their orders of magnitude and possible variations.

In the iterative minimisation of the sum of squares of differences between Y prediction and its actual measured value then begins the output controlled by the fourth statement of the second input card.

After succesful convergence it should print IFAIL IS 0 and then give the values of the parameters at the minimum.

APPENDIX 2

The Function VALUE Employed in the Program CURFIT

```
      REAL FUNCTION VALUE(N,PAR,X)
      DIMENSION PAR(N),R(200),C(200)
C  R IS THE RESPONSE FUNCTION ARRAY
C  C IS THE ARRAY OF THE GENERATED SPECTRUM
      DATA MC/1/ ,M/150/ ,IBAR/75/ ,R/... the response func./
C  IBAR IS THE CENTROID OF THE RESPONSE
      I=IFIX(X+0.5)
      IF (MC.EQ.1) GO TO 888
    2 S=0.
      DO 6 K=1,M
      J=IBAR+I-K
      IF (J.LT.1) J=1
      IF (J.GT.150) J=M
    6 S=S+R(J)*C(K)
      COUNT=S+PAR(2)+PAR(3)*I+PAR(8)*I**2+PAR(9)*I**3
C  PAR(2) IS CONSTANT BACKGROUND
C  PAR(3) IS BACKGROUND SLOPE 1
C  PAR(8) IS BACKGROUND SLOPE 2
C  PAR(9) IS BACKGROUND SLOPE 3
      MC=MC+1
      GO TO 999
  888 DO 4 J=1,M
      T=PAR(1)-FLOAT(J)
C  PAR(1) IS THE PEAK CENTROID
      GW=T*T/PAR(5)/PAR(5)
      PW=T*T/PAR(7)/PAR(7)
      GAUSS=0.
      PARA=0.
      IF (GW.LT.200.) GAUSS=PAR(4)*EXP(-GW)
C  PAR(4) IS THE GAUSSIAN HEIGHT
C  PAR(5) IS THE GAUSSIAN WIDTH
C  PAR(7) IS THE PARABOLA WIDTH
```

```
      IF (PW.LT.1.) PARA=PAR(6)*(1.-PW)
C  PAR(6) IS THE PARABOLA HEIGHT
    4 C(J)=GAUSS+PARA
      GO TO 2
  999 VALUE=COUNT
      RETURN
      END
```

REFERENCES

Ashcroft,N.W. and Mermin,N.D. ; 1976, Solid State Physics (Holt, Rinehart and Winston, New York)

Anderson,C.D. ; Phys. Rev. 43 (1933), 491

Arias-Limota,J.A. and Varlashkin,P.G. ; Phys. Rev. B1 (1970), 142

Bell,R.E. and Graham,R.L. ; Phys. Rev. 90(1953),644

Bergersen,B. and Stott,M.J. ; Solid State Commun. 7(1969),1203

Bergersen,B. and Taylor,D.W. ; Can. J. Phys. 52(1974),1594

Bergersen,B. and McMullen,T. ; Solid State Commun. 24(1977),421

Beringer,R. and Montgomery,C.G. ; Phys. Rev. 61(1942),222

Berestetskii,V.B.,Lifshitz,E.M.,and Pitaevskii,L.P. ; 1971, Relativistic Quantum Theory (Pergamon,Oxford)

Berko,S. and Plaskett,J.S. ; Phys. Rev. 112(1958),1877

Berko,S. and Erskine,J.C. ; Phys. Rev. Lett. 19(1968),307

Berko,S. and Mader,J. ; Appl. Phys. 5(1975),287

Bhattacharyya,F. and Singwi,K.S. ; Phys. Rev. Lett. 29(1972),22

Birtcher,R.C.,Lwin,Y.,and Koehler,J.S. ; Phys. Rev. Lett. 33(1974),899

Bisi,A.,Fiorentini,A.,and Zappa,L. ; Phys. Rev. 131(1963),1023 ; Ibid 134(1964),A328

Bisi,A.,Bussolati,C.,Cova,S.,and Zappa,L. ; Phys. Rev. 141(1966),348

Bosi,L. and Dupasquier,A. ; Phys. Rev. B11(1975),2485

Brandt,W.,Berko,S.,and Walker.W.W. ; Phys. Rev. 120(1960),1289

Brandt,W. and Spirn,I. ; Phys. Rev. 142(1966),231

Brandt,W. ; 1967, Positron Annihilation (ed. by Stewart,A.T. and Roellig,L.O. , Academic Press, London)

Brandt,W. ; Appl. Phys. 5(1974),1

Brandt,W.,Isaacson,D.,and Paulin,R. ; Phys. Rev. Lett. 35(1975),1180

Campbell,J.L.,Schulte,C.W.,and Jackman,T.E. ; J. Phys. F: Metal Phys. 7(1977),1985

Carbotte,J.P. and Kahana,S. ; Phys. Rev. A139(1965),213

Carbotte,J.P. ; Phys. Rev. 155(1967),197

Carbotte,J.P. and Salvadori,A. ; Phys. Rev. 162(1967),290

Chiba,T. and Tsuda,N. ; Appl. Phys. 5(1974),37

Connors,D.C. and West,R.N. ; Phys. Lett. A30(1969),24

Connors,D.C.,Crisp,V.H.C.,and West,R.N. ; Phys. Lett. A33(1970),180 ; J. Phys. F: Metal Phys. 1(1971),355

Cushner,S.,Erskine,J.C., and Berko,S. ; Phys. Rev. B7(1970),2852

De Benedetti,S.,Covan,C.E.,Konneker,W.R.,and Primakoff,H. ; Phys. Rev. 77(1950),205

De Benedetti,S. ; 1967, Positron Annihilation (ed. by Stewart,A.T. and Roellig,L.O. , Academic Press,London)

De Blonde,G.,Chuang,S.Y.,Hogg,B.G.,Kerr,D.P.,and Miller,C.M. ; Can. J. Phys. 50(1972),1619

Dekhtyar,I.Ya.,Levina,D.A.,and Mikhalenkov,V.S. ; Soviet Phys. Dokl. 9(1964),492

Dirac,P.A.M. ; Proc. Camb. Phil. Soc. 26(1930),361

Dlubek,G.,Brummer,O.,and Meyendorf,N. ; Appl. Phys. 13(1977a),67 ; Phys. Status Sol. A39(1977b),K95

Dojo,M. ; Nucl. Instr. and Methods 115(1974),425

Doyama,M. ; J. Phys. Soc. Japan 33(1972),321

Doyama,M. and Hasiguti,R.R. ; Crystal Lattice Defects 4(1973),139

Du Mond,J.W.M.,Lind,D.A.,and Watson,B.B. ; Phys. Rev. 75(1949),1226

Farrel,R.A. ; Rev. Mod. Phys. 28(1956),308

Feder,R. and Nowick,A.S. ; Phil. Mag. 15(1967),805
; Phys. Rev. B5(1972),1244

Frank,W. and Seeger,A. ; Appl. Phys. 3(1974),61

Fujiwara,K.,Hyodo,T.,and Ohyava,J. ; J. Phys. Soc. Japan
33(1972),1047

Gainotti,A.,Germognoli,E.,Schianchi,G.,and Zecchina,L. ; Phys.
Lett. 13(1964),9

Gemmel,D.S. ; Rev. Mod. Phys. 46(1974),129

Gol'danskii,V.I. and Prokop'ev,E.P. ; Soviet Phys. Solid State
6(1965),2641

Gol'danskii,V.I. ; 1967, Positron Annihilation (ed. by Stewart,A.T
and Roellig,L.O. , Academic Press,London)

Green,B. and Madansky,L. ; Phys. Rev. 102(1956),1014

Hautojarvi,P.,Tamminen,A.,and Jauho,P. ; Phys. Rev. Lett.
24(1970),459

Hautojarvi,P.,Vehanen,A.,and Mikhalenkov,V.S. ; Appl.Phys.
11(1976),191

Hendersen,B. ; 1972, Defects in Crystalline Solids (Edward
Arnold,London)

Herlach,D. and Maier,K. ; Appl. Phys. 11(1976),197

Herlach,D.,Stoll,H.,Trost,W.,Metz,H.,Jackman,T.E.,Maier,K.,
Schaefer,H.E.,and Seeger,A. ; Appl. Phys. 12(1977),59

Herman,F. and Skillman,S. ; 1963, Atomic Structure Calculations
(Prentice Hall)

Hlaing,T. ; 1976, Positron Annihilation in Metals (Ph.D. Thesis,
University of London, unpublished)

Hodges,C.H. ; Phys. Rev. Lett. 25(1970),284

Hodges,C.H. and Trinkaus,H. ; Solid State Commun. 18(1976),857

Hotz,H.P.,Mathiesen,J.M.,and Hurley,J.P. ; Phys. Rev. Lett.
170(1968),351

Hughes,A.E. and Pooley,D. ; 1975, Real Solids and Radiation (Wykeham Publications,London)

Jackman,T.E.,Schulte,C.W.,Campbell,J.L.,Lichtenberger,P.C., Mac Kenzie,I.K.,and Wormald,M.R. ; J. Phys. F: Metal Phys. 4(1974),L1

Jamieson,H.C.,McKee,B.T.A.,and Stewart,A.T. ; Appl. Phys. 4(1974),79

Kahana,S. ; Phys. Rev. 129(1963),1622

Kern,J. ; Nucl. Instr. and Methods 79(1970),233

Kerr,D.P. ; Can. J. Phys. 52(1974),935

Kim,S.M.,Stewart,A.T.,and Carbotte,J.P. ; Phys. Rev. Lett. 18(1967),358

Kim,S.M.,Buyers,W.J.L.,Martel,P.,and Hood,G.M. ; J. Phys. F: Metal Phys. 4(1974),343

Kim,S.M. and Buyers,W.J.L. ; J. Phys. F: Metal Phys. 6(1976),L67

Kirby,R.K.,Hahn,T.A.,and Rothrock,B.D. ; 1972, American Institute of Physics Handbook , p.4

Kirkegaard,P. and Eldrup,M. ; Computer Phys. Commun. 3(1972),240 ; 7(1974),401

Kittel,C. ; 1971, Introduction to Solid State Physics (John Willey,London)

Koehler,J.S. ; 1968, Vacancies and Interstitials in Metals (Proceedings of an International Conference , ed. by Seeger,A. , Amsterdam, 1970)

Kubica,P. and Stewart,A.T. ; Phys. Rev. Lett. 34(1975),852

Lee-Whiting,G.E. ; Phys. Rev. 97(1955),1557

Leighly,Jr.H.P. ;Appl. Phys. 12(1977),217

Leung,C.H.,McMullen,T.,and Stott,M.J. ; J. Phys. F: Metal Phys. 6(1976),1063

Lichtenberger,P.C.,Schulte,C.W.,and Mac Kenzie,I.K. ; Appl. Phys. 6(1975),305

Lucke,K. ; Material Sci. and Eng. 25(1976),153

Lynn,K.G.,Ure,R.,and Byrne,J.G. ; Acta Metallurgica 22(1974),1075

Lynn,K.G.,Mac Donald,J.R.,Boie,R.A.,Feldman,L.C.,Gabbe,J.D., Robbins,M.F.,Bonderup,E.,and Golovchenko,J. ; Phys. Rev. Lett. 38(1977),241

Mader,J.,Berko,S.,Krakauer,H.,and Bansil,A. ; Phys. Rev. Lett. 37(1976),1232

Mantl,S. and Triftshauser,W. ; 1976, in Proceedins of the Fourth International Coference on Positron Annihilation , Helsingor, paper E22.

Mantl,S. and Triftshauser,W. ; Phys. Rev. B17(1978),1645

Mogensen,E.O., Petersen,K.,Cotterill,R.M.J.,and Hudson,B. ; Nature, Lond. 239(1972),98

Moya,S. ; Phys. Status Sol. A23(1974),K171

Muirhead,H. ; 1965, The Physics of Elementary Particles (Pergamon Press,Oxford)

Myllyla,R. ; Nucl. Instr. and Methods 148(1978),267

Mac Kenzie,I.K.,Langstroth,G.F.O.,McKee,B.T.A.,and White,C.G. ; Can. J. Phys. 42(1964),1837

Mac Kenzie,I.K. ; Phys. Lett. A30(1969),115

Mac Kenzie,I.K. ; Phys. Status Sol. A12(1972),K87

Mac Kenzie,I.K. and Lichtenberger,P.C. ; Appl. Phys. 9(1976),331

Mac Kenzie,I.K. ; Phys. Rev. B16(1977),1705

McGervey,J.D. and Triftshauser,W. ; Phys. Lett. A44(1973),53

McKee,B.T.A.,Triftshauser,W.,and Stewart,A.T. ; Phys. Rev. Lett. 28(1972a),358

McKee,B.T.A.,Jost,A.G.D.,and Mac Kenzie,I.K. ; Can. J. Phys. 50(1972b),415

McKee,B.T.A.,Jamieson,H.C.,and Stewart,A.T. ; Phys. Rev. Lett. 31(1973),634

McMullen,T. and Hede,B. ; J. Phys. F: Metal Phys. 5(1975),669

McMullen,T. ; J. Phys. F: Metal Phys. 7(1977),2041

McNelles,L.A. and Jackman,J.L. ; Nucl. Instr. and Methods 127(1975),73

Nanao,S.,Kuribayashi,K.,Tanigawa,S.,Mori,M.,and Doyama,M. ; J. Phys. F: Metal Phys. 3(1973),L225

Ore,A. and Powell,J.L. ; Phys. Rev. 75(1949),1696

Perkins,A. and Carbotte,J.P. ; Phys. Rev. B1(1970),101

Petersen,K.,Nielsen,B.,and Evans,J.H. ; Phil. Mag. 34(1976),685

Rice-Evans,P.,Hlaing,T.,and Rees,D.B. ; J. Phys. F: Metal Phys. 6(1976a),1079

Rice-Evans,P.,Hlaing,T.,Chaglar,I. ; Phys. Rev. Lett. 37(1976b),1415

Rice-Evans,P. and Hlaing,T. ; J. Phys. F: Metal Phys. 7(1977),821

Rice-Evans,P.,Hlaing,T.,and Chaglar,I. ; Phys. Lett. A60(1977),368

Rice-Evans,P.,Chaglar,I.,and El Khangi,F.;Phys.Lett. A64(1978a),450

Rice-Evans,P.,Chaglar,I.,and El Khangi,F. ; Phys. Rev. Lett. 40(1978b),716

Routti,J.T. and Prussin,S.G. ; Nucl. Instr. and Methods 72(1969),125

Schilling,W. and Sonnenberg,K. ; J. Phys. F: Metal Phys.3(1973),322

Schroeder,H. and Schilling,W. ; Radiat. Eff. 30(1976),243

Scharma,S.C.,Berko,S.,and Warburton,W.K. ; Phys. Lett.A58(1976),405

Schumancher,D. ; 1968, Vacancies and Interstitials in Metals (Proceedings of an International Conference, ed. by Seeger,A. , Amsterdam, 1970)

Seeger,A. ; Phys. Lett. A40(1972),135

Seeger,A. ; J. Phys. F: Metal Phys. 3(1973a),248

Seeger,A. ; Crystal Lattice Defects 4(1973b),221

Seeger,A. ; Appl.Phys. 5(1975),85

Segers,D.,Dorikens-Vanpraet,L.,and Dorikens,M. ; Appl. Phys. 13(1977),51 ; Appl. Phys. 10(1976),121

Segre',E. ; 1953, Experimental Nuclear Physics (Wiley,New York)

Shafroth,S.M. and Marcus,J.A. ; Phys. Rev. 103(1956),585

Sharp,J.V.,Mitchell,A.,and Christian,J.W. ; Acta Metallurgica 13(1965),965

Singh,K.P.,Goodbody,G.S.,and West,R.N. ; Phys. Lett. A55(1975),237

Singh,K.P. and West,R.N. ; J. Phys F: Metal Phys. 6(1976),L267

Smedskjaer,L.C.,Fluss,M.J.,Chason,M.K.,Legnini,D.J.,and Siegel,R.W. ; J. Phys. F: Metal Phys. 7(1977),1261

Stewart,A.T. ; Can. J. Phys. 35(1957),168

Stewart,A.T. and Pope,N.K. ; Phys. Rev. 120(1960),2033

Stott,M.J. and West,R.N. ; J. Phys F: Metal Phys. 8(1978),635

Stroud,D. and Ehrenreich,H. ; Phys. Rev. 171(1968),399

Stump,R. ; Phys. Rev. 100(1955),1256

Sueoka,O. ; J. Phys. Soc. Japan 36(1974a),464 ; 37(1974b),875

Sumi,A. and Toyozawa,Y. ; J. Phys. Soc. Japan 35(1973),137

Tam,S.W. and Siegel,R.W. ; J. Phys. F: Metal Phys. 7(1977),877

Thompson,M.W. ; 1969, Defects and Radiation Damage in Metals (The University Press,Cambridge)

Triftshauser,W. and McGervey,J.D. ; Appl.Phys. 6(1975),177

Triftshauser,W. ; Phys. Rev. B12(1975),4634

Waite,T.R. ; Phys. Rev. 107(1957),463

Wallace,P.R. ; Solid State Phys. 10(1960),1

Weisberg,H. and Berko,S. ; Phys. Rev 154(1967),249

West,R.N.;1974, Positron Studies of Condensed Matter (Taylor and Francis,London)

West,R.N.,Borland,R.E.,Copper,J.R.A.,and Cusack,N.E. Proc. Phys. Soc. 92(1967),195

Yang.C.N. ; Phys. Rev. 77(1950),242

ACKNOWLEDGEMENTS

I would like to express my sincere gratitute to Dr. P. Rice-Evans for his excellent supervision and great contributions to the ideas expressed in the text and to Prof. E.R. Dobbs for his interest in this work.

I would also like to convey my appreciation to Dr. M.J. Lea for his advice with the cryogenic systems and Dr. T. Lake for his advice in computing and writing the program Curfit.

It is a pleasure to express my thanks to Dr. T. Hlaing , Mr. F. El Khangi and Mr. M. McGetrick for their collaboration in all aspects of the work.

I also express my thanks to Messrs W.A. Baldock, F.Grimes, A.King, A.K.Betts, B.Pashley, T.LeMotte, J.Sales and D.J.Gower for their technical support.

I would also like to thank the Computer Unit staff, Dr. P. Pal, Mr. P. Taylor, Mr. C. Kirton, Mr. J. Turner, and also the staff of the University of London Reactor Centre, especially Mr. E.A.Y. Caesar and Dr. G.D. Burholt.

Finally, I would like to acknowledge Bedford College for the award of a Tutorial Research Studentship, and also the Science Research Council for the fine research equipment that they have provided for positron annihilation studies at Bedford College.